Dyes and Pigments 199 (2022) 110074

Contents lists available at ScienceDirect

Dyes and Pigments

journal homepage: www.elsevier.com/locate/dyepig

Benzothiazole based fluorescent probes for the detection of biomolecules, physiological conditions, and ions responsible for diseases

Samarpita Das, Harish Kumar Indurthi, Pulkit Asati, Pallavi Saha, Deepak K. Sharma *

Department of Pharmaceutical Eng. and Tech, Indian Institute of Technology-Banaras Hindu University, Varanasi, UP, 221005, India

ARTICLE INFO

Keywords:
Benzothiazole
Fluorescent probes
Cancer
Alzheimer
Genetic disorder
Cardiovascular

ABSTRACT

Benzothiazole-based fluorescent probes are formed by decorating benzothiazole fluorophore with a small chemical fragment capable of detecting a particular biological species or physiological condition. Due to a variety of their photophysical mechanism, like, intramolecular charge transfer (ICT), excited-state intramolecular proton transfer (ESIPT), photoinduced electron transfer (PET), and aggregation-induced emission (AIE), these fluorescent probes selectively interact with various analytes and lead to change in their luminescence features that afford the detection of the analyte. These probes showed advantages of large Stokes shift, high quantum yields, and excellent color transitions. Benzothiazole fluorescent probes can be applied to diagnose various diseases or disorders by monitoring essential biomolecules by imaging cells or intracellular organelles. To date, several benzothiazole-based small molecular probes have been reported. The current review is mainly centered on the recent advances made by these fluorescent probes in the last five years.

1. Introduction

Biological systems are highly dynamic, and the processes that take place inside them are random and rapid. The molecular level of understanding of these fast and complicated cellular processes requires specially designed tools for gaining knowledge about them. For the past several decades, fluorescent probes have gained immense popularity for tracking and monitoring an array of different biological processes such as cellular dynamics, protein expression and localization, enzyme activities, and regulation of signaling cascades [1–4].Therefore, it is an extreme necessity to identify fluorophores that can turn into probes. The primary requirement of any fluorophore to become a probe is to have high sensitivity and excellent selectivity towards a specific target or a specific group of targets (e.g., biothiols, reactive oxygen species, etc.), resulting in a specific fluorescent response. These pre-requisites have urged researchers to synthesize sophisticated fluorescent molecules that can be efficiently applied to the field of bioimaging. For example, utilization of 'switch-on or switch-off' fluorescent probes exhibited fluorescent signals after binding to the target induced either by disruption or initiation of any photophysical event, such as excited-state intramolecular proton transfer (ESIPT) [5], intramolecular charge transfer (ICT) [6], Förster resonance energy transfer (FRET) [7], photo-induced electron transfer (PET) [8]

Benzothiazoles are a popular group of heterocyclic compounds that exhibited various pharmacological activities, such as antibacterial [9], anticancer [10], anti-inflammatory, analgesic antidiabetic, etc. [11] The concrete conjugated structure and excellent photophysical properties such as high quantum yields, elevated molar extinction coefficients, large Stokes shift, and good photostability of benzothiazoles have gained the attention of researchers to construct fluorescent probes and chemosensors [12]. These probes are mainly formed of two units, the benzothiazole moiety as the fluorophore and a small organic recognition unit that remains attached to the benzothiazole ring [Fig. 1(a)]. Due to the presence of a thiazole ring in them, benzothiazole fluorescent probes show excellent coordination ability [13]. Several fluorophoric benzothiazole scaffolds have been identified till date, but the most widely used among them are 2-(2-hydroxyphenyl) benzothiazole (HBT) and thiazole orange (TO) [Fig. 1(b)].

HBT exhibits fluorescence emission at 350–400 nm and 500–550 nm, amongst which emission at 500–550 nm is due to the ESIPT process [5]. Incorporating electron-withdrawing or electron-donating groups in HBT resulted in initiation or hindrance of ESIPT process, which results in ratiometric or "on-off" fluorescence response in the presence of the target under investigation [14]. Over the past couple of decades, TO has also gained considerable attention due to its remarkable 'turn-on' fluorescence response and less background signal. Several TO-based small

* corresponding author
E-mail address: deepak.phe@itbhu.ac.in (D.K. Sharma).

https://doi.org/10.1016/j.dyepig.2021.110074
Received 8 November 2021; Received in revised form 28 December 2021; Accepted 28 December 2021
Available online 31 December 2021

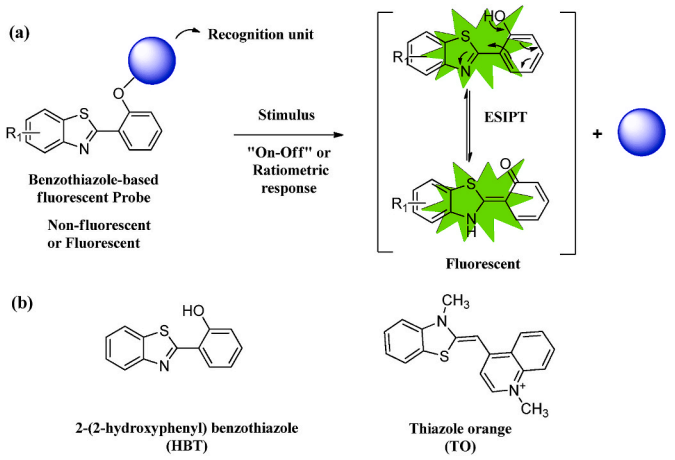

Fig. 1. (a) General mechanism of fluorescence response generated by benzothiazole-based small molecule fluorescent probes; (b) Chemical Structures of some common fluorophoric benzothiazole scaffolds.

molecular probes have been employed to detect various biomolecules and metal ions [1]. With the application of different strategies, they can evolve into a versatile probe for tracking many biomolecules.

In recent years, a significant amount of work has been done on benzothiazole-based molecular fluorescent probes to detect various classes of analytes and biological states. There are several excellent reviews on benzothiazole-based sensing and bioimaging probes [15,16]. However, a systematic review on benzothiazole probes based on their function in disease diagnosis and detection of physiological anomalies has not yet been documented. Herein, we have summarized the literature on benzothiazole probes that have appeared in the last five years and have classified them based on disease detection and abnormal physiology sensing applications. A comparison table is also included herewith to make understanding of application of benzothiazole-based probes easier (depicted in Table 1).

2. Role of benzothiazole based probes in biosensing and bioimaging

2.1. Detection of cancer

2.1.1. Detection of pH for identification of cancer

Intracellular pH (pHi) maintenance is crucial to various pathological and physiological processes such as endocytosis, cell proliferation, mobilization of ions across cell membranes, and resistance against multidrug therapies. Thus, the stability of pH is necessary for the survival of living organisms. Hence, precise determination of the intracellular pH value is of immense importance for the prediction of various human diseases.

Spiropyrans are photochromic ring systems that undergo reversible ring-opening phenomena to form merocyanine upon photochemical irradiation and change in pH of the system from acidic to alkaline. Zhu et al. have synthesized probe **1a**-**1c** by amalgamating benzothiazole with spiropyran to evaluate pH variation. These molecules individually exhibit poor resistance and strong shorter-wavelength emission that are fatal to cells, but when connected by electron-withdrawing, π-conjugated groups, the emission wavelength moves to near-infrared (NIR) regions, which is primarily desired. The π-conjugated groups maintain the spiropyran ring in closed form due to inhibition of ESIPT progress in neutral or basic pH. Once the pH decreased, the ring-opening phenomenon enhances longer-wavelength emission. All three probes demonstrated significant changes in absorption and emission spectra due to protonation under acidic pH and consequent loop opening of spiropyran. Probe **1a** showed an "off-on" response over a wide pH range whereas, probes **1b** and **1c** showed ratiometric responses [Fig. 2(a)]. The pKa values of probes **1a**, **1b**, and **1c** were obtained as 6.57, 4.90, and 3.95, respectively, implicating their suitability for detecting weakly acidic, intermediately acidic, and strong acidic conditions. The probes showed decent water solubility due to quaternization of π conjugated ring. They also exhibited good selectivity in terms of long emission wavelength. When incubated with probe **1b**, HeLa cells exhibited an increase in green fluorescence with a simultaneous disappearance of red fluorescence with the increased pH from 2.02 to 7.30, implying its ability to measure a wide range of pH [Fig. 2(b-c)]. Thus, excellent membrane permeability, staining ability with lesser cellular toxicity, and efficient imaging of pH changes within living cells make these probes, especially probe **1b**, essential for the early diagnosis of pH-associated anomalies [5].

Li et al. synthesized an aggregation-induced probe **2** to detect pH, which is crucial for finding out apoptosis and uncontrolled cell proliferation. Probe **2** exhibited multi-fluorescence emissions in different physical states, (yellow in non-polar solvents and solid state, and blue in protic solvents) pertaining to its tunable ESIPT and restricted intramolecular rotation processes. The variable fluorescent emissions attributed to its keto-enol tautomerism during the ESIPT process [Fig. 3]. The probe responded ratiometrically to pH alterations due to protonation and deprotonation processes that indirectly influenced the photophysical behavior. Moreover, the pH jump from 7 to 8 was very precipitous and well synced with the physiological pH, which makes the probe suitable for keeping track of pH fluctuations in both live cells and neutral water samples. In cell imaging experiment, probe **2** was used to image HeLa cells [17].

Ma et al. synthesized probe **3** for the detection of acidic pH. The fluorescence emission is predominant in the pH 3.44–6.46, with a pKa of 4.23. The more the acidity is, the higher will be the H^+ ion concentration which enhanced the fluorescence emission by inhibition of the PET process [Fig. 4(a)]. Probe **3** exhibits high selectivity towards H^+ ions over other interfering species like metal ions or cations, anions, and other endogenous bioactive molecules observed in the biological systems that might hamper its fluorescence intensity. The fluorescence response of the probe **3** is rapid and takes less than a minute. It was used for bioimaging of HeLa cell lines [Fig. 4(b)]. Due to the presence of acidic vacuoles in lysosomes, probe **3** was used to monitor cellular lysosomal activities [18].

Sun et al. synthesized ratiometric fluorescent probe **4** to track subtle pH changes in living cells over a neutral to acidic range. The probe has three absorption maxima at 292 nm, 365 nm, and 392 nm that greatly varied with pH range. At physiological pH of 7.4, the probe has a fluorescence maximum at 515 nm whose intensity slightly increased in basic pH whereas emission peak red-shifted to 565 nm in acidic environment due to protonation of the benzothiazole nitrogen and subsequent enhancement of the ICT process upon photoexcitation [Fig. 5(a)]. The probe was further utilized for imaging of MCF-7 cells to monitor intracellular pH fluctuations. It was noted that probe **4** penetrate through the cell membrane and not be phagocytized by the nucleus. *In vitro* fluorescence imaging exhibited decrease of green fluorescence with concurrent increase of the red signal with the increase of pH from 5.0 to 8.0, thereby establishing the ratiometric fluorescence response [Fig. 5(b)] [6].

2.1.2. Detection of enzymes for identification of cancer

Carboxylesterases (CEs) are a broad class of enzymes widely distributed in various human tissues, particularly liver and intestine, and associated with pathology of several diseases, such as non-small-cell lung cancer (NSCLC), neuroblastoma, colorectal cancer, etc. where they are specifically upregulated [19–22]. Also, they are employed in the determination of pharmacokinetic and pharmacodynamics profiles of ester drugs or prodrugs. Hence, CEs detection in biological systems is inevitable in diagnosis of diseases and the discovery and development of chemotherapeutic agents. However, owing to their substrate specificity

Table 1
Comparison of photophysical properties and biological assay of benzothiazole-based probes.

Probe	λ_{ex} (nm)	λ_{em}(nm)	Fluorescence type	Detection of biomolecule	Detection limit	Cell imaging	*In vivo* imaging	Ref.
1a	365	640	Turn-on	H^+ concentration	N.R.	HeLa cells	N.R.	[5]
1b		640	Ratiometric					
1c		675	Ratiometric					
2	405	398/484/551	Ratiometric	H^+ concentration	N.R.	HeLa cells	N.R.	[17]
3	360	432	Turn-on	H^+ concentration	0.26 μM	HeLa cells	N.R.	[18]
4	292/365/392	515/565	Ratiometric	H^+ concentration	N.R.	MCF-7	N.R.	[6]
5	325	460	Turn-on	Carboxylesterases (CEs)	4.02×10^{-5} U mL^{-1}	HepG2 cells	Zebrafish and mice	[23]
6	405	569	Ratiometric	Esterase	4.73×10^{-5} U mL^{-1}	MDA-MB-231 cells	N.R.	[24]
7	405	514/650	Ratiometric	Alkaline phosphatase (ALP)	0.072 mU/mL	HeLa cells	N.R.	[28]
8	450	680	Turn-on	Caspase-3	5.1 pg/mL	HeLa cells	N.R.	[29]
9a-9d	500	630–640	Turn-on	Lysosome associated membrane protein-1 (LAMP-1)	N.R.	A549, Huh 7.5, COS-7, HEK293 cells	N.R.	[36]
10a-10d	417	630–650	Turn-on	Lysosome	N.R.	MO3.13 and NHLF cells	N.R.	[37]
11	590	650	Turn-on	Peroxynitrite ($ONOO^-$)	30 nM	HeLa cells	N.R.	[38]
12	397	640	Turn-on	Nitroreductase (NTR)	2.8 ng/mL.	A549 cells	N.R.	[42]
13	332	423/505	Ratiometric	Soluble amyloid-β peptides (Aβ)	390 nM for Aβ-40 monomer	N.R.	N.R.	[44]
14	386–494	471–641	Ratiometric	Aβ-42	N.R.	HeLa cells	N.R.	[45]
15	300	500	Ratiometric	Amyloid fibrils	N.R.	HeLa cells	N.R.	[46]
16	450	654	Turn-on	Aβ-42	N.R.	N.R.	N.R.	[47]
17	526	652	Turn-on	Hydrogen Sulfide (H_2S)	38.3 nM	N.R.	N.R.	[48]
18	350	540	Turn-on	H_2S	41 nM	HeLa cells	N.R.	[49]
19a	550	582	Ratiometric	Bovine serum albumin (BSA)	N.R.	N.R.	N.R.	[50]
19b								
20		601	Turn-on	Cell membrane viscosity	N.R.	HeLa cells	N.R.	[51]
21	411	713	Turn-on	Cysteine (Cys)	102 nM	HeLa cells	Zebrafish and mouse models	[53]
22	470	551	Turn-on	Cys and Homocysteine (Hcy)	12.6 nM (Cys), 20.4 nM (Hcy)	SNU-423 cells	N.R.	[54]
23	413	530	Turn-on	Cys, Glutathione (GSH) and Hcy	0.12 μM	A549 cells	N.R.	[55]
24	315/335	390	Turn-on	Cys	0.32 μM	HeLa cells	N.R.	[56]
25	350	426/665	Ratiometric	GSH	0.35 mM	HeLa cells	N.R.	[57]
26	365	460	Turn-on	Cys	3.78×10^{-8} M	HeLa cells	N.R.	[58]
27	280	482	Turn-on	Cys, GSH and Hcy	2.0×10^{-8} M (Cys), 1.7×10^{-7} M (GSH), and 1.2×10^{-7} M (Hcy)	NCI–H226 cells	N.R.	[59]
28a	365	458/510	Ratiometric	Reactive oxygen species (ROS), hydrogen peroxide (H_2O_2). β-galactosidase activity	N.R.	HeLa cells	N.R.	[61]
28b		508	Turn-on					
29	350/410	540	Turn-on	Hypochlorous acid (HClO)	0.08 μM	HeLa cells	N.R.	[62]
30	433	524	Turn-on	Peroxynitrate ($ONOO^-$)	5.8×10^{-8} M.	HeLa cell	N.R.	[63]
31	415/650/732/820	500–530	Turn-on	H_2O_2	0.11–0.18 μM	N.R.	N.R.	[64]
32	550	548	Turn-on	Superoxide ($O^{2\cdot-}$)	N.R.	RAW 264.7 cells	Zebrafish and lung inflammation induced mice models	[65]
33	408	546/464	Ratiometric	Hypochlorite (OCl^-)	8.9 nM	HeLa cells	N.R.	[66]
36	370–390	530	Ratiometric	DNA	0.90 nM (ssDNA); 3.31 nM (antiparallel G4)	No	N.R.	[69]
37a-d	475	630	Turn-on	G-quadruplex DNA	2.55, 3.08, 5.86 and 8.52 nM for *telo21*	PC3 cells	N.R.	[70]
38	461	495	Turn-on	G4 structure of RNA of hepatitis C virus (HCV)	N.R.	Huh7 cells	N.R.	[71]
39	510	530	Turn-on	Peptide nucleic acids (PNAs)	N.R.	N.R.	N.R.	[72]
40a **and** 40b	557	643 to 850	Turn-on	DNA and RNA	0.084 μg/mL (DNA) and 0.237 μg/mL (RNA)	HeLa cells	N.R.	[73]
41a	425	646/678		DNA and RNA	N.R.	N.R.	N.R.	[74]
41b		645		RNA				
41c		698		RNA				
42	363	550	Turn-on	Nitroxyl (HNO)	0.19 μM	RAW 264.7 cells	N.R.	[77]
43	439	495	Turn-on	Ca^{2+} ions and α-Ketoglutarate	5–50 μmol/L in EtOH (α-KG)	N.R.	N.R.	[78]
44	392	492/552	Ratiometric	Formaldehyde	0.58 μM	MGC-803 cells	Zebrafish models	[81]
45	333/425	462/541	Ratiometric	Formaldehyde	4.1×10^{-4} M	N.R.	N.R.	[82]
46	465	556	Turn-on	Mitochondria	–	HeLa cells	Mice models	[83]
47	481/568	614	Turn-on	Mitochondrial viscosity	–	HeLa cells	N.R.	[84]

(*continued on next page*)

Table 1 (*continued*)

Probe	λ_{ex} (nm)	λ_{em}(nm)	Fluorescence type	Detection of biomolecule	Detection limit	Cell imaging	*In vivo* imaging	Ref.
48	449–479	505	Turn-on	Cu^{2+} ions and inorganic phosphate (PPi),	0.06 μM (Cu^{2+}) and 0.01 μM (PPi)	HeLa cells	N.R.	[85]
49	375	556/446	Ratiometric	Cu^{2+} ions	3.2×10^{-9} M.	HepG2 cells	N.R.	[86]
50	405	475	Turn-on	Cu^{2+} ions	1.34×10^{-6} M	MCF-7 cells	N.R.	[87]
51	380	580/429	Ratiometric	CN^- ions	69 nM	N.R.	N.R.	[88]
52	462	550	Turn-off	CN^- ions	0.11 μM	HeLa cells	N.R.	[89]
53		525	Turn-on	Cd^{2+} ions	0.1 μM	HeLa cells	N.R.	[90]
54	380	527/476	Ratiometric	Al^{3+} ions	99 nM	HSC cells	N.R.	[91]
55	398/446	568/582	Ratiometric	Al^{3+} ions	2.2 μM	HeLa cells	N.R.	[92]
56a and 56b	350/305	460	Turn-on	Zn^{2+} ions	2.53×10^{-6} (50a); 2.55×10^{-6} M (50b)	HEK293 cells	N.R.	[93]
57	445/433	543/475	Ratiometric	Zn^{2+} ions and PPi	60 nM	HeLa cells	N.R.	[94]
58	482	540	Turn-on	Ag^+ ions and Cys	17 nM (Ag^+) and 280 nM (Cys)	N.R.	N.R.	[95]
59	470	530	Turn-on	Hg^{2+} ions	N.R.	N.R.	N.R.	[96]
60	310	377/470	Ratiometric	Hg^{2+} ions	12 nM	TE-1 cells	N.R.	[97]
61	338	465/545	Ratiometric	Hg^{2+} ions	5.8 nM	N.R.	N.R.	[98]
62	411	573/520 and 573/540	Ratiometric	Zn^{2+} and Cd^{2+} ions	0.036 μM	HeLa cells	N.R.	[99]
63	367	450/530	Ratiometric (Hg^{2+}) Turn-off (Cu^{2+})	Hg^{2+} and Cu^{2+} ions	7.6×10^{-9} mol/L	HeLa cells	N.R.	[100]
64	338	422	Turn-off (Cu^{2+}) Turn-on (PO_4^{3-})	Cu^{2+} and PO_4^{3-} ions	2.11 and 31.6 ppb	N.R.	N.R.	[101]
65	410	480	Turn-on	Diethyl cyanophosphonate (DECP)	1.3 nM	N.R.	N.R.	[102]
66	330/450	460/546	Ratiometric	Benzoyl peroxide (BPO)	0.26 μM	A549 cells	N.R.	[103]
67	360	448	Turn-on	Hydrazine (N_2H_4)	N.R.	HeLa cells	N.R.	[104]
68a 68b	345 445	483 464	Turn-on	N_2H_4	0.37 μM 0.49 μM	HeLa cells	N.R.	[105]
69	375/450	445/495	Ratiometric	Phosgene gas ($COCl_2$)	0.14 ppm	N.R.	N.R.	[106]
70	300–450	464 ($NaHSO_3$) 498 (N_2H_4)	Ratiometric	$NaHSO_3$ and N_2H_4	6.3×10^{-7} M ($NaHSO_3$) and 1.7×10^{-5} M (N_2H_4)	N.R.	N.R.	[107]

N.R. = Not Reported.

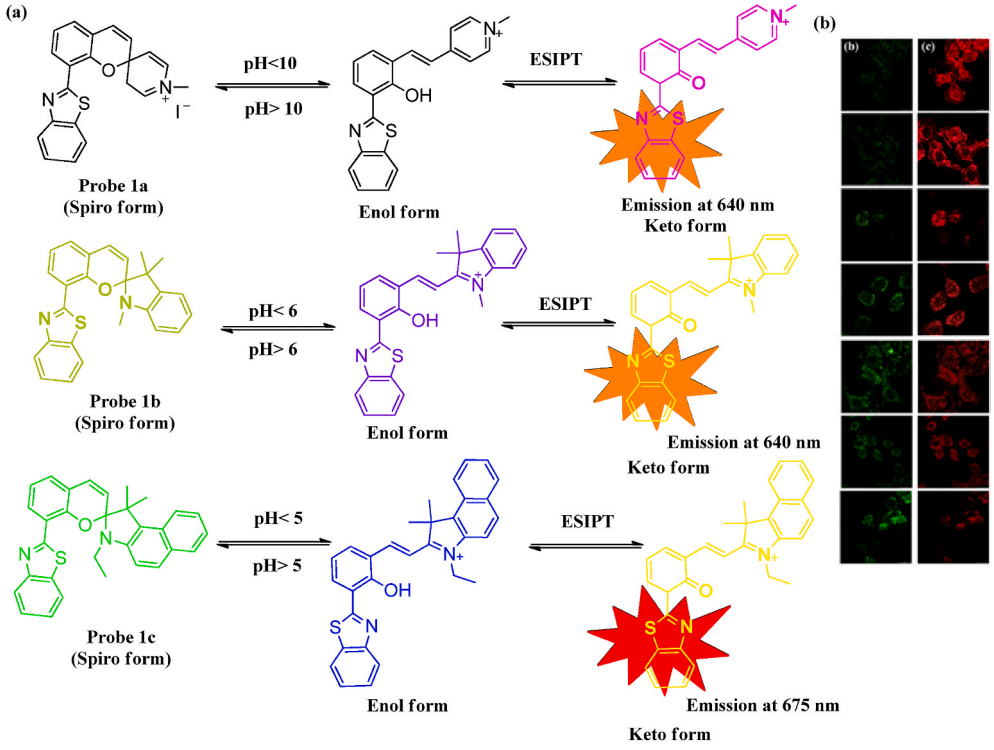

Fig. 2. (a) pH catalyzed ring opening of spiropyran-benzothiazole probes **1a**, **1b** and **1c**; (b) Confocal fluorescence images of HeLa cells incubated with probe **1b** in PBS buffers at various pH ranging from 2.02 to 12 collected at the channel of 475–550 nm and 600–700 nm, respectively. Reprinted (adapted) with permission from Fig. 6 in Ref. [5]. Copyright 2020 Elsevier.

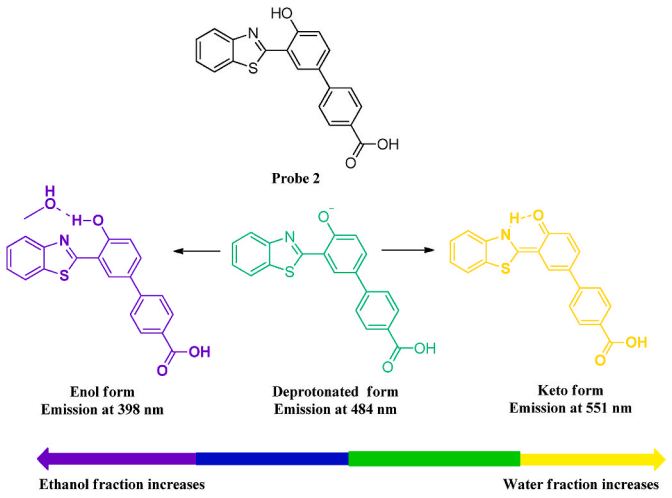

Fig. 3. pH-dependent protonation and deprotonation of probe **2** generating fluorescent response.

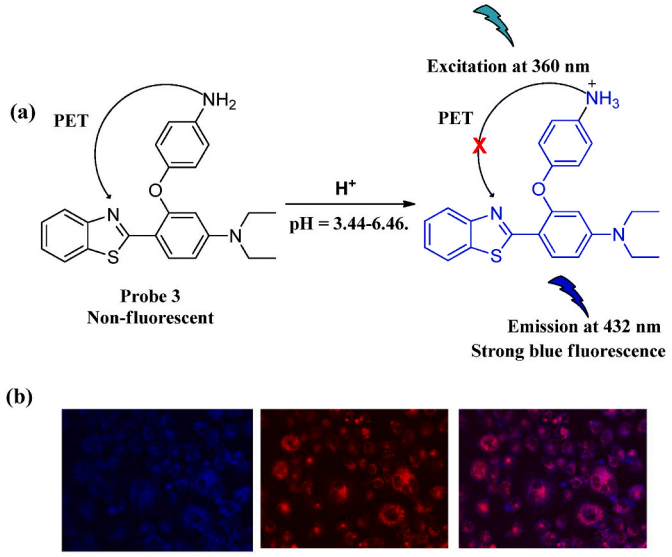

Fig. 4. (a) pH dependent "turn-on" fluorescence response of probe **3**; (b) Fluorescence images of living HeLa cells with probe **3** and LysoTracker Red DND-99. Reprinted (adapted) with permission from Fig. 8 in Ref. [18]. Copyright 2017 Elsevier.

and structural similarities, discrimination of CEs from other hydrolases using available acetyl group-based fluorescent probes becomes pretty challenging. Liu et al. synthesized sterically hindered pivaloyl ester fluorogenic probe **5** complementary to the active site of CE. Probe **5** showed excellent binding affinity to CE and exhibited high specificity, enhanced sensitivity (limit of detection = 4.02×10^{-5} U/mL), and catalytic efficacy. The off-on fluorescence signal generation of the probe has been attributed to the serine-triggered nucleophilic attack due to the proximity of the carbonyl group of probe **5** to the catalytic Ser-1221 residue of the CE active site. The probe absorbed at 325 nm and adequately emitted at 460 nm [Fig. 6(a)]. Greater than 80% cell viability of HepG2 cells and time-dependent enhancement of fluorescence signals of the probe suggested its promising potential as a bioimaging tool for detection of endogenous CEs in complex physiological systems. The *in vivo* bioimaging capacity of probe **5** for endogenous CEs was also observed in zebrafish [Fig. 6(b)] and nude mice models [Fig. 6(c)] [23].

Mao et al. synthesized probe **6** for detecting esterase activity intracellularly as a gradual decrease in the latter is an indicator of the onset of

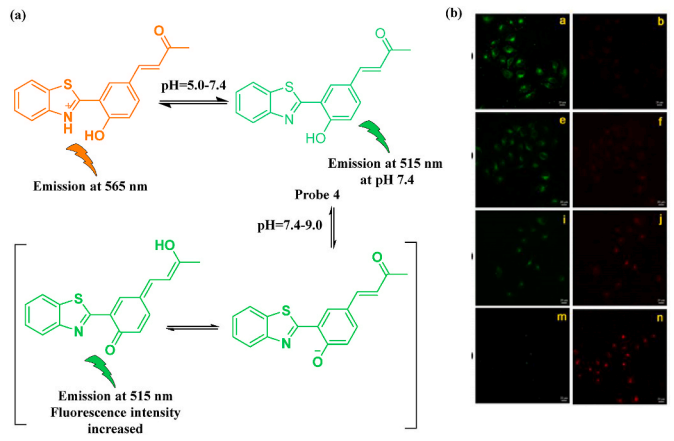

Fig. 5. (a) Detection of subtle pH changes over a neutral to acidic range by probe **4**; (b) Confocal microscopic images of MCF-7 cells incubated with probe **4** and further washed with PBS of various pH values at 8.0 (a–b), 7.0 (e–f), 6.0 (i–j), and 5.0 (m–n). Reprinted (adapted) with permission from Fig. 6 in Ref. [6]. Copyright 2017 Elsevier.

cellular apoptosis. Probe **6** differentiate viable cells from the dead ones and thus finds an inevitable role in pharmacological researches. The free probe emitted weak fluorescence at 410 nm due to electron-withdrawing acetyl group. After addition of esterase to the probe, the resultant mixture emitted a strong fluorescent signal at 569 nm (Fig. 7). The developed probe showed a 70-times enhancement of fluorescence intensity in proximity of esterase enzyme at a concentration of 0.02 U mL^{-1} with an extremely low limit of detection (LOD) i.e., 4.73×10^{-5} U mL^{-1} and high selectivity to esterase. Incubation of probe **6** with MDA-MB-231 living cells exhibit bright fluorescence due to activation by esterase but the intensity is curbed in paraformaldehyde or H_2O_2 pre-treated cells, due to inactivation of intracellular esterase in the presence of such oxidizing agents [24].

Alkaline phosphatase (ALP) is a hydrolytic enzyme involved in the dephosphorylation of phosphorylated proteins, carbohydrates, and nucleic acids [25,26]. Abnormal level of ALP in serum can be an indication of diabetes, bone disease, hepatopathy, prostate cancer, etc. [27] Thus, ALP is important biological marker for diagnosis of above mentioned diseases. In this context, Zhang et al. developed ESIPT-based ratiometric probe **7** based on a phosphorylated HBT derivative for sensing intracellular ALP activity. The free probe is hydrophilic and exhibits green fluorescence due to hindrance of the ESIPT process but upon exposure to ALP, the phosphate ester part of the probe gets hydrolyzed, thereby restoring the ESIPT process. A ratiometric signal is observed by decrease of the fluorescence peak at 514 nm, with concomitant emission at 650 nm [Fig. 8(a)]. The decrease in ratio of fluorescence intensity is linked linearly with the increase of ALP from 0 to 60 mU/mL, with LOD of 0.072 mU/mL. When Hela cells were separately stained with probe and the commercially available Mito Tracker Green, the probe stained the same regions in red as that of the fluorescent green domains of Mito Tracker Green [Fig. 8(b)]. Such selectivity and sensitivity of the probe makes it an excellent candidate for detection of ALP *in vitro* and *in vivo* [28].

Kim et al. reported novel "turn-on" excimer-forming probe **8** for targeting apoptotic protease caspase-3. The hydrophilic probe **8** is formed by the conjugation of the hydrophilic caspase-3 recognition sequence Ac-Asp-Glu-Val-Asp (Ac-DEVD) to the hydrophobic excimer-forming cyanovinylene-NH_2 (CV) unit by means of an amide bond. Upon exposure to the caspase-3 enzyme, the water-soluble DEVD peptide undergoes cleavage and releases the hydrophobic CV-NH_2 residue that gets aggregated in the solution to produce a red-emissive excimer [Fig. 9(a)]. HeLa cells pre-treated with probe **8** and then incubated with caspase-3 in the form of a metal nanoparticle functionalized protein

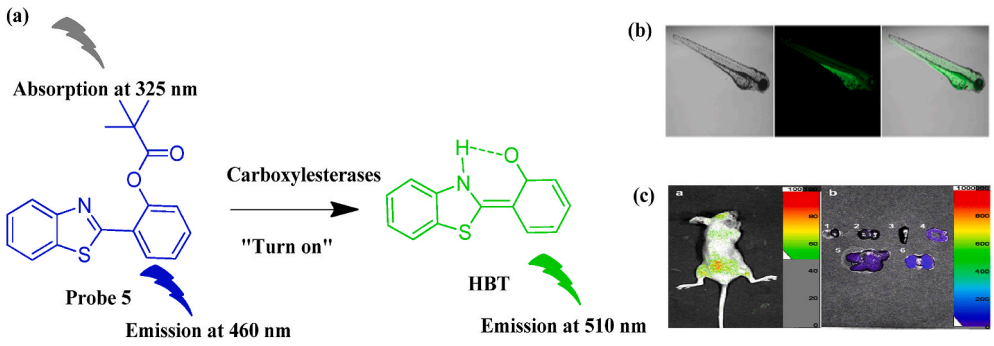

Fig. 6. (a) Ester hydrolysis by carboxylesterase enzyme leads to fluorescent color change of probe **5**; (b) Live imaging fluorescence images of zebrafish treated with probe **5** in DMSO; (c) Live fluorescence image of nude mice intravenously injected with probe **5**. Reprinted (adapted) with permission from Figs. 8 and 9 in Ref. [23]. Copyright 2020 American Chemical Society.

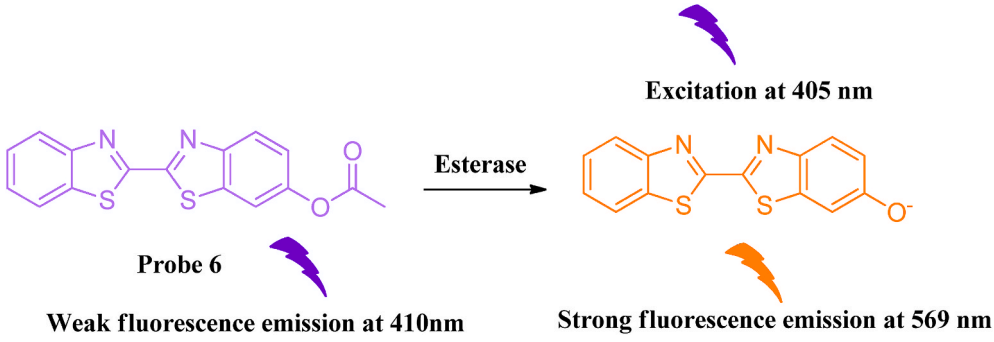

Fig. 7. Esterase catalyzed cleavage of probe **6** generates light emitting free fluorophore.

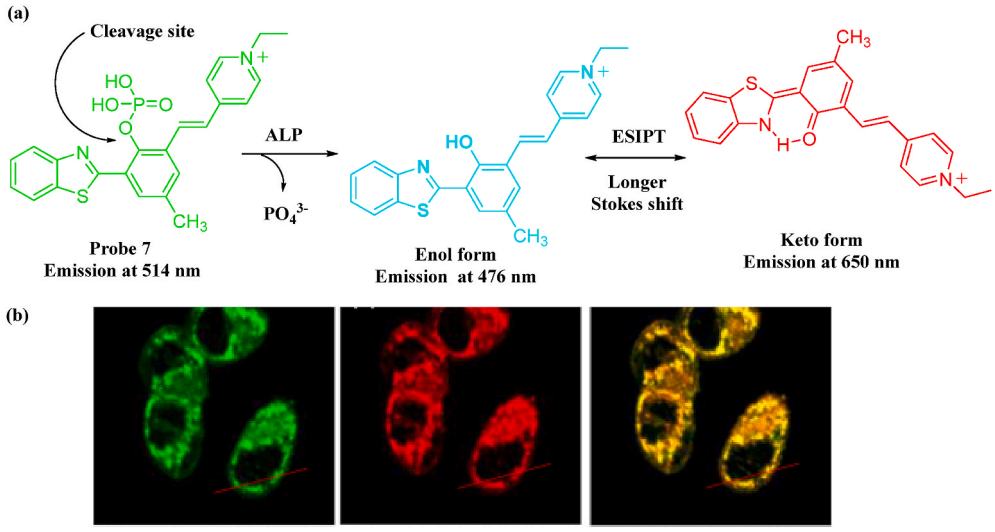

Fig. 8. (a) Proposed mechanism of dephosphorylation of probe **7** by ALP; (b) Fluorescent images of mitochondria localization in HeLa cells co-incubated with Mito Tracker Green and probe **7** (fluorescence emission in green channel, red channel and merged emission). Reprinted (adapted) with permission from Fig. 3 in Ref. [28]. Copyright 2019 American Chemical Society.

complex showed strong fluorescence signal in the red channel (550–690 nm) within the cells. The probe-stained HeLa cells showed no fluorescence in absence of Caspase-3 or presence of a caspase inhibitor, Z-VAD-fmk [Fig. 9(b)]. Probe **8** showed higher Stokes shift and near-infrared emission at 680 nm. The probe also exhibited an outstanding sensitivity with a LOD of 5.1 pg/mL and high selectivity towards caspase-3. Furthermore, cell-permeability and biocompatibility make the probe **8** an attractive tool for the functional study of this class of enzymes, both *in vitro* and *in vivo* [29].

2.1.3. Detection of lysosomal microenvironment for identification of cancer

Lysosomes play an invincible role in several essential cellular processes like endocytosis, autophagy, cellular metabolism, signal transduction, mitosis and homeostasis. Thus, dysfunction of lysosomes can lead to cancer and inflammations [30–35]. Therefore, lysosomal bioimaging are extremely crucial for detection of tumor growth, migration and invasion. For the purpose of visualization and understanding the engulfing mechanism of cellular lysosomes, an array of pyrene-benzothiazolium dye-based probe **9a-9d** were synthesized and

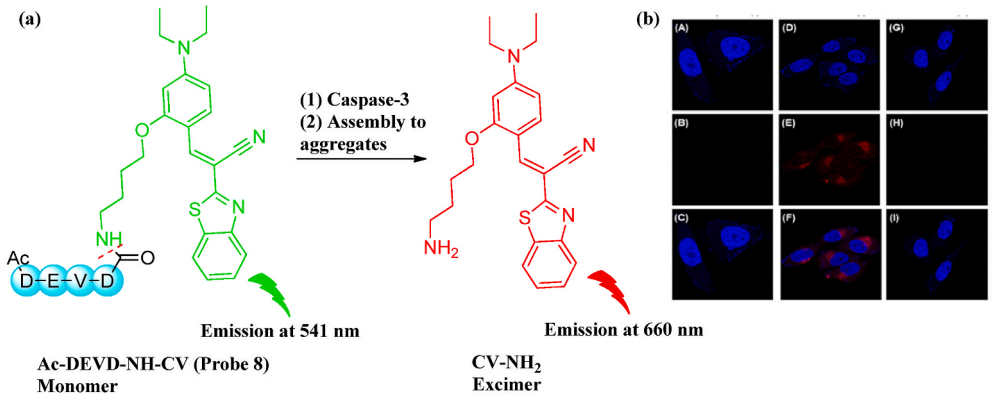

Fig. 9. (a) Caspase-3 activated "turn-on" excimer formation of probe **8**; (b) Confocal microscopic images of HeLa cells incubated with probe **8** and co-stained with DAPI before and after exposure to caspase-3 in the absence or in the presence of Z-VAD-fmk, a caspase-3 inhibitor. Reprinted (adapted) with permission from Fig. 4 in Ref. [29]. Copyright 2017 American Chemical Society.

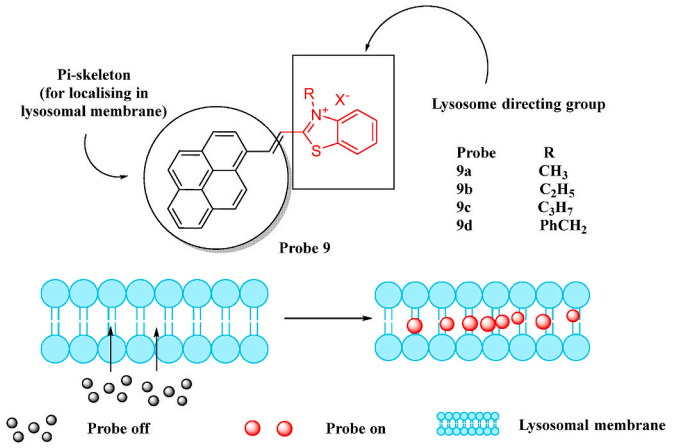

Fig. 10. Detection of engulfing mechanism of lysosomes by probe **9a-9d**.

used as suitable means of bioimaging of living cells. The selectivity of these probes towards lysosomes was further evaluated with respect to expression-dependent visualization of fluorescently marked lysosome associated membrane protein-1 (LAMP-1) in both cancer (A549, Huh 7.5) as well as normal (COS-7, HEK293) cell lines. The dyes **9a-9d** were successfully used as an alternative to LAMP-1 for imaging of lysosome in tumor cell models and exhibited remarkable fluorescence turn-on response at 630–640 nm. The large Stokes' shift of 140 nm can be attributed to the strong ICT process [Fig. 10]. The distinct advantage of these probes is that the emission from them remain unaffected by the solvent polarity due to the rigid chromophore structure. Moreover, the absorbance or emission of the probes remain unaltered in different pH environments (pH = 3–10). These probes helped to eliminate significant background fluorescence resulting from the LAMP-1 expression-dependent methods. The probes enabled long term staining of cellular lysosomes for up to 24 h and their lipophilicity enhanced their accumulation in hydrophobic domains of lysosomes. These probes found to be accumulated mainly in the hydrophobic domains of the lysosomes rather than in their acidic compartments [36].

Abeywickrama et al. generated cyanine (Cy) based fluorescent probes **10a-10d** by amalgamating Cy with HBT. The synthesized probes showed bright red-emission at 630–650 nm owing to attachment of the HBT component [Fig. 11]. They also exhibited a Stokes shift of 130 nm and elevated fluorescence quantum yields of 0.1–0.5. Out of these, probes **10a**, **10b**, and **10d** were efficiently selective for lysosomes in MO3.13 and NHLF cell lines. Lysosome directing property of probes were due to the presence of the phenyl benzothiazolium cyanine **(F)** component [37].

Ren et al. reported the synthesis of a benzothiazole-bearing pyronine fluorescent red-emission dye (probe **11a)** for specific bioimaging of lysosomes. The electron-withdrawing benzothiazole unit of the probe is positioned *meso* to the pyronine scaffold, as a result of which, both absorption and emission wavelengths experienced large red shifts, such as

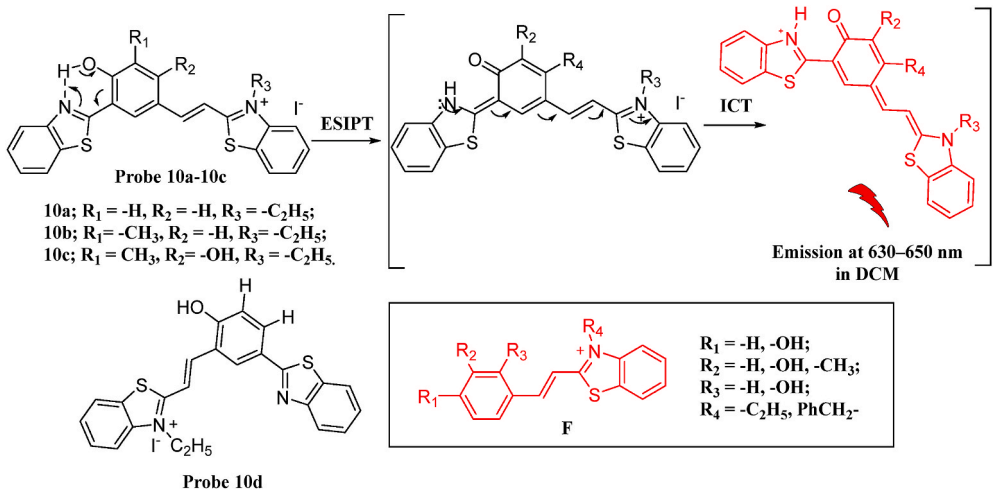

Fig. 11. Lysosome identifying activity of benzothiazole-based probe **10a-10d**.

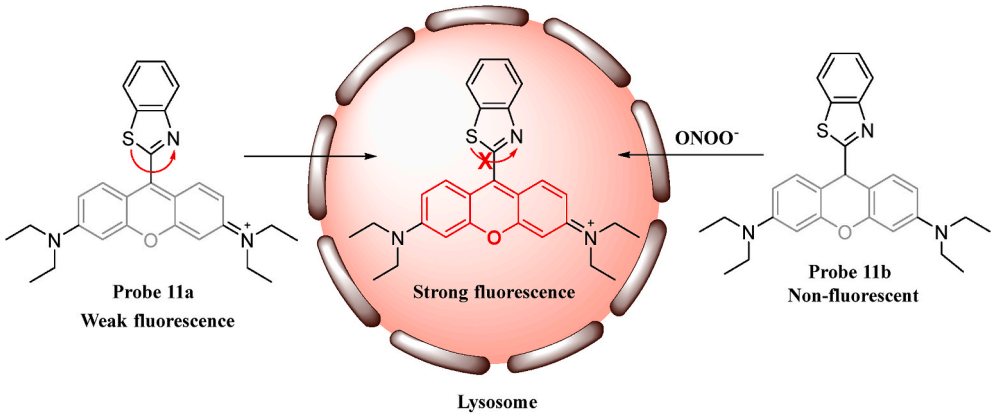

Fig. 12. Bioimaging of lysosomes and specific ROS by probe **11a-11b**.

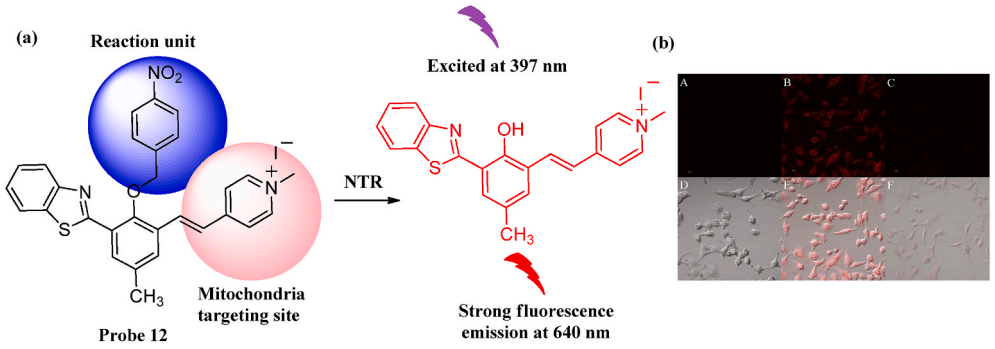

Fig. 13. (a) NTR catalyzed conversion of probe **12** to corresponding fluorophore for hypoxia imaging; (b) Fluorescent and bright-field images of NTR inhibition experiment conducted in A549 cells in absence and presence of probe **12** (A-B and D-E) and also in cells treated with dicoumarol followed by probe **12** (C and F). Reprinted (adapted) with permission from Fig. 6 in Ref. [42]. Copyright 2020 Elsevier.

590 nm and 650 nm, respectively, as compared to that of classic rhodamines which are 550 nm and 570 nm, respectively [Fig. 12]. The probe acts as a fluorescent molecular rotor responding to viscosity changes inside lysosomal micro-environment and can thus be utilized for investigating drug-induced viscosity changes in lysosomes. Ren et al. further explored probe scaffold and came up with a dihydro derivative (probe **11b**) for detecting reactive oxygen species (ROS), which was found to be extremely selective and sensitive for endogenous peroxynitrite ($ONOO^-$) detection with rapid "Off-On" fluorescence response. The LOD was calculated as 30 nM. In bioimaging studies, HeLa cells incubated with probe **11a** showed bright intracellular red fluorescence suggested fair cell membrane permeability and activation of probe by surrounding intracellular microviscosity [38].

2.1.4. *Detection of hypoxia for identification of cancer*

Hypoxia is one of the main reasons behind tumor progression and can lead to upregulation of several reductive enzymes, such as nitroreductases (NTRs), that take part in reduction of nitroaromatic scaffolds to amines or hydroxylamines in the presence of an electron donor, such as reduced nicotinamide adenine dinucleotide (NADH) [39–41]. Thus, detection of NTRs present inside mitochondria leads to accurate detection of hypoxic status of tumor cells. With the vision of developing

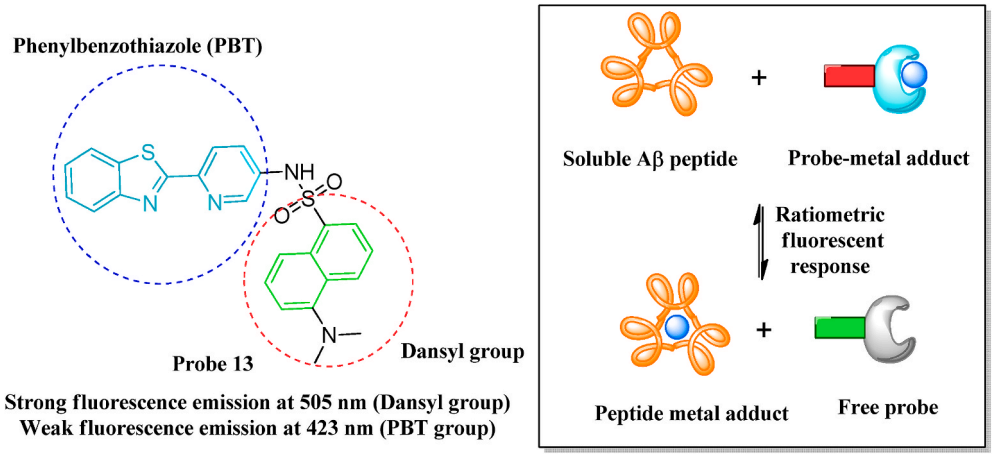

Fig. 14. Fluorescence detection of soluble Aβ proteins by probe **13** for diagnosis of AD.

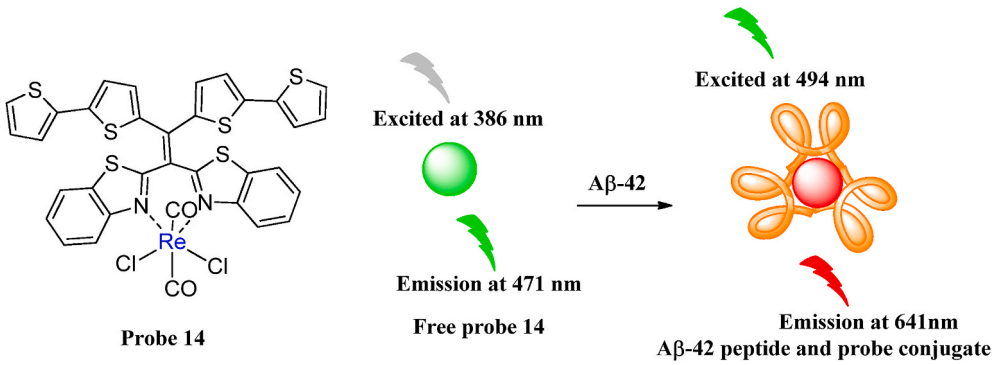

Fig. 15. Detection of Aβ-42 peptide aggregates by probe **14**.

mitochondria-targeting fluorescent probe, Yang and colleagues synthesized an efficient turn-on fluorescence probe **12** to indirectly evaluate the hypoxic condition of tumor cells by detecting their NTR concentrations. When incubated with NTR enzymes, the 4-nitrobenzyl group of the probe **12** underwent reduction reaction and subsequent cleavage, thereby, releasing the fluorescent moiety HBT-Py, which exhibited emission wavelength at 640 nm with a higher Stokes shift of 243 nm due to inherent ESIPT mechanism along with ICT process. [Fig. 13(a)]. The probe displayed a LOD 2.8 ng/mL. Incubation of probe **12** with hypoxic A549 cells displayed a bright red fluorescence signal confirmed the NTR expressed under hypoxic conditions. However, when incubated with a NTR inhibitor, dicoumarol, the probe-loaded cells showed a weak fluorescence indicating specificity of probe **12** towards NTR [Fig. 13(b)] [42].

2.2. Diagnosis of Alzheimer's disease (AD)

2.2.1. Detection of amyloid peptides for identification of AD

Alzheimer's disease (AD) is widely prevalent amongst the elderly population and is mainly associated with development of amyloid plaques inside the brain, consisting of amyloid-β peptides (Aβ). Recent studies, however, have suggested that soluble Aβ are more reliable biomarkers for the early diagnosis of the disease [43]. With the view of detection of soluble Aβ proteins, Li et al. have reported ratiometric fluorescence probe **13** from which soluble Aβ peptides competitively displace the chelated metal ions. Zn^{2+} and Cu^{2+} exhibit high chelation affinity towards Aβ, which induces Aβ nucleation and aggregation. As a result, Aβ forms co-ordinate bonds with metal-bound chelators and regulates their fluorescence intensity. Thus probe **13**, formed by two fluorescing units, the dansyl group and the metal-chelating 2-pyridyl-benzothiazole (PBT) group, is introduced to soluble Aβ, probe-metal adduct undergoes sequestration by the peptides and gives off ratiometric fluorescence response for Zn^{2+} and Cu^{2+} ions [Fig. 14]. This phenomenon occurs due to the lower binding affinity of metal ions to the probe in contrast to that of soluble Aβ. A proper linear curve is obtained for the increasing concentration of soluble Aβ in the presence of Zn^{2+} ions. Titrating assays showed excellent selectivity towards soluble Aβ species and prevented interference by any exogenous agents or the other proteins. This assay can also be used for rapid quantitative detection of soluble Aβ species from biological fluids, like artificial cerebrospinal fluid (ACSF), plasma and serum, and serves as an inexpensive, sensitive and simplified approach for sensing of soluble Aβ species in the early stages of diagnosis for AD [44].

A wide array of photophysical properties exhibited by luminescent transition-metal complexes, based on rhenium [Re(I)], iridium [Ir(III)], and ruthenium [Ru(II)], are well-suited for imaging of small as well as large biomolecules, such as Aβ peptides, which have a crucial role to play in progression of AD. In order to label and image these Aβ peptides fibrillation, Gabr et al. reported fluorescent probe **14** based on bis (benzothiazole) chelated oligothiophene units conjugated with tricarbonyl rhenium complexes of tetraarylethylene (TAE) ligands. The photophysical properties and the Aβ-peptide binding affinities of the formed complexes greatly varied with the number of thiophene rings associated. The complexes displayed red-shifts in both absorption (λ_{abs} = 386–494 nm) and emission wavelengths (λ_{em} = 471–641nm) accompanied by a 34-folds enhancement of luminescence [Fig. 15]. The emission response of the probe was found selective for Aβ-42 fibrils compare to other biomacromolecules, like, calf thymus DNA, human IgG, human serum albumin, pepsin, and casein. The higher binding efficacy and attractive photophysical properties of these complexes pose them as suitable alternatives of thioflavin T as Aβ probes [45].

With a vision to overcome the shortcomings of positively charged Thioflavin-T (ThT) in the tracking of amyloid fibrils, due to lack of permeability through the blood brain barrier, Mora et al. synthesized a ThT-inspired neutral fluorescent probe **15**. The probe in its aqueous solution showed a narrow maximum absorption peak at around 300 nm and a broad maximum emission peak at 500 nm. When introduced to amyloid fibrils, the probe undergoes a large blue-shift in its emission spectrum [Fig. 16] unlike ThT and also a remarkable enhancement in its emission intensity that makes it a suitable candidate for ratiometric sensing of the amyloid fibrils. Molecular docking studies established the binding of the probe in the inner core of the fibrils [46].

Rajasekhar et al. synthesized a novel "turn-on" hemicyanine scaffold based benzothiazole-coumarin probe **16** for the detection of amyloid-β (Aβ-42) that serve as toxic biomarkers of AD. The probe upon binding to Aβ-42 aggregates exhibits emission at 654 nm wavelength with an enhanced red fluorescence (almost 30 folds) and chromogenic change from light red to purple. High selectivity towards Aβ-42 fibrils over other

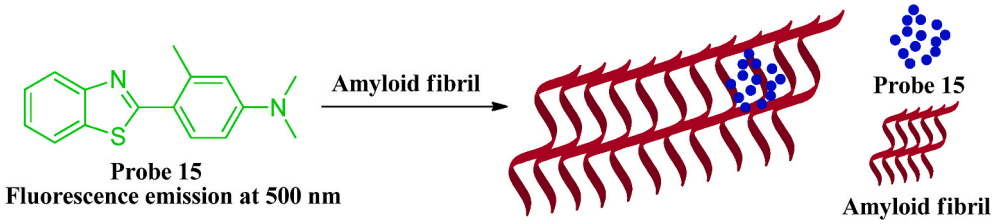

Fig. 16. Fluorescence detection of amyloid fibrils by probe **15**.

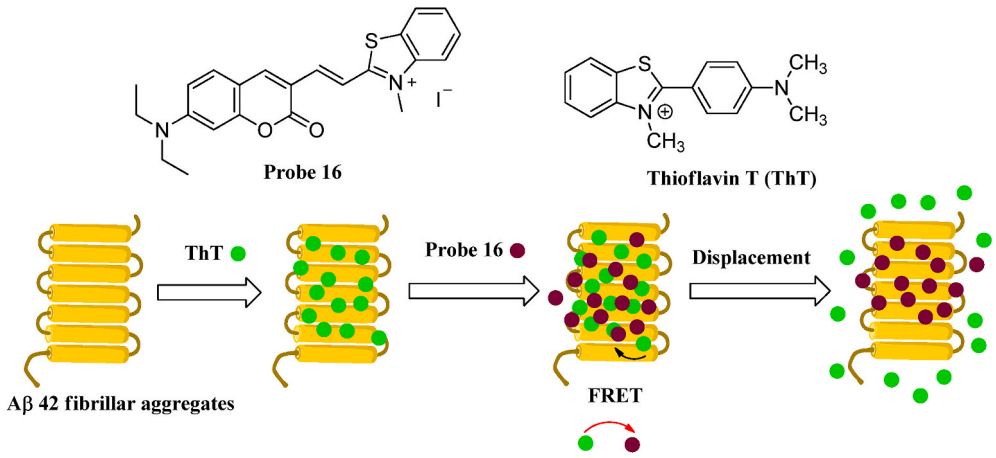

Fig. 17. "Turn-on" detection of Aβ-42 peptides for diagnosis of AD by probe **16** and ThT.

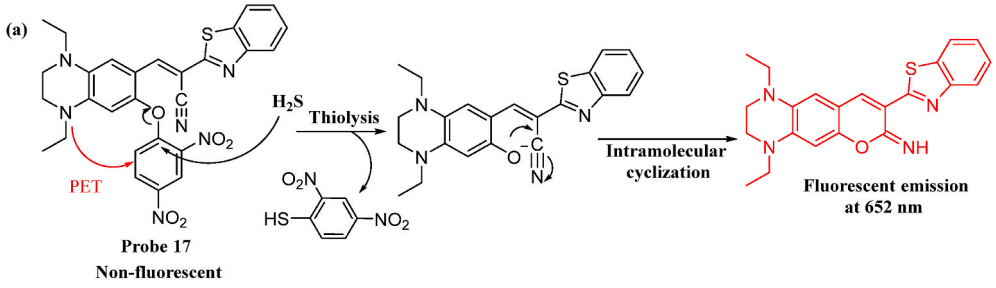

Fig. 18. Hydrogen sulfide catalyzed conversion of probe **17** to corresponding fluorescing species.

unconventional protein aggregates with a nanomolar binding affinity of 1.72×10^7 M^{-1} was observed for this probe. It also displaced ThT from its complex with Aβ-42 fibrils pertaining to high binding affinity of the former [Fig. 17]. The red shift in the absorption spectra and colorimetric optical output of the probe in response to Aβ-42 has been attributed to sudden hydrophilic to hydrophobic micro-environment change. The molecular docking studies carried out on the probe showed the presence of multiple binding sites in the fibril. The binding affinity of the docked probe with Leu, Val, Phe and Gly amino acid residues was found to be the highest in comparison to that of other sites [47].

2.2.2. *Detection of other signaling molecules in AD*

Hydrogen sulfide (H_2S) is an environmental pollutant generated from industrial wastes, and is responsible for occurrence of toxicities in the human body after long term exposure to elevated concentrations. Moreover, H_2S serves as an endogenous signaling molecule, which in high levels in the brain and blood can cause associated diseases, namely, Down's syndrome, hyperglycemia and AD. Zhong et al. synthesized a novel NIR emission fluorescent turn-on probe **17** for detection of H_2S. This probe undergoes HS^- triggered thiolysis followed by cyclization to produce 1,4-diethylpiperazine-modified iminocoumarin-benzothiazole fluorophore which exhibited significant enhancement in the fluorescence intensity. Apart from serving as the reaction site for H_2S, the 2,4-dinitrophenyl (DNP) group in probe **17** exhibited a strong electron-withdrawing effect which resulted in the quenching of the fluorescence intensity of the probe due to a donor-excited PET process [Fig. 18]. There are several advantages of using this probe for H_2S detection, such as, fluorescent "turn-on" response, NIR emission at 652 nm, large Stokes shift of 126 nm, almost 200-folds elevated signal-to-noise ratio, effective detection of H_2S. The LOD was found 38.3 nM in PBS. The probe was used for determining the purity of red wine and natural waters [48].

Chen et al. formulated a "turn-on" fluorescent probe **18** for the

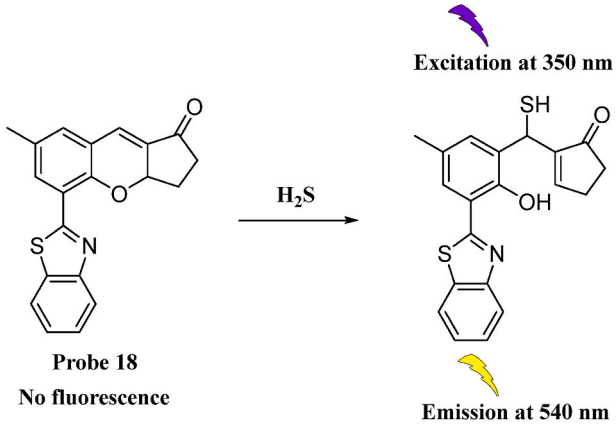

Fig. 19. Turn-on fluorescence response of probe **18** in presence of hydrogen sulfide.

detection of H_2S. The probe design is based on a ESIPT based fluorophore, HBT, with AIE characteristics. The free probe does not exhibit fluorescence due to obstruction of the ESIPT process by the phenol hydroxyl group in vicinity of the lactone moiety. Upon addition of H_2S, the probe **18** undergoes cleavage of the heterocyclic ring in the middle giving a strong "turn-on" fluorescence signal at 540 nm, with a simultaneous raise in the absorption band at 350 nm [Fig. 19]. H_2S induces a drastic fluorescence enhancement of nearly 80-folds when the amount of H_2S reaches greater than 25 μM. The detection limit of **18** for H_2S was determined as 41 nM. The probe provides benefits of pH independency over a range of 6–10, high selectivity over other biologically interfering species, such as GSH, Hcy, etc., and excellent sensitivity. Furthermore, probe **18** was also applied to detection of H_2S in HeLa cells. The

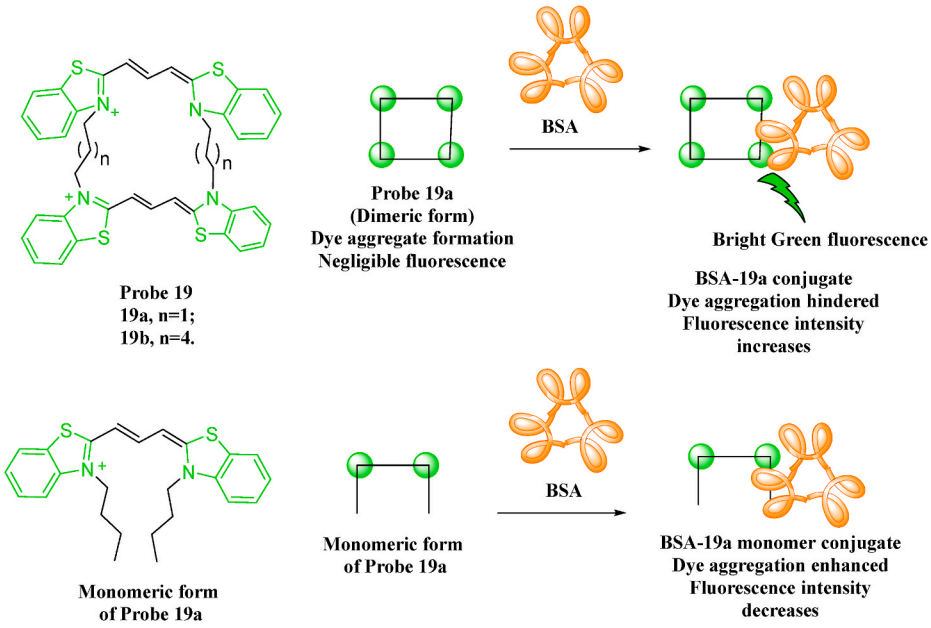

Fig. 20. Detection of BSA by probes **19a** and **19b**.

microscopic images of the probe incubated HeLa cells showed no fluorescence but upon addition of H_2S, the images showed notable increase in fluorescence intensities in living cells [49].

The aggregates of bovine serum albumin (BSA) produced by thermal pathways exhibit amyloid-like properties; thus, their nature of aggregation can extrapolate to the understanding of aggregation of amyloid proteins in neurodegenerative diseases like AD. In their work, Patlolla et al. synthesized two dimeric carbocyanine dyes (probes **19a** and **19b**) for detection and estimation of BSA. The dyes formed H-dimers and H-aggregates in their aqueous solutions. When the dye **19a** was introduced to BSA, its dimeric form bound to the latter with a high binding affinity ($K_a = 1.49 \times 10^5\ M^{-1}$). Fluorescence intensities of the dimeric dyes enhanced proportionally with time upon interaction with BSA and was found to be better than that of ThT [Fig. 20]. Further addition of surfactant SDS to the dimeric dye resulted in a 200-fold increase in the fluorescence intensities in presence of BSA. Protein aggregation conditions were found to promote the dye binding process and leads to fluorescence intensity enhancement upon interaction between the dimeric dye and BSA. Fluorescence microscopy images of **19a** revealed fibrillar character of aggregated BSA within half an hour of incubation and the bright green fluorescence of the dye was collectively increased after 24 h of incubation due to disaggregation of **19a** in presence of BSA. These self-aggregating dimeric dyes demonstrate a promising approach for non-covalent labeling applications in serum protein identification [50].

2.2.3. *Detection of cell membrane viscosity in AD*

Alteration of membrane viscosity has been closely associated with diseases involving carrier mediated transport and receptor binding, such as, diabetes, cancer and AD. Hence, its detection is of great significance for understanding the intricate biological processes related to viable cell function and its subsequent death. Wang et al. synthesized a viscosity susceptible cell membrane fluorescent dye **20** by linking *N, N*-diethylaminobenzaldehyde with a benzothiazole to sense changes in viscosity of the phospholipid bilayer. The dye **20** undergoes free rotation around the double bond between the phenyl and the benzothiazole rings. Due to this twisting around double bond, the ICT state led to quenching of the fluorescence emission of this hemicyanine dye. As soon as the solution viscosity increased, it limited the excited state rotation around the double bond, thus, preventing occurrence of twisted ICT with the gradual enhancement of fluorescence. The dye **20** exhibited a turn-on fluorescent response at 601 nm in response to increase of viscosity from 0.89 to 865 cp [Fig. 21], with a linear relationship. The dye was specific for response towards viscosity changes with a molar extinction coefficient ranging between 3.34×10^4–$2.64 \times 10^5\ M^{-1}\ cm^{-1}$ and decent photostability. The low cytotoxicity of **20** makes it applicable for live cell imaging and has been successfully applied to study of viscosity changes in cell membranes of HeLa cell lines [51].

2.3. *Detection of oxidative stress for the early diagnosis of cancer, AD and other neurodegenerative disorders*

Oxidative stress may be described as a disbalance between the

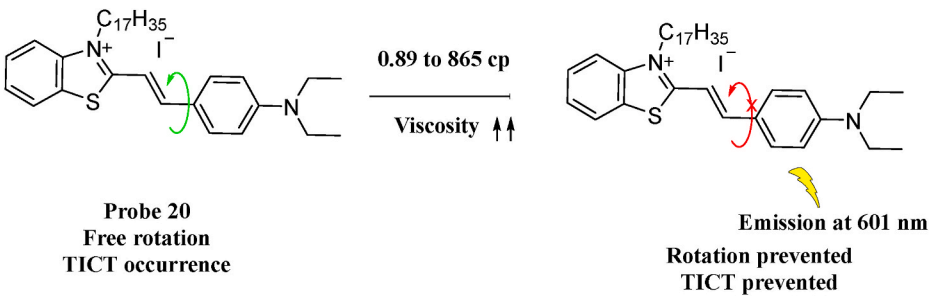

Fig. 21. Viscosity dependent fluorescence response of dye **20**.

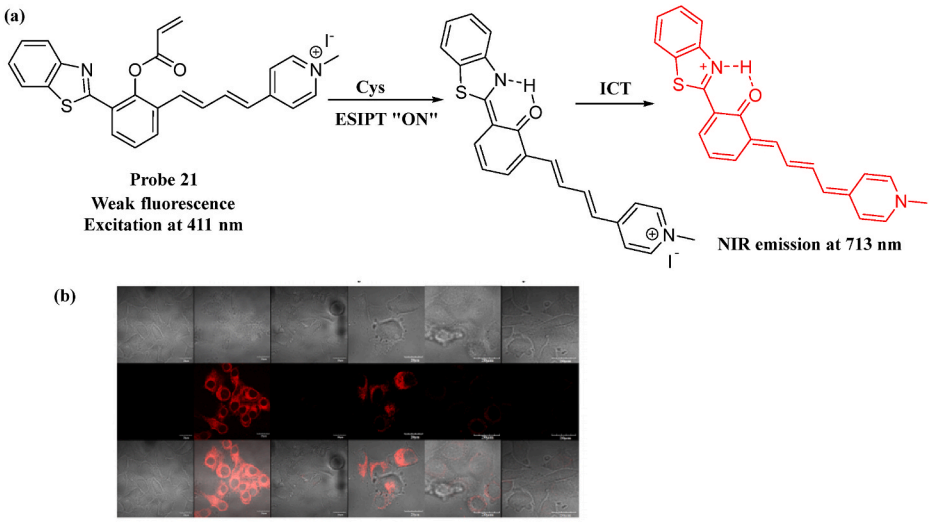

Fig. 22. (a) Selective determination of Cys by probe **21**; (b) Confocal fluorescence and bright-field images of HeLa cells only stained with probe **21**; cells pretreated with thiol trapping agent and stained with probe **21**; and thiol trapper pre-treated cells treated with Cys, GSH, or Hcy, and stained with probe. Reprinted (adapted) with permission from Fig. 4 in Ref. [53]. Copyright 2020 American Chemical Society.

production of ROS (free radicals) and antioxidants, which leads to tissue damage. ROS are unstable and highly reactive species interacting locally to exchange electrons with other molecules to become stable. The free radicals react with biological macromolecules, such as, lipids, proteins, nucleic acids, carbohydrates, etc. to produce a free radical chain reactions which lead to grave consequences like lipid peroxidation, protein or DNA damage, fragmentation. These further lead to cancer, AD, diabetic vascular damage and other neurodegenerative disorders. Hence, detection of oxidative stress at a tissue level is of immense importance for diagnosis of some fatal disorders [52].

2.3.1. *Detection of biothiols for measurement of intracellular oxidative stress*

Cysteine (Cys) is a precursor of the intracellular biothiol, Glutathione (GSH), and plays a crucial role in homeostasis and preventing intracellular oxidative stress. Thus, the development of efficient techniques for the detection of Cys is of utmost importance. Long et al. synthesized a NIR two-photon fluorescent probe 21 for determination of Cys from the conjugation of HBT derivative as a fluorescing unit, acrylate as the cysteine trapper, and an *N*-methylpyridinium ion as the organelle targeting and water-soluble unit and was achieved by a specific conjugate addition-cyclization reaction between acrylate and Cys. The probe exhibited an "off-on" fluorescent signal generation (emission at NIR of 713 nm) with a significantly large Stokes shift of 302 nm in contact with Cys. The butadienyl *N*-methylpyridinium moiety in probe **21** extend the π-conjugation system of HBT enabling the ESIPT phenomenon. Besides this, a push-pull effect due to the presence of the electron-donating phenolic OH and the electron-withdrawing *N*-methylpyridinium in the probe led to the ICT effect. High selectivity and sensitivity of the probe for detection of Cys over Homocysteine (Hcy), GSH, and hydrogen sulfide was observed [Fig. 22(a)]. Moreover, high quantum yields and strong red fluorescence with a sizeable two-photon action cross-section of released fluorophore of the probe are highly desirable for bioimaging of living samples. When living HeLa cells stained with probe **21** were

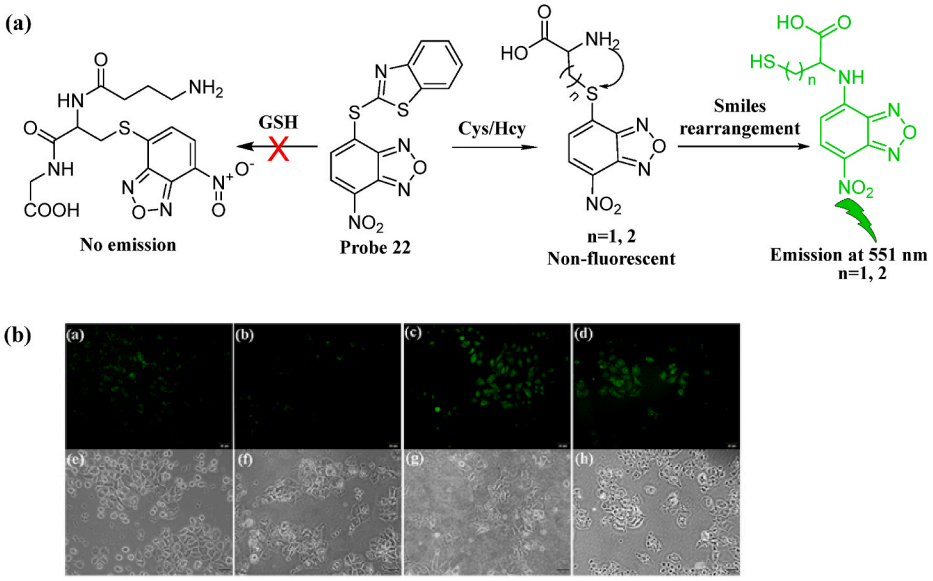

Fig. 23. (a) Selective detection of Cys and Hcy by probe **22**; (b) Fluorescence and bright field images of living SNU-423 cells incubated with probe **22** (a and e), SNU-423 cells incubated with biothiols trapper followed by probe **22** (b and f), SNU-423 cells treated with biothiols trapper, probe and Cys (c and g), SNU-423 cells treated with biothiols trapper, probe and Hcy (d and h). Reprinted (adapted) with permission from Fig. 6 in Ref. [54]. Copyright 2019 Elsevier.

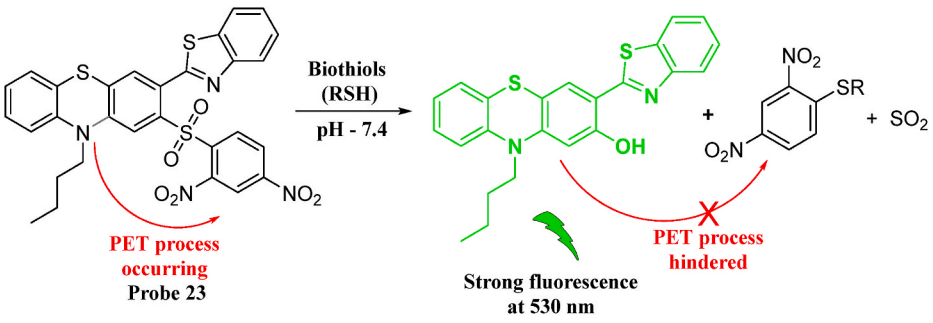

Fig. 24. Detection of biothiols like Cys, Hcy and GSH by probe **23**.

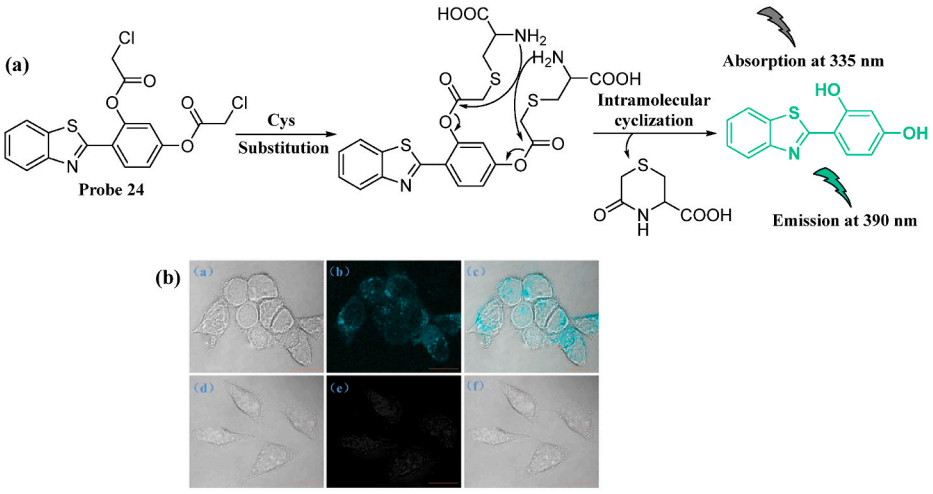

Fig. 25. (a) Selective estimation of Cysteine by probe **24**; (b) Confocal microscopic images (bright field, fluorescence and merged images) of HeLa cells incubated with probe **24** with and without treatment of a biothiols trapping agent, NEM. Reprinted (adapted) with permission from Fig. 4 in Ref. [56]. Copyright 2018 Elsevier.

excited with a two-photon near-infrared light at 820 nm, the cells exhibited bright red fluorescence, but in the presence of a thiol-trapping reagent, NEM, the bright signal was significantly inhibited, implying monitoring of endogenous Cys by the probe. [Fig. 22(b)]. The probe successfully demonstrated its application in imaging Cys in viable cells, zebrafish, and mouse models [53].

Li et al. developed probe 22 to detect Cys and Hcy. The detection of biothiols by the probe was aided by forming a yellow-green fluorescent amino-nitrobenzoxadiazole from a Cys/Hcy-activated nucleophilic substitution reaction of benzothiazole thioether, followed by Smiles rearrangement. Compared to glutathione, the probe showed higher selectivity towards Cys/Hcy with strong fluorescence emissions at 551 nm, whereas no fluorescent signal was obtained for other amino acids [Fig. 23(a)]. Probe **22** detection limit for Cys and Hcy was determined as 12.6 nM and 20.4 nM, respectively. The probe can thus be easily exploited for sensing intracellular Cys/Hcy in living cells due to their reduced toxicity, low limit of detection, cheaper cost, higher sensitivity, and simple mechanism. Probe **22** also finds application in examining exogenously and endogenously produced Cys/Hcy in SNU-423 cells [Fig. 23(b)] [54].

Ma et al. reported the design and development of a new fluorescent probe 23 that emits green light in the presence of Cys, Hcy, and GSH, which participate in several nucleophilic and redox reactions in both prokaryotes as well as eukaryotes. The probe comprises a 2,4-dinitrobenzenesulfonate moiety (DNBS) as the detection unit, which undergoes cleavage in the presence of biothiols and thus, acts as a selective reaction switch for biothiols. The sensing mechanism is owing to the biothiol-induced scission of the DNBS group, resulting in subsequent inhibition of the PET process of the probe [Fig. 24]. The probe sensitivity towards Cys could be confirmed by a gradual elevation of the fluorescent intensity at 530 nm with a concurrent increase of the Cys concentration. The probe also showed favorable properties of high selectivity, a significant "turn-on" fluorescence signal, a better sensitivity with LOD of 0.12 μM, and an elevated Stokes shift of 117 nm. Moreover, the probe's membrane-permeability and visualization of biothiols could be confirmed by confocal fluorescence imaging in viable A549 lung adenocarcinoma cell lines [55].

Yu et al. reported a turn-on fluorescent probe 24 to detect amino acid Cys. The probe contained the ESIPT fluorophore, HBT, and two chloroacetate groups decorated on the fluorophore that served as reaction points for Cys. The free probe absorbs maximally at 315 nm, but the absorption peak shifts to 335 nm after incubation of Cys [Fig. 25(a)]. The isobestic point was observed at around 325 nm. It exhibited enhanced fluorescence intensity for Cys at 390 nm. Fluorescence emission spectra were screened, and it was observed that only Cys triggered a significant rise in the fluorescence intensity, whereas the other ions and amino acids failed to achieve apparent fluorescence enhancement. Though the fluorescent intensity enhancement caused by Hcy was quite significant, nothing compared to that of Cys. Probe **24** was successfully applied for bioimaging intracellular Cys in viable HeLa cells without any risk of cytotoxicity [Fig. 25(b)] [56].

GSH is involved in the maintenance of intracellular signal transduction, redox homeostasis, and gene regulation. Zhou et al. synthesized a NIR ratiometric probe 25. The acetyl group in probe **25** serves as a recognition site for GSH and triggers the ICT process [Fig. 26]. The free probe in its aqueous solution exhibited strong emission at 426 nm with a simultaneous weak NIR fluorescence at 665 nm, but upon exposure to GSH, the short fluorescence emission gradually decreased, and the NIR fluorescence emission significantly improved. The LOD for probe **25** was calculated as low as 0.35 mM. Furthermore, probe **25** was effectively

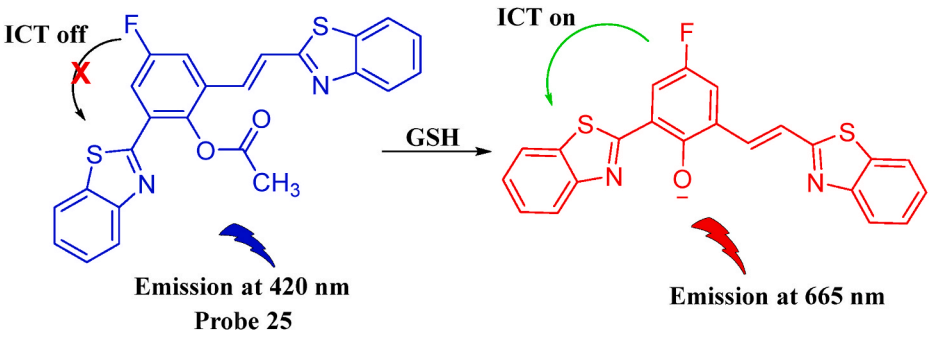

Fig. 26. Selective detection of Glutathione for maintenance of homeostasis by probe **25**.

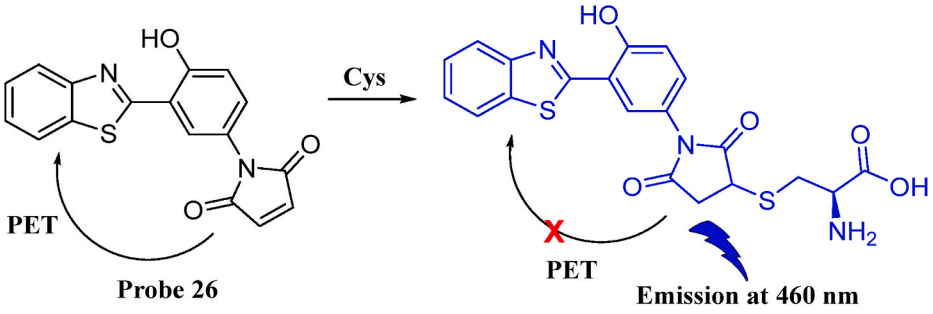

Fig. 27. Proposed mechanism of detection of Cys, Hcy and GSH by probe **26**.

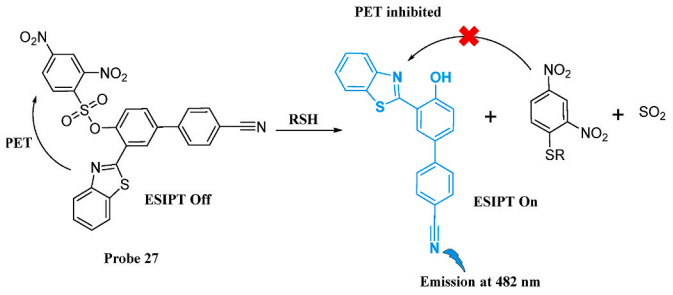

Fig. 28. Mechanism of detection of biothiols by probe **27**.

used for bioimaging of GSH in viable HeLa cells [57].

Zhao et al. fabricated a probe 26 by combining HBT, an ESIPT fluorophore, with a maleimide group to detect Cys, Hcy, and GSH. The maleimide unit strongly quenches the emissivity of the free probe via the process of PET, but upon exposure to any of the biothiols, the extended π-conjugation of the probe is disrupted, and the fluorescence is restored, owing to the ESIPT process [Fig. 27]. The probe exhibited a large Stokes shift (90 nm), a rapid response time (30 s), and an elevated signal-to-noise ratio (23-folds) along with the perks of excellent selectivity and sensitivity to thiols with a LOD as low as 3.78×10^{-8} M. In cell imaging study, living HeLa cells showed strong blue fluorescence in the presence of probe **26** and Cys. A quenching of the fluorescent signal was also confirmed by incubating the probe-treated cells with Cys and a biothiol

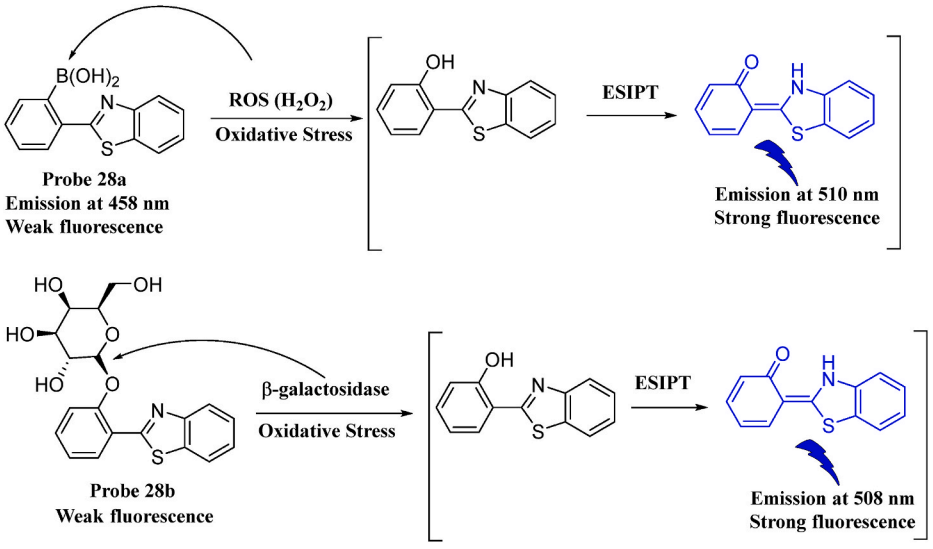

Fig. 29. Fluorescence detection of ROS and β-galactosidase hyperactivity by probes **28a** and **28b** for determination of oxidative stress associated with stress-induced premature senescence.

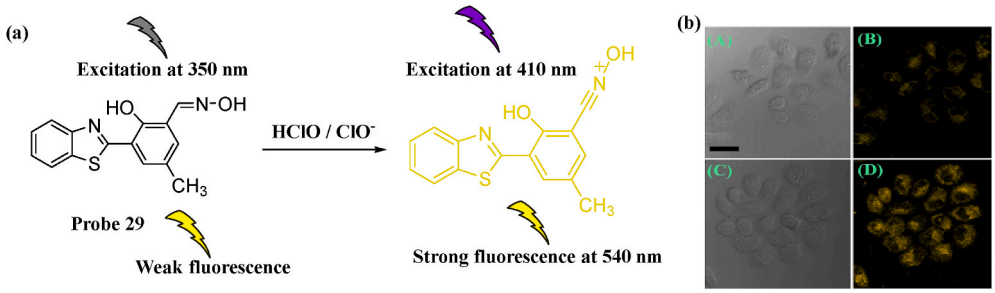

Fig. 30. (a) Detection of endogenous hypochlorous acid by probe **29**; (b) Fluorescence and bright-field images of live HeLa cells incubated with probe **29**. Reprinted (adapted) with permission from Fig. 4 in Ref. [62]. Copyright 2018 Elsevier.

trapper, indicating specificity and selectivity of the probe towards Cys [58].

Chen et al. reported synthesizing an ESIPT-based fluorescent probe 27 to detect biothiols using DNBS as the sensing unit. The DNBS moiety serves as the electron acceptor that quenches the benzothiazole fluorescent intensity due to the occurrence of PET and corresponding hindrance of the ESIPT process. Upon being introduced to biothiols, the probe undergoes conversion to 4′-hydroxy-3'-(benzothiazol-2-yl)-4-biphenylcarbonitrile and exhibits emission at 482 nm pertaining to the ESIPT process [Fig. 28]. Probe **27** exhibits a large Stokes shift (202 nm) and high sensitivity to biothiols with LOD of 2.0×10^{-8} M, 1.7×10^{-7} M, and 1.2×10^{-7} M for Cys, GSH, and Hcy, respectively. Probe **27** was efficiently applied to the bioimaging of thiols in living NCI–H226 cells [59].

2.3.2. *Detection of reactive oxygen species for determination of oxidative stress determination*

Reactive oxygen species (ROS) are metabolic byproducts generated by living cells as a part of their daily metabolic processes. When overtly stressed, the cells produce excessive ROS that triggers the living organisms to evolve response mechanisms to adapt to the stress and utilize them as signaling molecules. Excessive production of ROS leads to the destruction of cell organelles and biomolecules, which causes an inflammatory response that accounts for the development of diabetes and cancer [60].

Makau et al. developed HBT-based fluorescent probes for monitoring of oxidative stress and β-galactosidase activity inside tumor cells. Probe 28a detect ROS, H_2O_2 and 28b evaluate the enzymatic profile of β-galactosidase [Fig. 29]. These probes were assessed for ratiometric imaging of intercellularly accumulated H_2O_2 and the degree of β-galactosidase activity in HeLa cells with or without treatment of H_2O_2. It was observed that fluorescence intensity was directly proportional to the H_2O_2 concentration and was enhanced by nearly 3.5 times in H_2O_2-treated cells. Furthermore, **28b** was successfully used to image elevated levels of β-galactosidase activity in the doxorubicin-treated population of HeLa cells which showed bright fluorescence in the blue channel with contrast to the Doxorubicin-untreated cells [61].

Nguyen et al. fabricated a "turn-on" fluorescent probe 29 to detect hypochlorous acid generated by the intracellular reaction of chloride ion (Cl^-) with H_2O_2 and acts as a ROS, indirectly affecting various physiological processes. The probe comprises HBT and hydroxylamine as the ESIPT fluorophore and recognition units, respectively. The detection mechanism attributed to specific oxidation of oxime unit to nitrile group by HClO and subsequent generation of a highly emissive derivative showing yellow fluorescence at a wavelength 540 nm [Fig. 30(a)]. The probe displays a large Stokes shift of 190 nm and a rapid fluorescence response for HClO at 540 nm. Furthermore, bioimaging studies on live HeLa cell lines showed cell permeability of the probe with emission of bright yellow fluorescence [Fig. 30(b)] and thus, paved the way for its application to HClO detection in living cells [62].

Shen et al. formulated a fluorescent probe 30 to detect peroxynitrite using the ESIPT process. Upon exposure to peroxynitrite, the probe underwent oxidative deprotection or cleavage of the pyridine hydrazone moiety that led to a strong fluorescence emission (40-fold enhancement) at 524 nm [Fig. 31] with LOD of 5.8×10^{-8} M. The probe exhibited a rapid fluorescence response towards $ONOO^-$ within a period of 60 s. The probe was also successfully used for live HeLa cell imaging [63].

Wang et al. formulated probe 31 for detecting H_2O_2 in water samples collected from various sources. The principle of this method is based on the oxidative coloration of the probe via Fenton reaction, resulting in a green radical [Fig. 32] exhibiting absorbance at 415 nm, 650 nm, 732 nm, and 820 nm, which were directly proportional to H_2O_2 concentrations over a range of 0–40 μM and the sensitivities of the proposed method at the four wavelengths were determined as 4.19×10^4 M^{-1} cm^{-1}, 1.73×10^4 M^{-1} cm^{-1}, 2.18×10^4 M^{-1} cm^{-1}, and 1.96×10^4 M^{-1} cm^{-1}, respectively. The LOD of probe **31** at the above-mentioned wavelengths were respectively found to be 0.18 μM, 0.12 μM, 0.10 μM, and 0.11 μM. The absorbance of the formed radical was found to be quite stable in ultrapure, underground, and reservoir water samples for nearly 30 min. Furthermore, this probe can also be utilized to detect H_2O_2 variations during the oxidative decolorization of rhodamine B in an alkali-activated H_2O_2 system [64].

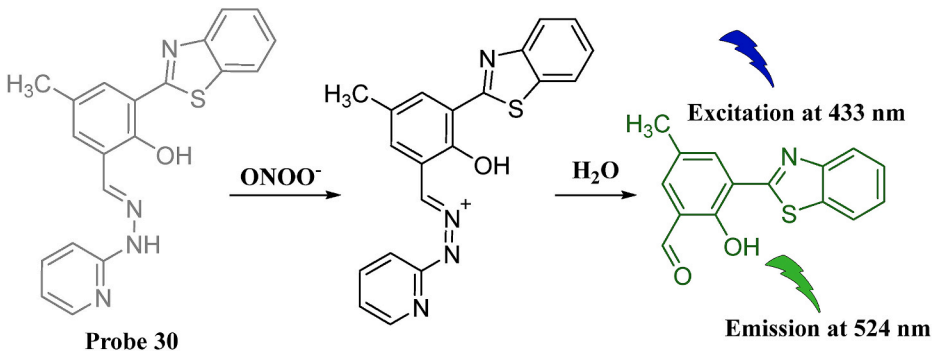

Fig. 31. Detection of endogenously produced peroxynitrite by probe **30**.

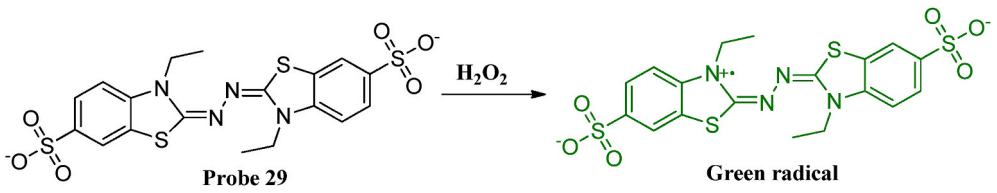

Fig. 32. Fluorescent response of probe **31** in presence of hydrogen peroxide.

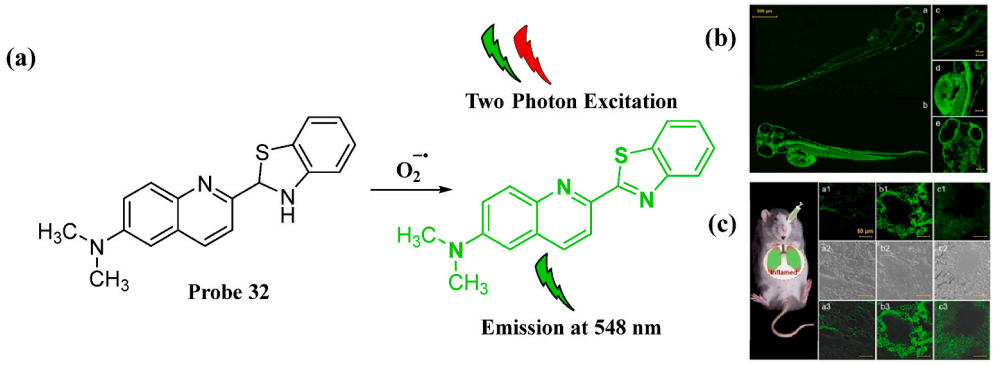

Fig. 33. (a) "Turn-on" response of probe **32** in presence of superoxide ions; (b) Two Photon fluorescence images of probe **32** in zebrafish. Reprinted (adapted) with permission from Fig. 4 in Ref. [65]. Copyright 2016 Elsevier; (c) Two Photon fluorescence images of $O_2^{\bullet -}$ level by using probe **32** in inflammatory lungs slice of mice. Reprinted (adapted) with permission from Fig. 5 in Ref. [65]. Copyright 2016 Elsevier.

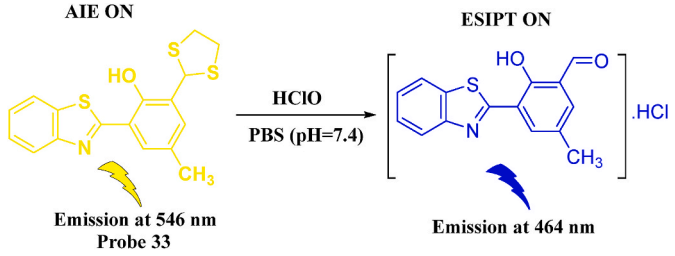

Fig. 34. Proposed mechanism of ratiometric fluorescence response of probe **33** in presence of hypochlorous acid.

Li et al. reported the synthesis of a quinoline-based two-photon fluorescent probe 32 for tracing superoxide ($O^{2\cdot-}$) ions in living organisms to monitor oxidative stress conditions or lack of homeostasis in them. The probe exhibited a specific "turn-on" green fluorescence response at 548 nm due to extension of the π-conjugation system and moderate ICT process [Fig. 33(a)]. Furthermore, low cytotoxicity and greater biocompatibility towards viable RAW 264.7 cells and organisms like zebrafish and lung inflammation induced mice models [Fig. 33(b and c)] establishes this probe as suitable trackers of endogenous superoxide in living cells and *in vivo* [65].

Hypochlorite (OCl^-), a chemical substance commonly used as a bleaching agent and in the treatment of industrial wastewater, has proven to be beneficial for human health up to a certain limit but, in

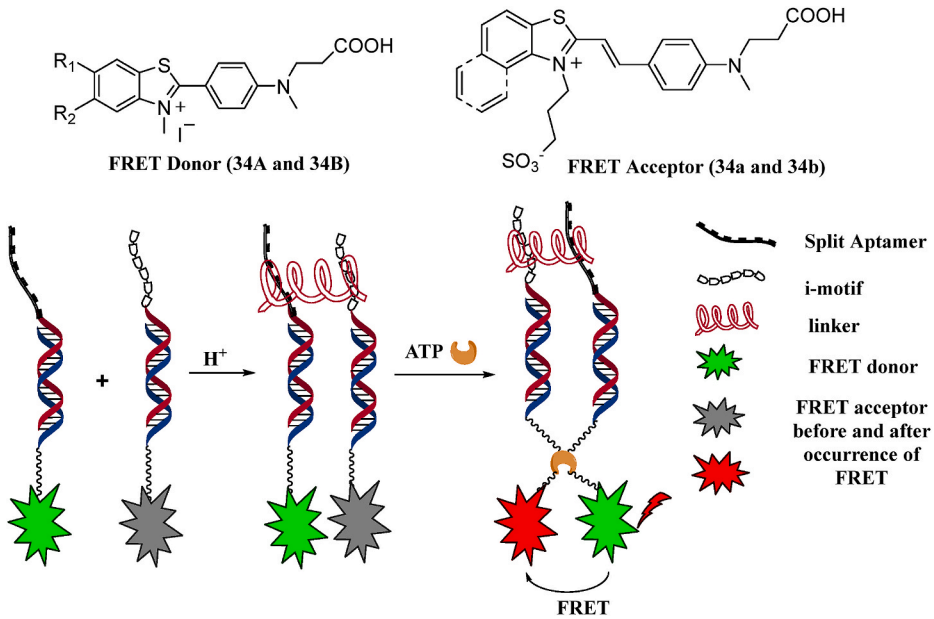

Fig. 35. Benzothiazole-based proximity-dependent DNA aptasensors **34A-B/34a-b** that in close proximity exhibit FRET responses.

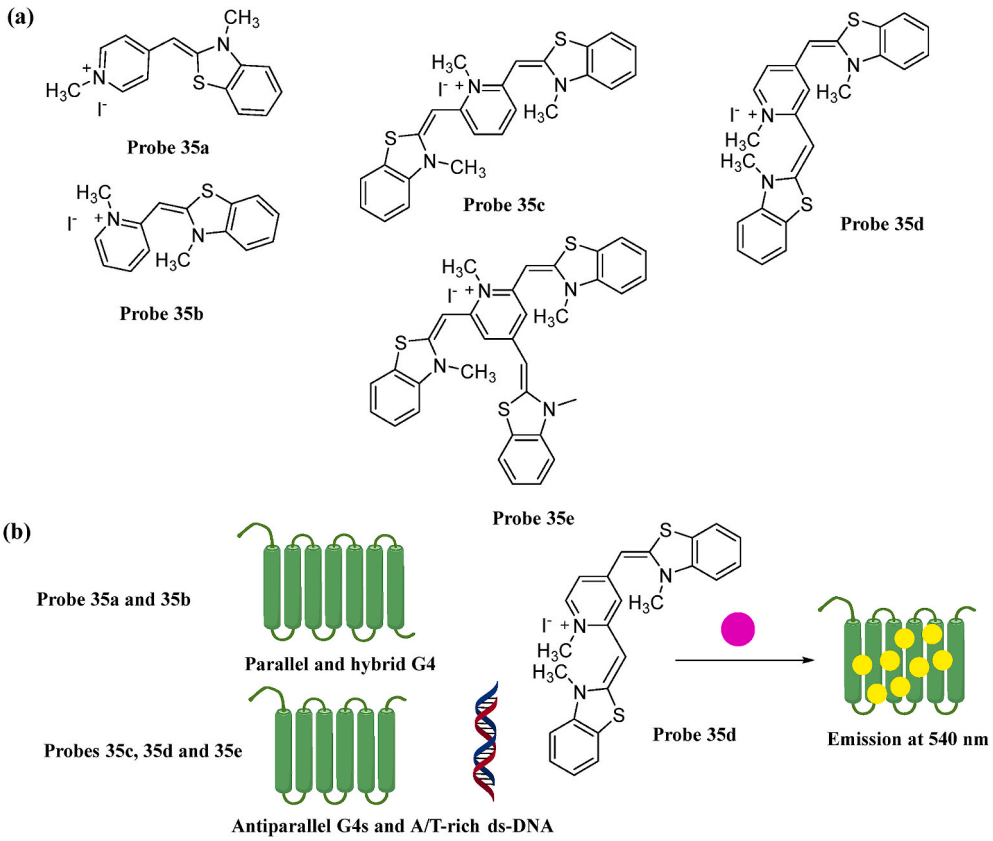

Fig. 36. (a) Chemical structures of probes **35a-e**; (b) Specificity of **35a-e** towards various DNA fragments and fluorescence response of DNA G-quadruplexes in presence of probe **35d**.

excess amounts, is capable of causing severe damage to the CVS, human red blood cells, neuronal network, lungs, and kidney. Chang et al. reported ratiometric fluorescent probe 33 for detection of hypochlorite with high sensitivity and selectivity due to selective reaction of dithiolane functional groups with OCl^- over other ROS or reactive nitrogen species (RNS). Probe **33**, in its free form, exhibited two absorption peaks at 303 nm and 358 nm in the absence of hypochlorite. But, upon adding OCl^- (10 equiv.), the two absorption peaks remarkably decreased due to rapid oxidation of the probe with a corresponding change in fluorescent signals from yellow (546 nm) to blue (464 nm) [Fig. 34]. The probe showed good sensitivity to hypochlorite with a low LOD of 8.9 nM. Furthermore, application of probe **33** in bioimaging of hypochlorite in living HeLa cells established its good cell penetrability and potential to selectively detect OCl^- in living cells [66].

2.4. Diagnosis of genetic disorders

The application of highly fluorescent probes for the qualitative and quantitative detection of nucleic acids (DNA, RNA, PNAs) has opened new avenues for widespread investigations in the fields of biochemistry, chemical biology, and clinical diagnosis. For example, DNA which, apart from being the genetically encoded double-helical nucleotide strands, takes part in forming adopt higher-ordered and functionally useful structures, like, G-quadruplex (G4) which are of special biological significance in maintenance of DNA telomeres, regulation of DNA transcription, and antitumor chemotherapy [67,68].

2.4.1. Detection of nucleic acids for the identification of genetic disorders

Wang and group synthesized two carboxylated FRET pairs, 34A/34a and 34B/34b, that show bright green and red fluorescence when labeled to DNA [Fig. 35]. The two dyes exhibit an efficient FRET system which is at par with the most widely used Cy3/Cy5 pair. The produced FRET pair is bound to two parts of a split ATP aptamer controlled by a bimolecular i-motif. The synthesized pH-induced switching fluorescent ATP aptasensors exhibited good sensitivity, excellent selectivity, and reconfiguration. Modification in the length of the linker of the switching unit helped to understand the effects of DNA proximity reactions in several physiological processes. These FRET pairs also exhibited large-Stokes shift, elevated photostability and pH non-dependency [67].

High-throughput approaches towards genome-based profiling of G4s have been gaining popularity in the past several years, but these methods are extremely time-consuming and laborious. Hence, they have been replaced with modern fluorescent and luminescent probe-based bio-physical methods. Several such probes based on benzothiazole orange were developed by Turaev et al. with one, two or three methylbenzothiazolylmethylidene functionalities in their pyridinium core (35a-e) and evaluated for their fluorogenic sensitivity towards various DNA structures [Fig. 36(a)]. The single-functionalized analogs showed sensitivity towards parallel and hybrid G4s, whereas the bi- and trifunctionalized analogs exhibited high sensitivities to G4s and A/T-rich ds-DNA. However, these were also capable of distinguishing G4s from mixed-sequence double-stranded DNA (dsDNA). Benzothiazole orange exhibited a 160-times stronger enhancement in the fluorescence quantum yield when complexed with TBA31 (a structure of a-G4 in conjunction with a dsDNA containing a CACTGG-TAGGTTGGTGTGGTTGGGGCCAGTG sequence) and was comparable to the free dye. Among these, 2,4-substituted derivative 35d showed excellent fluorescence quantum yields when complexed with G4s from oncogene promoters, and the results were comparable to those of Thioflavin-T [Fig. 36(b)]. Through the use of several known compounds with high to low affinities for oncogene promoter and telomeric G4s and well-established assay techniques, the probe **35d** exhibited widespread applicability in FID assays for profiling of G4 ligands [68].

TO-conjugated quantum dots (**probe** 36) were developed as

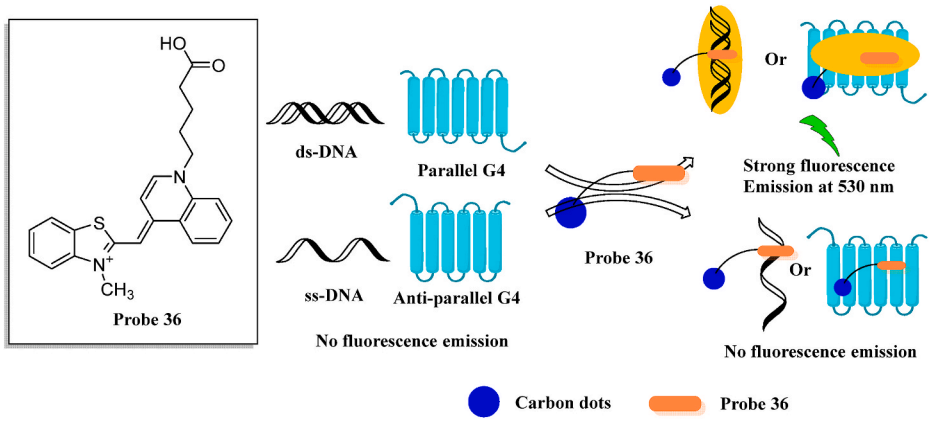

Fig. 37. Probe **35** serving as ratiometric fluorescent nanoprobes by for the detection of DNA.

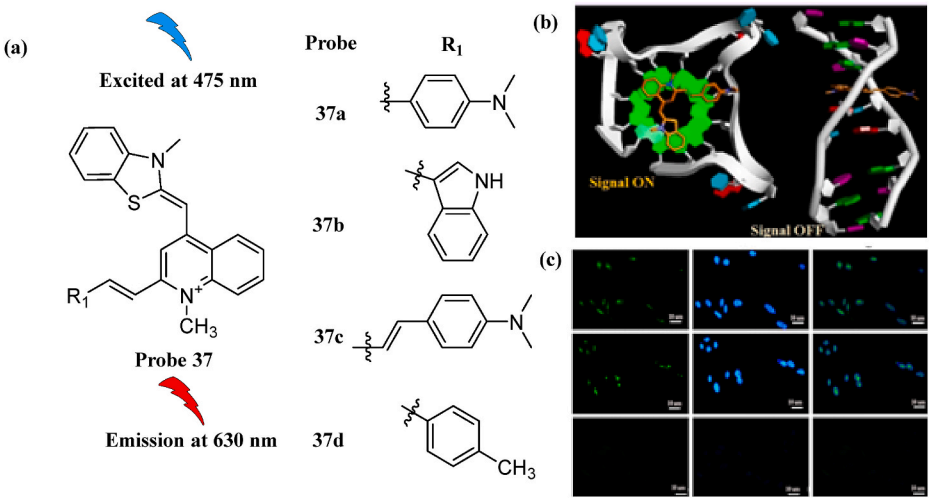

Fig. 38. Chemical Structures of probe **37a-d**; (b) Proposed detection mechanism of DNA by probe **37**. Reprinted (adapted) with permission from graphical abstract in Ref. [70]. Copyright 2016 American Chemical Society.; (c) Fluorescence images of PC3 cells (fixed) stained with probe **37a** and then DAPI without and with DNase or RNase treatment. Reprinted (adapted) with permission from Fig. 10 in Ref. [70]. Copyright 2016 American Chemical Society.

ratiometric fluorescent nanoprobes by Jin et al. to detect DNA. The probe covalently attached to the surface of the carbon dots serves as their recognition unit and fluorescence response counterparts. The free nanoprobes led to blue emission owing to the photophysical properties of the dots, while the benzothiazole unit of TO remains non-fluorescent. Upon introduction to DNA, a turn-on fluorescence response was observed from these TO-functionalized dots due to emission at 530 nm and gradual enhancement in the fluorescence intensity with a gradual increase in the amount of target DNA, while the fluorescence of CDs remains unchanged, that led to ratiometric detection of the target DNA [Fig. 37]. These nanoprobes exhibited decent selectivity and sensitivity towards dsDNA and parallel G4 as compared to single-stranded DNA (ssDNA) and antiparallel G4 with LOD of 0.90 and 3.31 nM, respectively. These carbon dots showed a higher binding affinity towards target DNA compared to the standard probe TO. Thus, was capable of expanding the scope of the nanoprobe to other targets by replacing specific recognition units [69].

With the vision of staining G4 structures, Lu and coworkers functionalized TO with various styryl features at the ortho-position to yield a series of probes (37a-d) [Fig. 38(a)]. The binding kinetic analysis of the series of probes revealed that dyes exhibited selectivity towards G4 over ssDNA, duplex DNA, and RNA. Probe 37a exhibited almost 10-folds more selectivity compared to its analogs 37b-d. The dyes were excited at 475 nm and emitted a fluorescence signal at 630 nm. Molecular docking studies were carried out on these probes to explain the mechanism of a remarkable fluorescent signal differentiation between G-quadruplex DNA and other types of nucleic acids by insertion of a small substituent [Fig. 38(b)]. The results revealed a similar binding mechanism of the produced dyes to G-quadruplex or duplex DNA like TO. However, the enhancement or quenching of the fluorescent signal greatly depended on and varied with the spatial length and orientation of the ortho-position styryl substituents. The one with a p-(dimethylamino)styryl moiety offers selectivity towards telomeric G4 than dsDNA and has also been applied to live-cell imaging of PC3 cells [Fig. 38(c)]. The LODs of **37a-37d** has been calculated as 2.55, 3.08, 5.86 and 8.52 nM, respectively [70].

Luo et al. proposed synthesizing a new G4-targeted fluorescence "turn-on" probe 38 for the direct imaging of innate noncanonical G4 structure of RNA of hepatitis C virus (HCV) in living host cells. The probe was used for several unperceivable and unachieved applications at first, such as detecting individual virus-infected cells with high sensitivity using small-molecule staining and real-time tracking of the viral RNA genome at a subcellular level inside host cells, and non-stop monitoring of the propagation of infection by native HCV. Probe **38** gets excited at 461 nm and exhibits fluorescence at 495 nm that is increased by 1693-folds in the presence of the viral genome with a significant enhancement of quantum yield from nearly 0.01% to 31.4% [Fig. 39(a)]. Live-cell imaging of HCV viral particles, such as CG2a and other RNAs, was

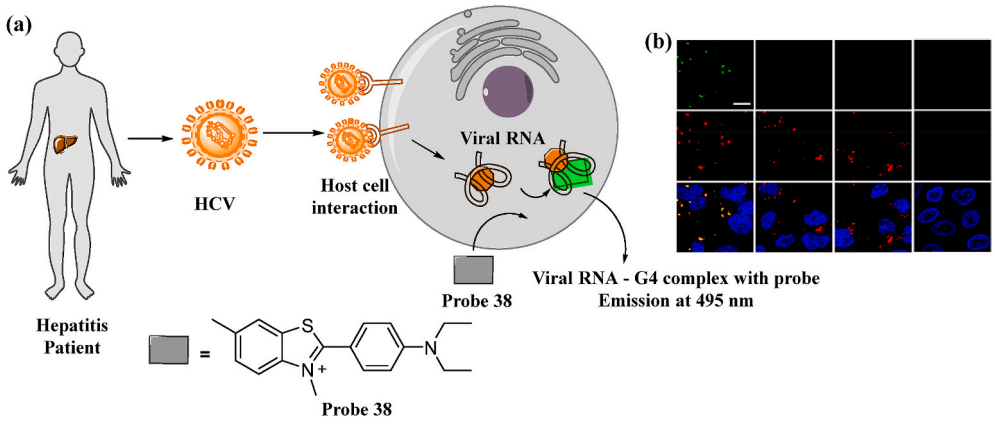

Fig. 39. (a) Proposed mechanism of bioimaging of G4 structure of RNA of HCV by probe **38**; (b) Cellular imaging of the G4 structure formed by RNA using probe **38**, and Cy5. Reprinted (adapted) with permission from Fig. 2 in Ref. [71]. Copyright 2019 American Chemical Society.

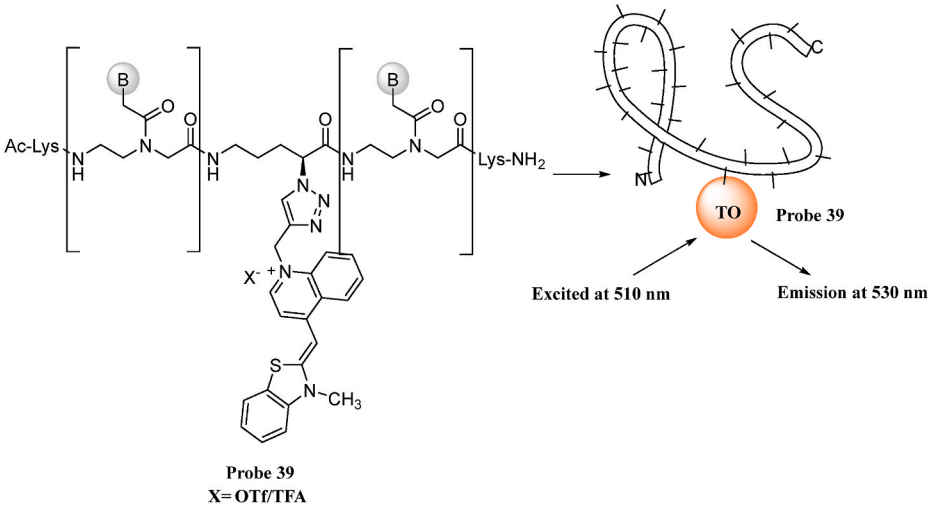

Fig. 40. Fluorescent illumination of Thiazole-orange linked α-azido D-ornithine-based PNAs (probe **39**).

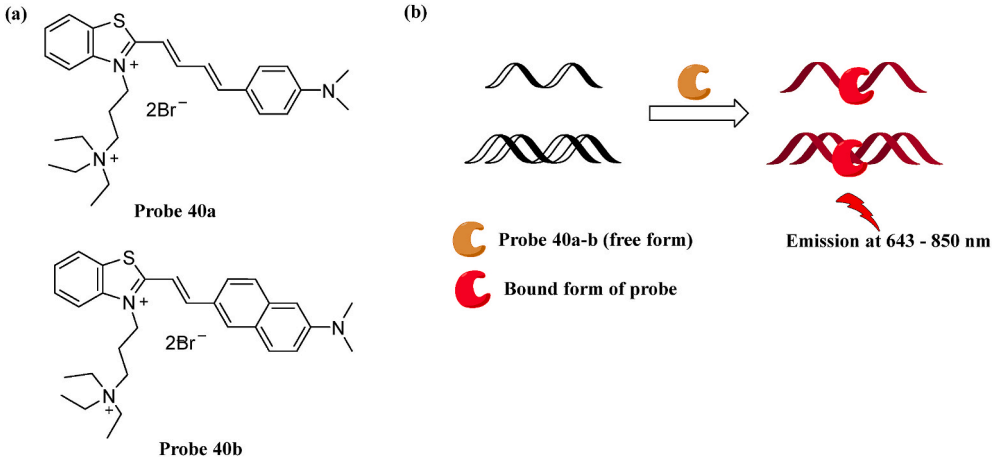

Fig. 41. (a) Chemical structures of probes **40a** and **40b**; (b) Binding of probes **40a** and **40b** with nucleic acids.

performed in Cy5-tagged liposomes transfected Huh7 cells [Fig. 39(b)]. Such a viral RNA detecting fluorogenic probe-based light-up system provides some edge to live-cell viral analysis and opens new avenues for medical diagnosis, viral biology, and drug development [71].

Peptide nucleic acids (PNAs) are small bio-mimetic sequences made of a polyamide backbone consisting of *N*-(2-aminoethyl)glycine or other amino acids attached to nucleobases via an amide linkage and perform a variety of functions in molecular biology for nucleic acid detection. Gahtory et al. formulated a convenient click strategy for on-resin-functionalization of α-azido D-ornithine-based PNAs (39) [Fig. 40].

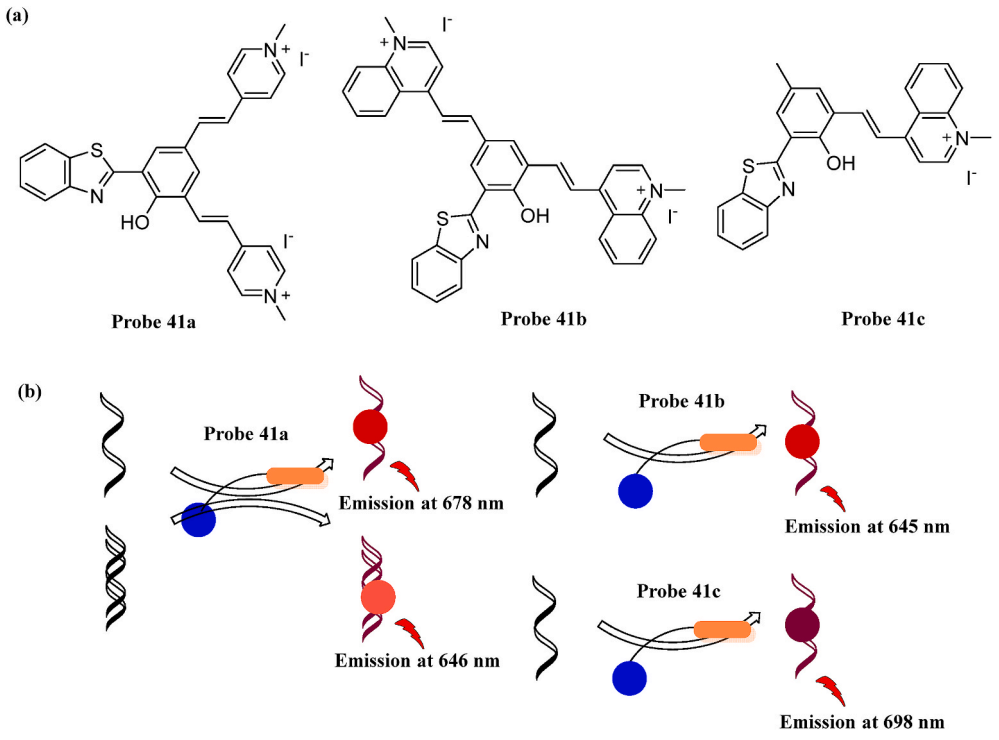

Fig. 42. (a) Chemical structures of probes **41a-c**; (b) Specificity of probes **41a-c** towards various nucleic acids and corresponding fluorescence response.

Once the azido group is attached to the resin, it reacts with to detect single-nucleotide polymorphism. The study revealed that TO clicked PNA probe when combined with fluorophore/quencher-labeled DNA exhibited increased sensitivity towards antisense DNA detection. Since antisense detection is independent of the TO-label, the proposed sensing method using azido-D-ornithine containing PNA can be used for more advanced functionalization and detection strategies [72].

Wang et al. synthesized a set of NIR fluorescent dyes **40a** and **40b** from hemicyanine attached to tetraalkyl ammonium group for detecting nucleic acid [Fig. 41(a)]. The dye showed fluorescent emission within a range of 643–850 nm in presence of DNA and RNA (0–200 μg/mL) [Fig. 41(b)]. Probe **40a** exhibited a 32.8-folds and 33.5-folds enhancement in fluorescent emission towards DNA and RNA, while probe **40b** exhibited a 33.0-folds and 38.8-folds enhancement, respectively. The probes also showed better photostability as compared to conventional Cy7 dyes owing to localization of electrons on the terminal nitrogen and p-π conjugation. In addition to this, the dyes also provide the benefits of large fluorescence Stokes shifts, selectivity to nucleic acids as compared to metal ions and other biomolecules and water solubility. Both dyes showed immense affinity towards RNA as compared to DNA. The dyes were also applied for nucleic acid imaging in viable and fixed HeLa cell lines [73].

Zhu et al. designed "off-on' cyanine dyes **41a-c** with aza units by fusing pyridinium or quinolinium ions with suitable aldehydes to develop efficient RNA specific probes in aqueous solution [Fig. 42(a)]. Positively charged heterocyclic rings act as suitable nucleic acid intercalators due to their attractive ionic interactions with the phosphate backbone. The maximal emission wavelengths of **41a-c** are 646 (upon addition of DNA) and 678 (upon addition of RNA), 645 (upon addition of RNA) and 698 nm (upon addition of RNA), respectively [Fig. 42(b)]. Cyanine dyes have comparatively poor photostability, but, when the photostability of the synthesized probes was tested keeping cyanine dye cy7 as the reference standard, it was found that upon irradiation, the absorption of probes **41a-c** ranged between 31 and 95%, whereas the same for cy7 was 9% only. The variance in the photostability of these probes could be attributed to the modulation in the length of the conjugated chain and bulkiness of the end group. The probes showed some good photophysical properties like, larger Stokes shift ranging between 235 and 282 nm, NIR emission wavelength of about 640–698 nm and decent selectivity towards nucleic acids. Probe **41a** exhibit sensitive fluorescent response towards both DNA and RNA with an increase from 0 to 8.9% in its quantum yield in response to RNA. Probes **41b** and **41c**

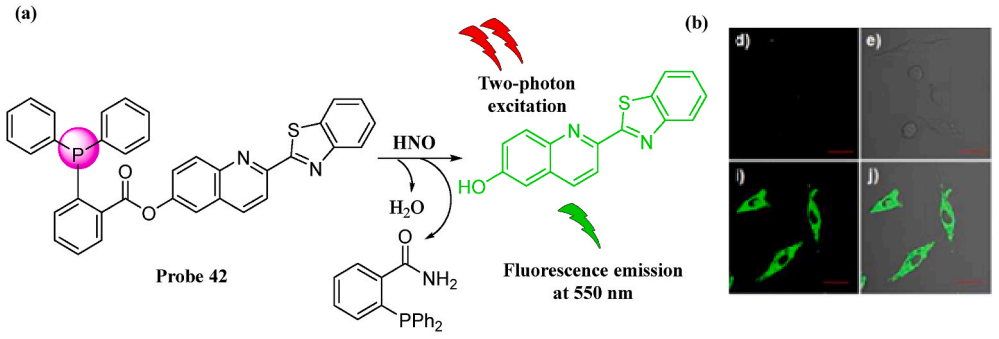

Fig. 43. (a) Two-photon probe **42** emitting light in presence of HNO; (b) Exogenous nitroxyl imaging in RAW 264.7 living cells. Two photon model obtained in green channel and merged channel, λ_{ex} = 730 nm. Reprinted (adapted) with permission from Fig. 5 in Ref. [77]. Copyright 2018 American Chemical Society.

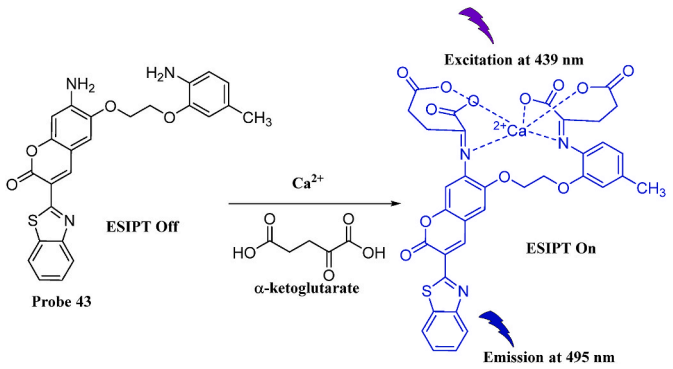

Fig. 44. Proposed detection mechanism of α-Ketoglutarate by probe **43**.

responded specifically to RNA in aqueous solution [74].

2.5. Diagnosis of cardiovascular (CVS) disorders

Nitroxyl (HNO), generated endogenously in living cells due to nitric oxide synthase activity, plays vital role in various physiological processes, such as potentiation of β-agonist dobutamine, inhibition of aldehyde dehydrogenase activity by reacting with thiols, and treatment of various CVS complications by upregulation of calcitonin gene-related peptide (CGRP) [75]. Moreover, HNO activates voltage-gated potassium ion channels and modulates resistant arteries' relaxation in human vascular systems [76]. Research on physiological functions of HNO has gained some momentum over the last few years, but any specific molecular mechanism is still unknown to us due to lack of effective tools for determination. In their work, Li et al. proposed the synthesis of a novel two-photon **probe** 42 with 2-(diphenylphosphino)benzoate as the HNO identification unit attached to the quinonline-benzothiazole fluorophore. When HNO donor was added to the probe solution, the intensity of fluorescence emission at 550 nm showed a significant enhancement due to elimination of the triphenylphosphine group as phosphine oxide and formation of an intermediate aza-ylide which turned into an amide derivative via Staudinger ligation [Fig. 43(a)]. Probe **42** showed excellent selectivity with lesser interferences from biological reductants (GSH), higher sensitivity with LOD of 0.19 μM and rapid response time of about 20 min. Probe **42** displayed higher biocompatibility pertaining to high cell penetrability and low biotoxicity when applied to imaging of alterations in exogenous and endogenous concentrations of nitroxyl in living RAW 264.7 cells [Fig. 43 (b)] [77].

2.6. Diagnosis of metabolic disorders

2.6.1. Detection of metabolites for identification of metabolic disorders

α-Ketoglutarate (α-KG), a major metabolite in the Krebs' energy cycle has recently been established as a surrogate biomarker for nonalcoholic fatty liver disease (NAFLD) and various other types of cancers. Gan et al. reported the fabrication of a novel "turn-on" probe 43 for detection of α-KG. Using benzothiazole-coumarin as framework for the new probe, the researchers designed a probe for calcium ion (Ca^{2+}) recognition that indirectly leads to α-KG measurement. The free probe exhibited a weak fluorescence at 495 nm when excited at a wavelength of 439 nm [Fig. 44]. When α-KG and Ca^{2+} were introduced to the probe solution, the emission fluorescence intensity at 495 nm was enhanced by a remarkable 7.6-folds without any significant change in the excitation or emission wavelengths. The probe was found to detect α-KG selectively even in the presence of other amino acids and interfering species like glutaric acid with a quantitative limit ranging in between 5 and 50 μmol/L in EtOH for α-KG [78].

Formaldehyde serves as an important source of reactive carbonyl species (RCS) in organisms. Formaldehyde is also associated with the abilities like cognition and spatial memory, but in abnormally elevated concentrations, it could participate in dementia, diabetes, cancer, and other neurodegenerative diseases [79,80]. In order to prevent this, Hao et al. synthesized a ratiometric fluorescent probe 44 for the detection of formaldehyde. The detection mechanism is a three-step process starting imine formation by condensation of formaldehyde with probe **44**, which undergoes 2-aza-Cope rearrangement, and finally hydrolysis resulted in aldehyde fluorophore [Fig. 45(a)]. The extended π-conjugation in fluorophore and aldehyde moiety reduces the energy gap between the HOMO and LUMO, leading to red shift in the emission spectra. Probe **44** has been efficiently employed in detecting formaldehyde with exceptional selectivity under physiological conditions compared to other interfering biological analytes. The probe displayed a LOD of 0.58 μM. The fluorescence response of the probe increased by 35.7 folds in the presence of formaldehyde. The probe was also successfully used for ratiometric imaging of formaldehyde in both viable MGC-803 cells [Fig. 45(b))] as well as in zebrafish models [Fig. 45(c)] [81].

Zhou et al. designed a novel ratiometric probe **45** by using HBT as the ESIPT fluorophore and pro-aza-Cope rearrangement scaffold as the recognition site of formaldehyde. The fluorogenic activity of the probe is ascribed to the conversion of the electron-dense pro-aza-Cope rearrangement group to an electron-lacking aldehyde group by means of aza-Cope rearrangement. In absence of formaldehyde, the free probe absorbed maximally at around 333. Upon addition of formaldehyde upto a concentration of 15 mM to the probe solution (20 μM), the peak at 333 nm decreased with a simultaneous elevation of a band at 425 nm. When excited at 350 nm, the free probe exhibited a fluorescence

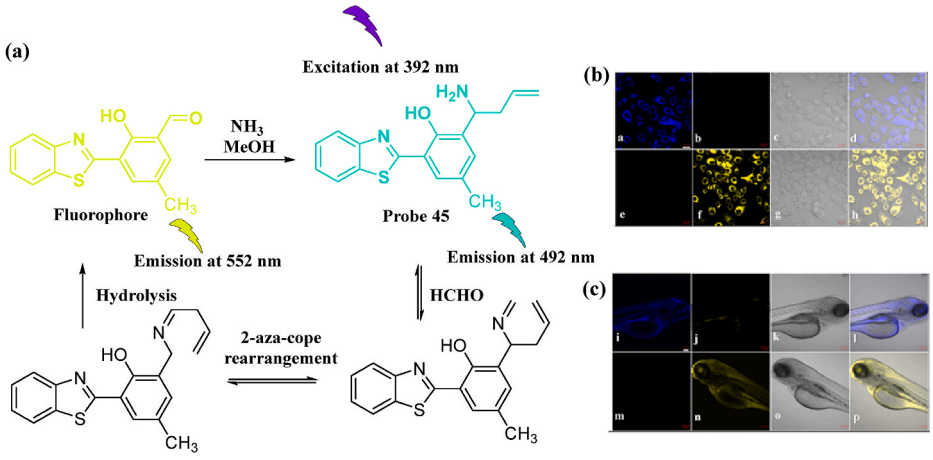

Fig. 45. (a) Synthetic route and sensing mechanism of probe **44** for formaldehyde; (b) Confocal fluorescence images of live MGC-803 cells incubated with probe **44** with and without subsequent treatment by formaldehyde. Reprinted (adapted) with permission from Fig. 4[A] in Ref. [81]. Copyright 2020 Elsevier; (c) Confocal fluorescence images of zebrafish incubated with probe **44** with and without subsequent treatment by formaldehyde. Fluorescence images in blue and yellow channels. Reprinted (adapted) with permission from Fig. 4[B] in Ref. [81]. Copyright 2020 Elsevier.

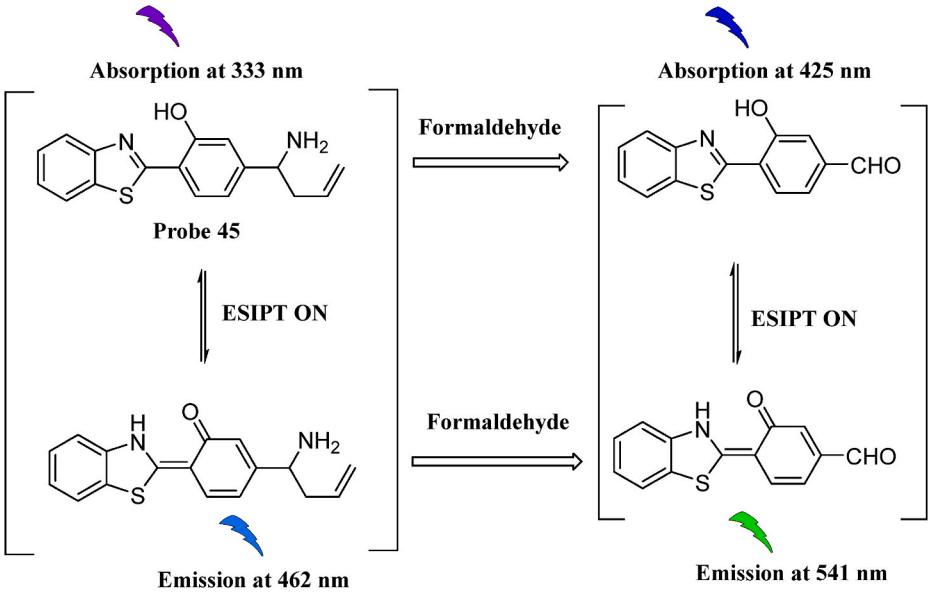

Fig. 46. Ratiometric fluorescence response of probe **45** in response to formaldehyde.

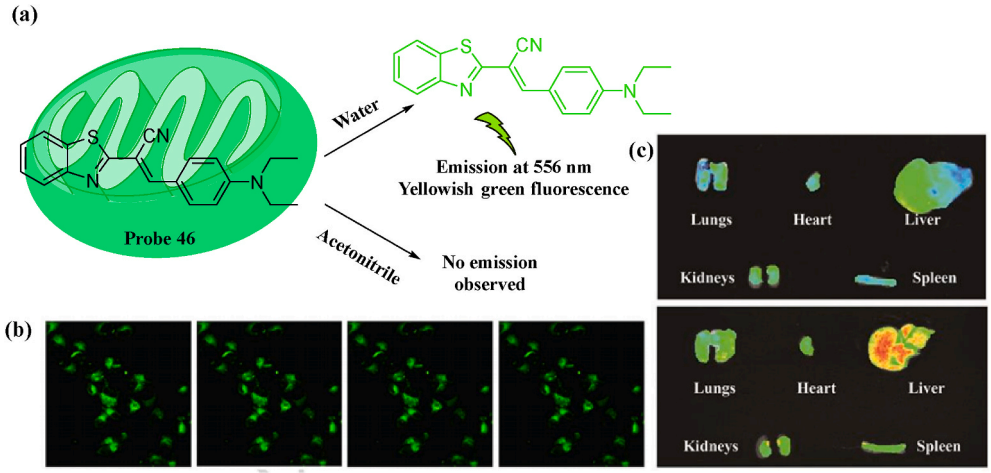

Fig. 47. (a) Determination of mitochondrial dysfunction by fluorescence emission of probe **46**; (b) Fluorescent images of HeLa cells stained with probe **46** from 0 to 360s when excited at 560 nm. Reprinted (adapted) with permission from Fig. 6 in Ref. [83]. Copyright 2017 Elsevier; (c) *Ex vivo* fluorescence images of major organs excised from sacrificed mice before and after injection of probe **46**. Reprinted (adapted) with permission from Fig. 7 in Ref. [83]. Copyright 2017 Elsevier.

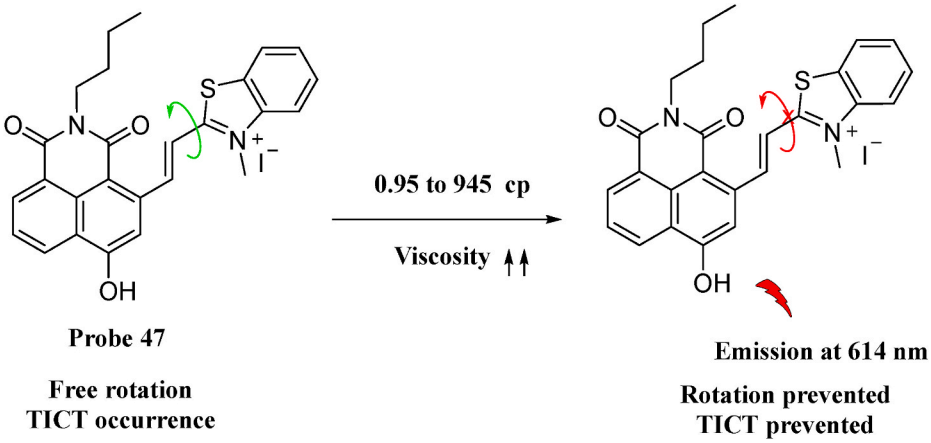

Fig. 48. Effect of viscosity on fluorescence emission of probe **47**.

emission band at 462 nm but when admixed with formaldehyde (0–30 mM), the emission band at 541nm increased by 39 folds (red shift of 79 nm) with a simultaneous fall of the emission peak at 462 nm (Fig. 46). The detection limit of the probe was calculated as 4.1×10^{-4} M. The probe has high selectivity and has been applied for detecting formaldehyde in calf serum [82].

2.6.2. Imaging of organelle dysfunction for detection of metabolic disorders

Mitochondrial dysfunction can be correlated to a variety of diseases, such as metabolic diseases, neurodegenerative anomalies, cancer, etc. Hence, proper investigations of the mitochondrial structure and functions are essential for maintaining normal physiological functions. Inspired by this, Lu et al. synthesized a fluorescent **probe** 46 for tracking mitochondrial activity. The AIE properties of the probe were tested in an acetonitrile-water mixture. The probe exhibited weak fluorescence due to its high solubility in acetonitrile. Nevertheless, as the amount of water was gradually increased in the mixture (fw > 80 vol%), yellow-green fluorescent emission was visible at 556 nm [Fig. 47(a)], which was earlier absent when the volume of acetonitrile was maximum. The probe exhibited low cytotoxicity and high photostability that paved the way for its successful bioimaging applications. The probe showed significant level of cell penetrability in living HeLa cells with stable green fluorescence [Fig. 47(b)] and ex vivo imaging studies on nude mice [Fig. 47 (c)], making it suitable for long-term bioimaging application [83].

Abnormal mitochondrial viscosity can be linked to several diseases, such as, diabetes and neurodegenerative disorders. Hence, its monitoring is mandatory for early diagnoses of the abovementioned health conditions. Wei et al. designed and synthesized probe **47** by linking 1,8-naphthalimide derivatives and benzothiazoles using a *C*–C double bond. The alkenyl linker between the two aromatic systems acts as the viscosity response site. In absence of viscosity, the linker single bond rotates freely. But, gradually as the viscosity is increased from 0.95 cP to 945 cP, the fluorescence emission peak at 614 nm increased by 20.34-folds [Fig. 48]. The fluorescence quantum yield of the probe was calculated as 80.8%. The probe **47** also showed negligible effect of solvent polarity, pH and other biologically interfering fluorescent species. It has been successfully applied for live cell imaging of HeLa cells for monitoring the fluctuation of the mitochondrial viscosity in them [84].

2.7. Detection of toxic and harmful substances in environment as well as biological systems

2.7.1. Detection of toxic metal ions and other ionic analytes

2.7.1.1. Detection of copper ions. Detection of Cu^{2+} ions in the human body is highly essential as a moderate concentration of the same is regulated throughout the body to maintain normal physiological functions. The permissible limits of Cu^{2+} in the blood are 15.7–23.6 μM, and any deviation from this value may lead to the occurrence of various diseases. Thus, tracking of Cu^{2+} in life functions is of utmost importance. Inorganic phosphate (PPi), generated upon hydrolysis of adenosine triphosphate (ATP) in living cells, has several important roles in energy conversions and metabolic processes of the biological systems. Selective identification and differentiation of PPi from other phosphorus-containing anions with the identical charge and structure obtained from other phosphoric acid derivatives in the body are thus of great importance. Therefore, the design of a specific Cu^{2+} sensor that can sequentially detect PPi serves as a cost-effective and convenient alternative to other chemical sensors involving other quenchers' interference. Li et al. conducted a study where they developed an extremely selective fluorescent **probe** 48 for the sequential recognition of Cu^{2+} and PPi. The addition of Cu^{2+} ions in probe **48** resulted significant redshift of about 30 nm in absorption wavelength from 449 nm to 479 nm and decline in the fluorescence intensity of the band at 505 nm [Fig. 49]. The

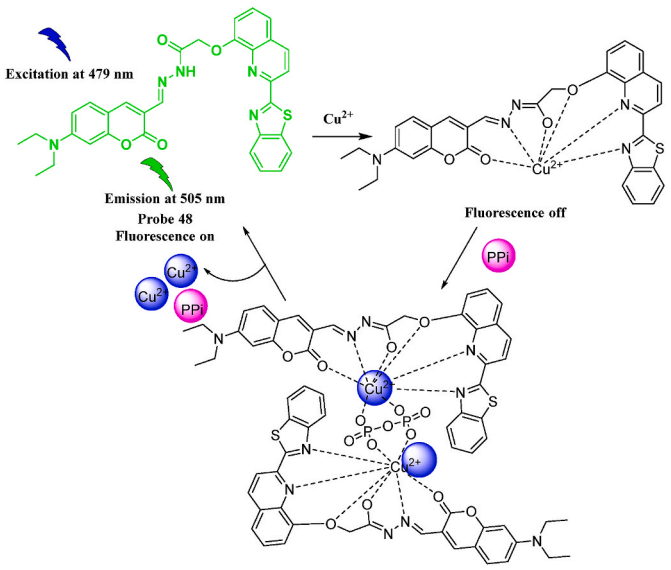

Fig. 49. Possible mechanism of interaction of the probe **48** with Cu^{2+} and subsequent binding of complex with PPi.

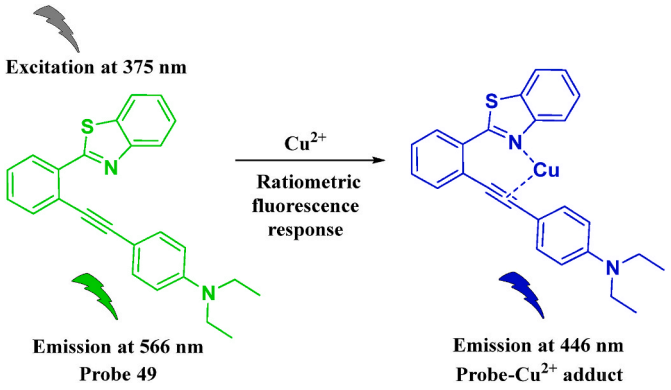

Fig. 50. Detection of Cu^{2+} ions by ratiometric and reversible fluorescence conversion of probe **49**.

probe showed binding to Cu^{2+} with LOD of 0.06 μM and the complex bound with PPi with LOD of 0.01 μM. The stable pH range of the sensor and complex combination was evaluated as 3–8. Further studies demonstrated the sequential "on-off" fluorescent signals in HeLa cells treated with probe **48** in the presence of Cu^{2+} and PPi [85].

Zhao et al. synthesized ratiometric and reversible probe 49 for the detection of Cu^{2+} ions. The free probe exhibited fluorescence emission at 566 nm with a large Stokes shift of 190 nm ($\lambda_{ex} = 375$ nm) and forms a complex with Cu^{2+} ions that cause the remarkable fluorescence enhancement of almost 578-fold. Introduction of Cu^{2+} to the probe solution led to a decrease in the emission peak at 566 nm with the simultaneous appearance of a new peak at 446 nm with a Stokes shift of 71 nm [Fig. 50]. The DFT calculations confirmed co-ordinate bond formation between Cu^{2+} ions and *N*-atoms of the thiazole ring on one side and alkyne on the other. The LOD for copper ions was calculated as 3.2×10^{-9} M. *In vitro* cell imaging experiments suggested that the probe **49** can permeate through the cell membrane and hence could be applied to identify Cu^{2+} ions in viable HepG2 cells [86].

Tang and colleagues synthesized ESIPT-based fluorescence probe **50** for detection of Cu^{2+} at a neutral pH. The sensing mechanism is based on the Cu^{2+}-induced hydrolytic cleavage of the picolinate ester moiety from the probe in order to liberate the ESIPT fluorophore with dual-wavelength emission enhancement. When Cu^{2+} is introduced, the

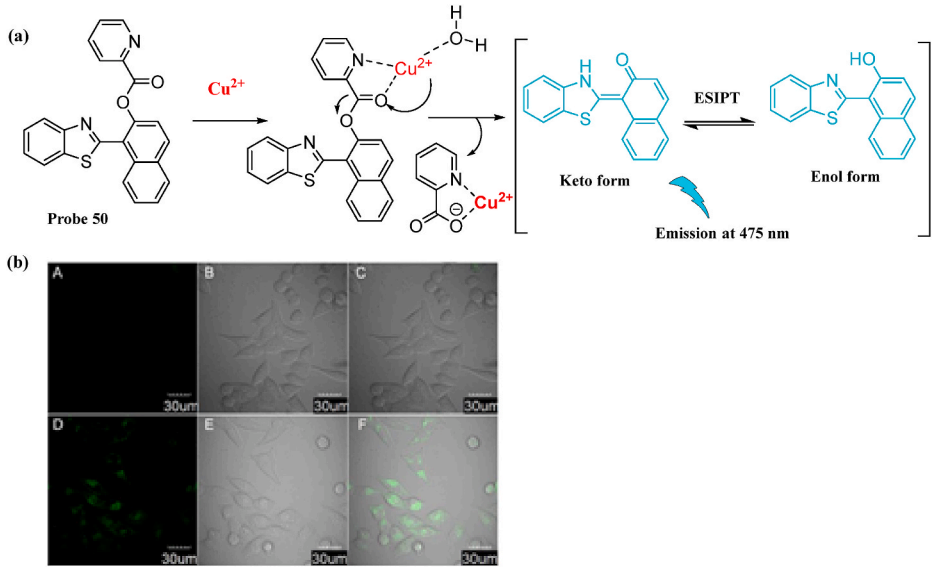

Fig. 51. (a) The sensing mechanism of probe **50** for Cu^{2+} ions; (b) Fluorescence images of MCF-7 cells incubated with probe **50** with and without Cu^{2+} ions observed from dark field, bright field, merged image. Reprinted (adapted) with permission from Fig. 8 in Ref. [87]. Copyright 2016 Elsevier.

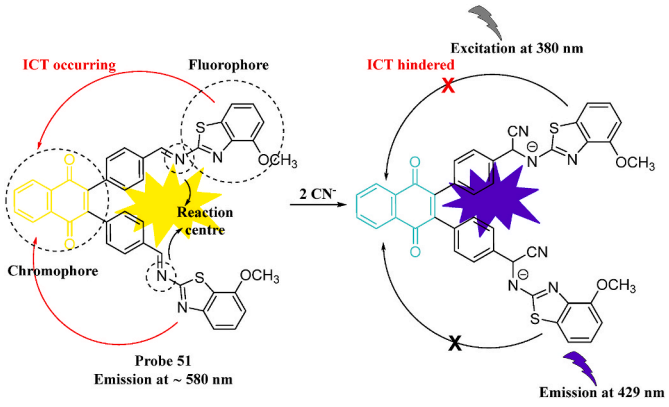

Fig. 52. Fluorescent response mechanism of probe **51** in presence of CN^- ions.

probe exhibits a bathochromic shift in its fluorescence emission at 475 nm [Fig. 51(a)]. The free probe itself showcases higher fluorescence emission under alkaline conditions (pH = 8–10) due to its hydroxide ion induced hydrolysis. However, the Cu^{2+} promoted enhancement of fluorescence was mainly obtained in the pH of 6–8, implying the use of this probe for detection of Cu^{2+} in near neutral conditions. Probe **50** was successfully used to detect and track Cu^{2+} in viable MCF-7 breast cancer cells and real water samples with LOD of 1.34×10^{-6} M [Fig. 51(b)] [87].

2.7.1.2. Detection of cyanide ions. According to the World Health Organization (WHO), cyanide (CN^-) is one of the most toxic anions found in nature, and thus its maximum tolerable limit in drinking water has been fixed at 1.9 μM. Owing to the lethal toxic consequences of CN^-, qualitative and quantitative tools have been employed to detect them. Out of all the methods developed, reaction-based sensors displayed excellent selectivity and sensitivity towards CN^- but due to poor aqueous solubility and extended response time, their applications have been limited. With the vision of overcoming such problems, Kumar and colleagues synthesized quinone-benzothiazole imine-based chemosensor 51 that indicates the presence of CN^- in an aqueous buffer by an immediate color change from yellow to bluish-green. The free sensor exhibited a band at 275 nm corresponding to π-π* transition and a shoulder at 344 nm due to the ICT transitions. As the amounts of CN^- in the chemosensor solution increased gradually, the absorbance peak at 344 nm diminished with a simultaneous increase of a new band at 667 nm, responsible for the observed color change. Addition of CN^- to the receptor led to an elevation of the fluorescence intensity at 429 nm [Fig. 52], with the formation of an excimer due to inhibition of ICT by

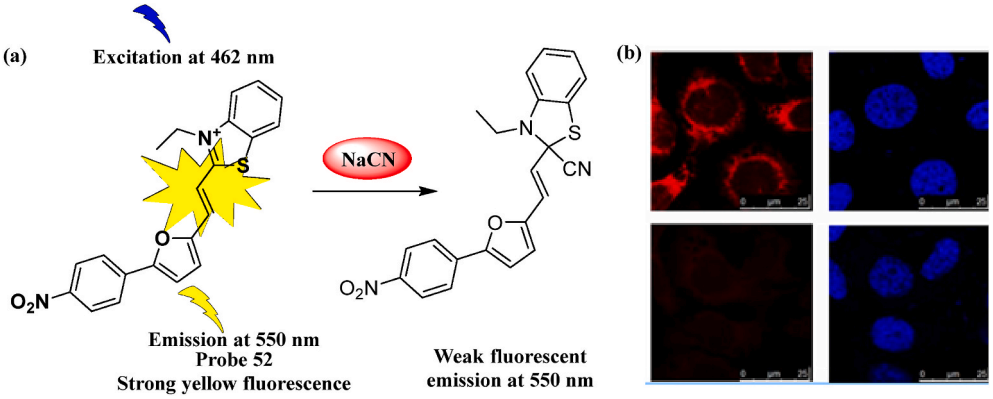

Fig. 53. (a) Suggested mechanism of interaction between probe **52** and CN^- ions; (b) Confocal laser scanning microscopy images of probe **52** stained HeLa cells, co-stained with DAPI in absence and in presence of CN^- ions. Reprinted (adapted) with permission from Fig. 6 in Ref. [89]. Copyright 2018 Elsevier.

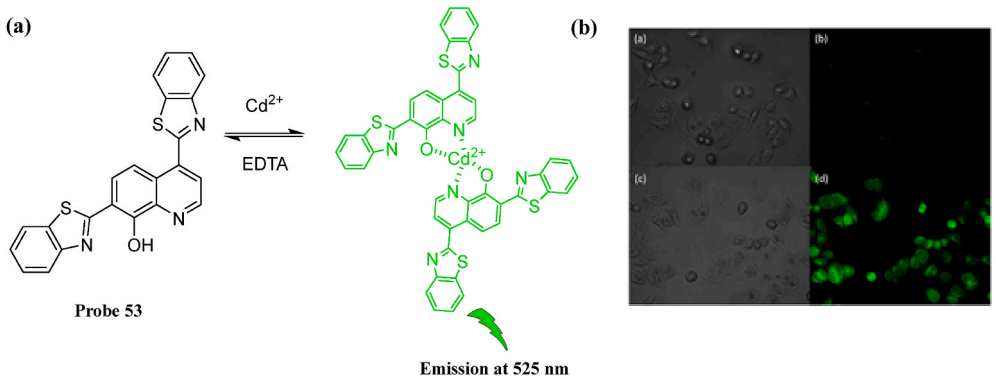

Fig. 54. (a) Proposed sensing mechanism of probe **53** for Cd^{2+} ions; (b) Confocal fluorescence images of Cd^{2+} in living HeLa cells incubated with probe **53** and those incubated with probe followed by Cd^{2+} ions. Reprinted (adapted) with permission from Fig. 9 in Ref. [90]. Copyright 2019 Elsevier.

nucleophilic addition of CN^- to the imino carbon atom, causing color change from yellow to blue under UV lamp. The synthesized sensor attaches to 2 equiv. of CN^- with a binding constant of $5.55 \times 10^4\ M^{-1}$. The receptor also exhibits a low LOD of 69 nM, which is much below the WHO's acceptable limit of cyanide in drinking water (1.9 μM). Similar findings were also observed in theoretical studies. The sensor **51** also detected cyanide fluorometrically in samples of tap water and food materials, like, almond, cassava flour, potato, etc. [88].

Wang et al. synthesized a novel chromogenic and fluorescent dual-channel signal probe 52 to detect CN^- ions. The probe showed high selectivity towards detection of CN^- ions and overcame interference of other anions usually present in water samples and the human body. The fluorescence intensity and absorption intensity of the probe peak at 550 nm and 462 nm, respectively, gradually dropped to a minimum in presence of CN^- [Fig. 53(a)]. The LOD of CN^- were calculated as 0.11 μM and 0.16 μM for fluorescence and absorbance, respectively. The emission properties of the probe attributed to the nucleophilic addition of CN^- to the 2nd position of the benzothiazole moiety. Irreversible hindrance of the π-conjugation and ICT process between furfural and benzothiazole led to the chromogenic alteration and fluorescent characterizations. Furthermore, the probe exhibited some excellent photophysical properties and enhanced biocompatibility, which allowed their practical applications in CN^- tracing of HeLa cell lines [Fig. 53(b)] [89].

2.7.1.3. Detection of cadmium ions. Cadmium has been identified as one of the most toxic heavy metal pollutants widely used in electroplating, agriculture, battery industries, and military affairs and can induce cancer in humans upon exposure. Due to the high risk associated with human exposure to cadmium, the synthesis of fluorescent chemosensors for detecting cadmium ions (Cd^{2+}) in biological and environmental samples has attracted much attention over the past few decades. Lu and co-workers thus generated probe **53** to detect Cd^{2+} ions in living systems. The free probe exhibited a weak fluorescence that was gradually enhanced by the formation of coordination complexes with different metal ions such as Al^{3+}, Zn^{2+}, etc. in methanol (consisting of 1% water), but in the presence of Cd^{2+} ions, the probe exhibited strong green fluorescence [Fig. 54(a)]. Unlike most other chemosensors, which undergo serious interferences from other transition metal ions, the probe exhibited good selectivity towards Cd^{2+} over a broad pH range of 4–12, which could further be improved by increasing the amount of water to 30% in the water-methanol solution. The fluorescence intensity was linearly increased at 525 nm with the subsequent increase in Cd^{2+} concentration within the range of 0–5 μM, and the LOD was calculated as 0.1 μM. Thus, the developed fluorophore served as a successful tool for fluorescence imaging of Cd^{2+} in living HeLa cells [Fig. 54(b)] [90].

2.7.1.4. Detection of aluminum ions. Aluminum is a metal found in abundance in nature and is widely employed in packaging

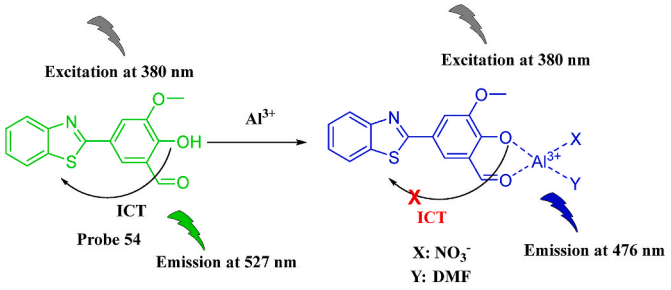

Fig. 55. Ratiometric detection of Al^{3+} ions by probe **54.**

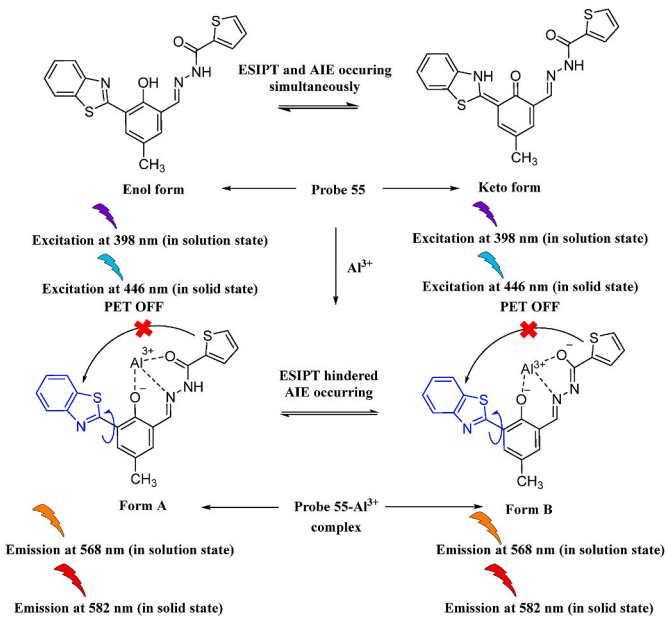

Fig. 56. Proposed mechanism of detection of Al^{3+} by probe **55** in water samples or inside cells.

pharmaceuticals and food additives, which may induce accumulation of its ionic form, Al^{3+} in water samples from various sources and human bodies. Detection of presence of Al^{3+} in humans is necessary as its accumulation in the human body above the tolerable limit might lead to occurrence of neurodegenerative disorders like AD, Parkinson's disease, amyotrophic sclerosis, and encephalopathy. Tian and co-workers synthesized fluorescent probe 54 for the ratiometric detection of Al^{3+}. The probe showed high selectivity and sensitivity towards Al^{3+} with a blue

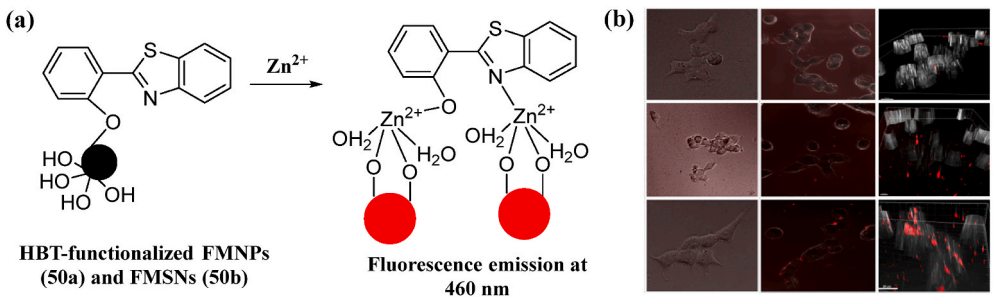

Fig. 57. (a) Detection of cellular zinc by HBT-functionalized fluorescent magnetite nanoparticles **56a** and mesoporous silica nanoparticles **56b**; (b) Fluorescence images of the HEK293 cells treated with **56a** and **56b** in absence of Zn^{2+} ions (Column I), in the presence of Zn^{2+} ions (Column II) and 3D reconstruction of cells treated with **56a** and **56b** in the presence of Zn^{2+} ions (Column III). Reprinted (adapted) from open access from Fig. 17 in Ref. [93].

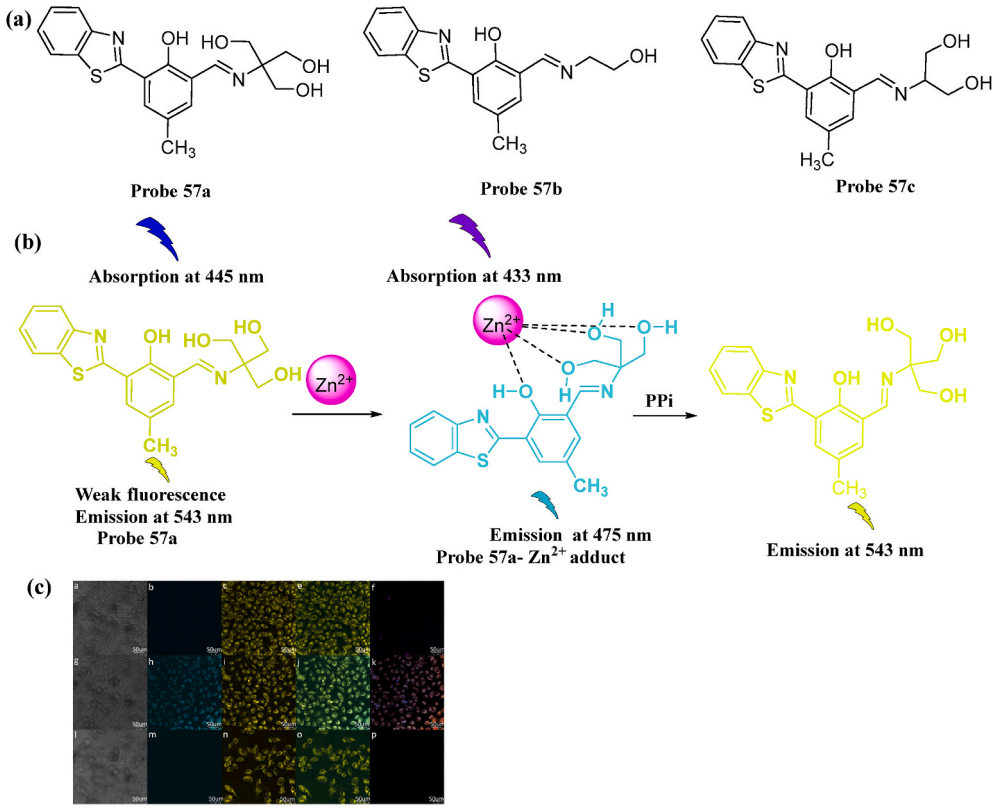

Fig. 58. (a) Chemical structures of probe **57a-c**; (b) Proposed detection mechanism of Zn^{2+} and PPi by probe **57a**; (c) Confocal fluorescence images of HeLa cells, incubated with the probe **57a** (a–f), HeLa cells treated with probe **57a** and then exposed to Zn^{2+} (g–k), HeLa cells incubated with probe **57a**, Zn^{2+} and then exposed to PPi. Reprinted (adapted) with permission from Fig. 9 in Ref. [94]. Copyright 2017 American Chemical Society.

shift in the fluorescence spectrum due to the synergistic mechanism of the inhibition of ICT [Fig. 55]. A good linear correlation was obtained between the absorbance ratios and the Al^{3+} concentration (0–12 μM) having a LOD of 99 nM, which substantiates the ratiometric detection of Al^{3+} by the probe. The probe was further used to detect Al^{3+} in the local river waters, on test strips and to monitor Al^{3+} concentration in human stromal cells (HSC) by fluorescence imaging experiments [91].

Chen et al. developed an ESIPT and AIE active Schiff-base probe 55 for the ratiometric detection of Al^{3+} in water samples and living cells. Probe **55** showed two absorption peaks at 398 nm and 300 nm in solution state. Addition of Al^{3+} resulted in the decrease of the absorption peak intensities with simultaneous increase of peak at 475 nm accompanied by colorless to pale-green color change of the probe solution. Probe **55** in its free solid-state exhibited red fluorescence at 582 nm with an excitation peak at 446 nm, which can be attributed to the occurrence of AIE process. Probe showed an orange fluorescence in solution state with emission maxima at 568 nm [Fig. 56]. The probe exhibited LOD of 2.2 μM. The crystallographic studies on the probe revealed that its interaction with Al^{3+} is pertaining to the chelation of Al^{3+} by means of the phenolic O atom, the N atoms in –C═N- groups, the O atom of the carbonyl group and three water molecules, thereby forming a hexa-coordinated structure. The probe was further explored for its bio-imaging and monitoring of Al^{3+} in living cells and was successfully achieved in viable HeLa cell lines [92].

2.7.1.5. Detection of zinc ions. Zinc is an essential element vital for growth and development in humans. They serve to be structural components of many proteins, like co-factors to several enzymes, receptors and transcription factors of cellular signaling pathways. Thus, they are essential to be detected in the human body. With a view of achieving zinc ion (Zn^{2+}) detection in cells, HBT-functionalized fluorescent magnetite nanoparticles (56a) and mesoporous silica nanoparticles

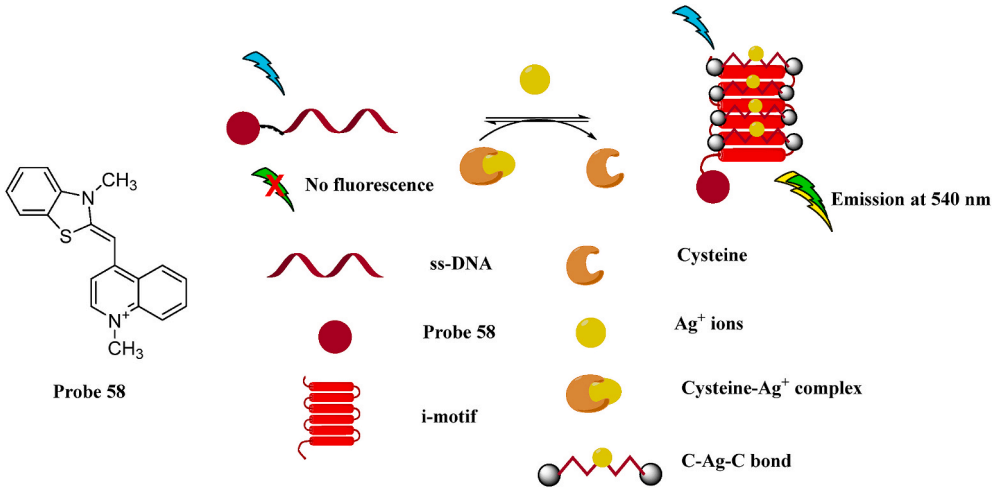

Fig. 59. Detection of Ag^{+} ions promoted folding of *C*-rich ss-DNA into i-motif DNA by means of probe **58**.

(56b) were developed by Erami et al. The covalent fusion of magnetite and silica scaffolds with the fluorescent HBT moiety rendered the nanoparticles some amount of stability and also made them sensitive and selective optical tools for Zn^{2+} detection [Fig. 57(a)]. The presence of the benzothiazole moiety further induced efficient Zn^{2+} ion uptake and desired cell viability (80% for **56a** and 92% for **56b**, respectively), with the potential of signal generation in the normal human kidney epithelial (HEK293) cell lines [Fig. 57(b)]. LODs were calculated as 2.53×10^{-6} and 2.55×10^{-6} M for **56a** and **56b**, respectively. However, both the probe were extremely sensitive; **56b** showed better Zn^{2+} signaling due to enhanced cellular penetration. These factors successfully establish this fluorescent probe-based NP formulation approach as a suitable and beneficial alternative for Zn^{2+} detection [93].

Chang et al. fabricated ratiometric fluorescent probes, 57a-c for the detection of zinc ions [Fig. 58(a)]. All the three probes exhibited yellow fluorescence in their free states and blue-shifted fluorescence upon adding Zn^{2+} ions [Fig. 58(b)]. The probes also exhibited selectivity towards the Zn^{2+} ions over other metal ions and showed fluorescence enhancement at 475 nm. The detection limit of probe **57a** was 7 nM for zinc ion. Probe **57a**-Zn^{2+} complex was further employed in the detection of PPi with a LOD of 60 nM. The complex was also able to trace enzyme-catalyzed degradation of PPi, therefore serving as an effective tool for tracking Zn^{2+} ion and PPi in biological systems. Moreover, the confocal microscopic images of viable HeLa cell lines substantiate the fair cell permeability of probe **57a** and specific identification of Zn^{2+} ions in living cells [Fig. 58(c)] [94].

2.7.1.6. Detection of silver ions. Kang et al. came up with a label-free TO-based optical probe 58 for the detection of silver (Ag^{+}) ions due to their toxic effects on human health as well as nature. TO serves as the recognition site for any structural change in i-motif DNA at neutral pH. The Ag^{+} ions aid the folding process of a *C*-rich ss-DNA sequence into i-motif DNA structure at physiological pH, and the folding can be reversed by chelation with Cys. This folding mechanism can be signaled by a change in the fluorescence emission of TO from none in the free molecular state to strong fluorescence at 540 nm after the insertion of i-motif DNA [Fig. 59]. The fluorescence intensity gradually increased with the increase in the Ag^{+} ion concentration. This probe is extremely rapid, highly sensitive, and favorably selective for sensing Ag^{+} and Cys with LOD of 17 and 280 nM, respectively. The resultant probe is label-free, hence less toxic and economical. It further shows a successful role in binding with i-motif to quantify Ag^{+} in the real samples [95].

2.7.1.7. Detection of mercury ions. Jiao et al. fabricated a novel coumarin-based fluorescent probe for the detection of Hg^{2+} ions.

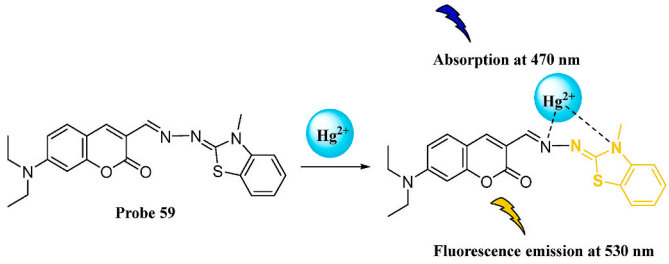

Fig. 60. Fluorescence response of probe **59** in presence of Hg^{2+} ions.

Inspired by the favorable photophysical features exhibited by coumarin, its diethylamino derivatives were used for the presence of electron-donating groups that suitably bridge with 3-methyl-2-benzothiazolinone hydrazone using a C═N bond. The crystallographic data revealed that the two aromatic rings of the probe were almost coplanar. Probe **59**, when excited at 470 nm showed weak fluorescence at 530 nm, which gradually enhanced by almost four folds with the increase of the Hg^{2+} ions [Fig. 60]. The probe also delivered excellent sensitivity and selectivity towards Hg^{2+} ions tracing amongst other similar metal ions [96].

Zhang et al. synthesized probe **60** for the ratiometric detection of Hg^{2+} ions. The thiophosphate moiety in probe **60** hindered the ESIPT process of HBT, and thus, exhibited emission at 377 nm when excited at 310 nm. But, as soon as Hg^{2+} ions were added to the probe solution, the thiophosphate group got cleaved off from the entire skeleton. The liberated free HBT fluorophore resulted in a strong fluorescence enhancement at 470 nm without any significant interference of other cations [Fig. 61]. The probe demonstrated a rapid response time of a minute and great selectivity towards Hg^{2+} ions with the detection limit of 12 nM. Fluorescence imaging techniques further established the bioimaging of Hg^{2+} in living TE-1 cells [97].

Zhou et al. designed and synthesized a ratiometric fluorescent probe **61** for the selective monitoring of Hg^{2+} ions by amalgamating HBT, an ESIPT fluorophore with thioacetal as the Hg^{2+} reactive site. The probe exhibits fluorescence response in presence of Hg^{2+} ions due to the reaction of the latter with the electron-rich dithioacetal moiety, followed by its subsequent removal thereby exposing the electron-deficient aldehyde group. An ICT process takes place in the molecule due to flow of charge from benzothiazole, the electron-donor, to aldehyde, the electron acceptor, thus, leading to a significant bathochromic shift in the fluorescence signals of the probe **61** generating a ratiometric response. The free probe emits maximally 465 nm upon excitation at 338 nm in neutral pH at ambient temperature but upon addition of Hg^{2+}, the

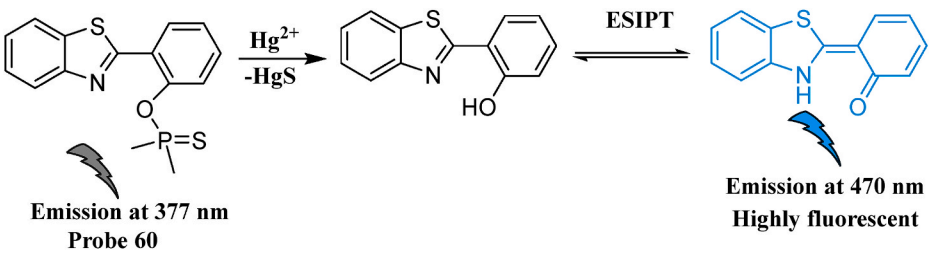

Fig. 61. Proposed mechanism of Hg^{2+}-promoted deprotection of probe **60** to corresponding fluorophore.

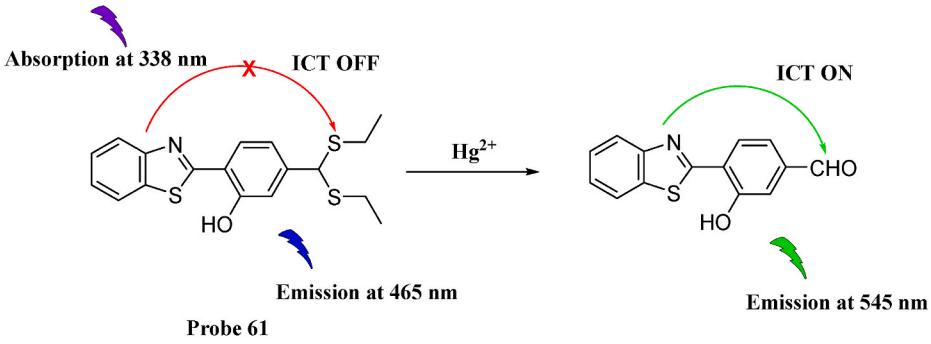

Fig. 62. Fluorescence response of probe **61** in presence of Hg^{2+} ions.

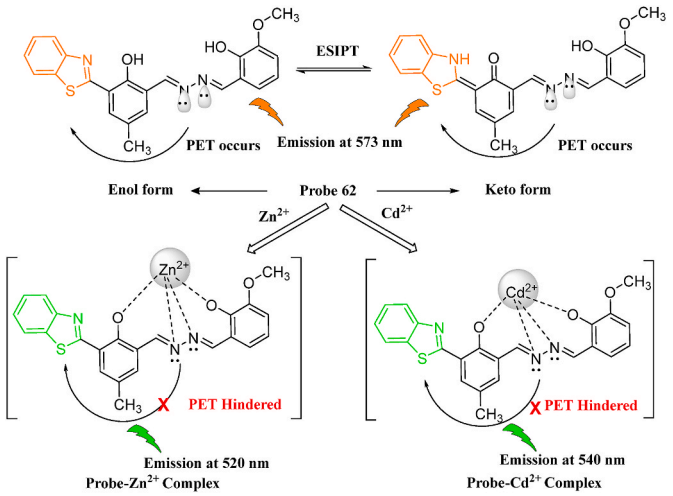

Fig. 63. Mechanism of dual detection of Zn^{2+} and Cd^{2+} ions by means of quenching of fluorescence response of probe **62**.

emission band shifts to 545 nm with gradual increase in its intensity concurrent with increasing concentrations of Hg^{2+} and a subsequent dip in the intensity of the band at 465 nm [Fig. 62]. **61** shows high sensitivity, better selectivity, decent collinearity with the increasing concentrations of Hg^{2+} ranging from 0 to 35 M and a detection limit as low as 5.8 nM [98].

2.7.1.8. Dual detection of two ionic species. Li et al. synthesized probe 62 for dual detection of Zn^{2+} and Cd^{2+} ions, using Cys as an auxiliary reagent. The free probe exhibits weak orange fluorescence at wavelength of 573 nm, but after adding Zn^{2+} or Cd^{2+}, the probe fluorescence undergoes a blue-shift to generate yellow fluorescence at 520 nm and 540 nm, respectively. When Cys was added, the fluorescence peak position of Zn^{2+}-probe **62** complex remains unchanged, i.e., at 520 nm, while the position of the same for the Cd^{2+}-probe **62** complex shifted back to 573 nm from 540 nm; emitting similar signals as the free probe [Fig. 63]. This helps to easily distinguish between Zn^{2+} and Cd^{2+} ions when they are present together. The probe was further tested for its application in bioimaging in living HeLa cells and showed fair cell permeability and selectivity towards Zn^{2+} and Cd^{2+} ions in living cells. When incubated with probe **62**, the HeLa cells showed orange fluorescence. As soon as Zn^{2+} ions were added, strong green fluorescence appeared. Similarly, the addition of Cd^{2+} also led to the occurrence of green fluorescence. The detection limit was as low as 0.036 μM [99].

Gu and colleagues developed probe **63** for dual-tracing of Hg^{2+} and Cu^{2+}. The probe consisted of two reactive centers, namely, a thioacetal moiety for Hg^{2+}, and electronegative atoms, O and N, of HBT for Cu^{2+}. Upon introduction of Hg^{2+} to the probe, it exhibited ratiometric fluorescent color change from green to blue, whereas, in the presence of Cu^{2+}, the probe's fluorescence was quenched, giving no colored emission at all. The free probe absorbed maximally at 367 nm due to the π→π* transition of the HBT chromophore. The probe gets excited at 346 nm and produces two corresponding emissions bands at 450 nm pertaining to the enol emission and 530 nm associated with the keto emission. The probe itself shows a strong green fluorescence due to the presence of the thioacetal group as the electron-donating fragment and occurrence of ESIPT process between H and N of HBT. Once the dithioacetal group cleaves off in presence of Hg^{2+}, the probe gets oxidized and showed a blue shift in emission to 450 nm from 530 nm due to the alteration in the π-conjugation [Fig. 64(a)]. However, Cu^{2+} led to quenching of the fluorescence emission of the probe [Fig. 64(a)]. The LOD was calculated to be 7.6×10^{-9} mol/L. Moreover, high sensitivity and selectivity towards these two cations without other metal ion interferences were also observed. The probe was also efficiently applied to fluorescent imaging of Hg^{2+} and Cu^{2+} in viable HeLa cells [Fig. 64(b)] [100].

Kaur et al. reported an HBT based Schiff-base **64** for the detection of Cu^{2+} and PO_4^{3-} ions. Addition of Cu^{2+} ions to the probe leads to hydrolysis of the imine and consecutive formation of complex between Cu^{2+} and 4-amino-HBT, with the consequent inhibition of the fluorescence emission resulting in "turn-off" response of probe for Cu^{2+}. Subsequent addition of PO_4^{3-} ions helps to decomplex the Cu^{2+}-HBT complex and thereby restores the fluorescence emission at 422 nm through release of the 4-amino-HBT (Fig. 65). The interference studies

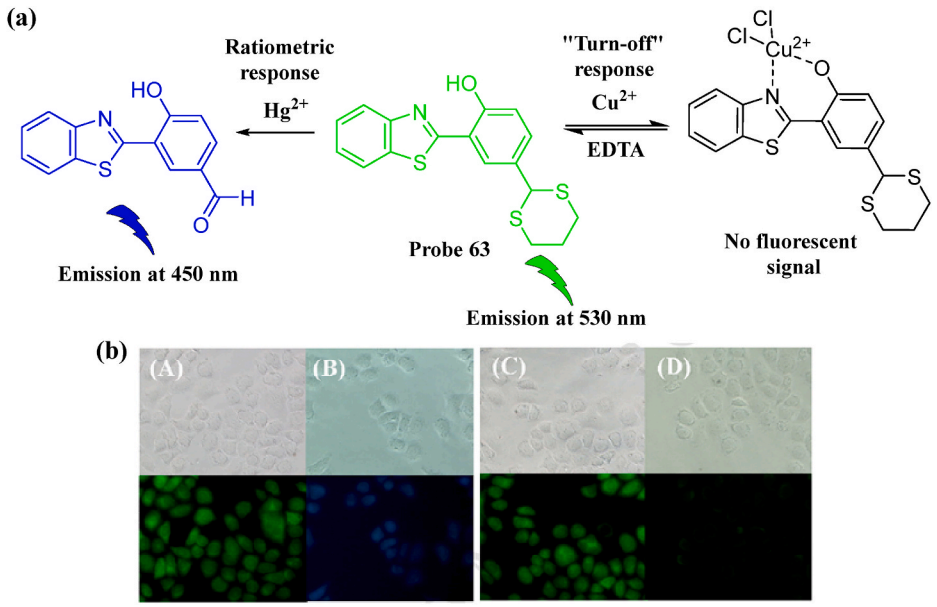

Fig. 64. (a) Proposed sensing mechanism of probe **63** for dual detection of Hg^{2+} and Cu^{2+} ions; (b) Bright field and Fluorescence images of HeLa cells incubated with probe **63** in the absence (A) and in the presence (B) of Hg^{2+} ions, and in the absence (C), and presence (D) of Cu^{2+} ions. Reprinted (adapted) with permission from Fig. 6 in Ref. [100]. Copyright 2016 Elsevier.

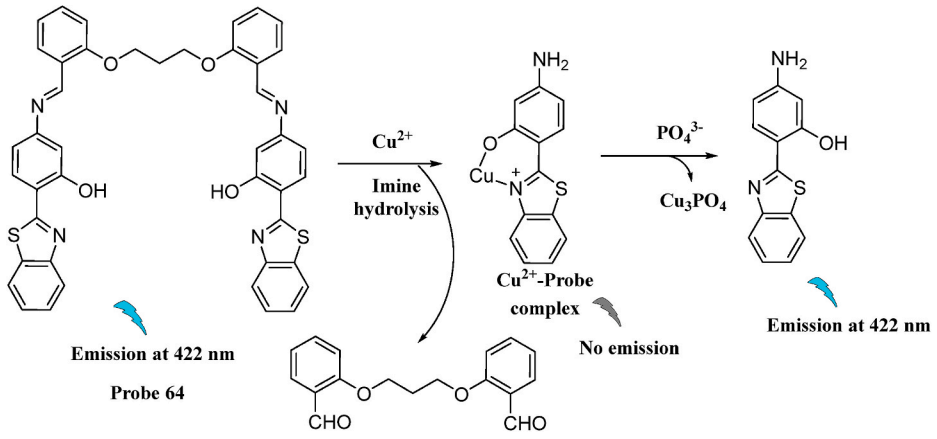

Fig. 65. Dual detection of Cu^{2+} and PO_4^{3-} ions by probe **64**.

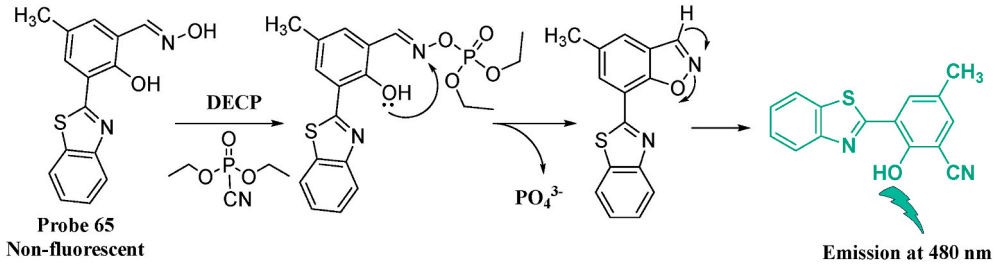

Fig. 66. Proposed mechanism of selective detection of DECP, by "turn-on" response of probe **65**.

demonstrated the selectivity of probe towards Cu^{2+} and PO_4^{3-} by showing no significant changes in the emission of probe in presence of other metal ions or phosphates such as pyrophosphate, AMP, ADP, ATP, etc. The detection limits of the probe for Cu^{2+} ions and were calculated as 2.11 and 31.6 ppb, respectively [101].

2.7.2. *Detection of various molecular toxicants*

An HBT-based fluorophore was amalgamated with an oxime reaction center to serve as an ESIPT fluorescent probe 65 to detect diethyl cyanophosphonate (DECP), a nerve gas mimic, in both its solution as well as gas phases. The free probe exhibited weak fluorescence due to occurrence of PET from oxime nitrogen to the benzothiazole fluorophore. The probe exhibited a 60-fold fluorescence enhancement at 480 nm in the

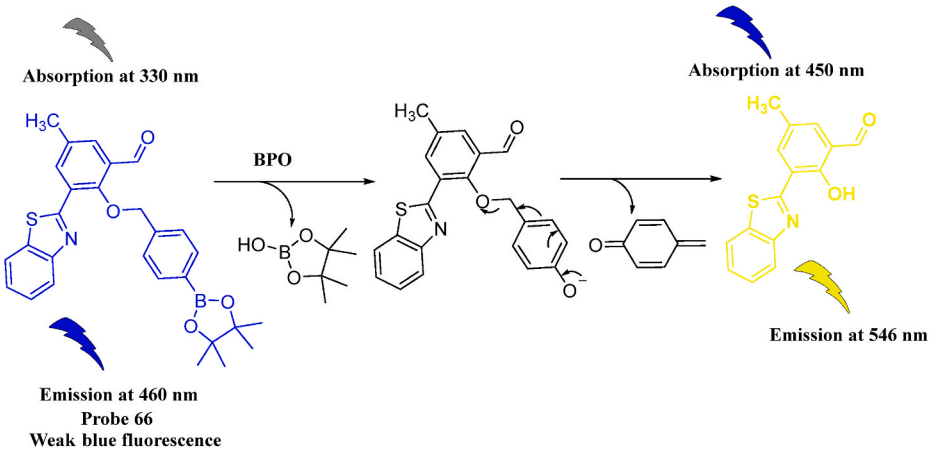

Fig. 67. Ratiometric fluorescence response of probe **66** in presence of benzoyl peroxide.

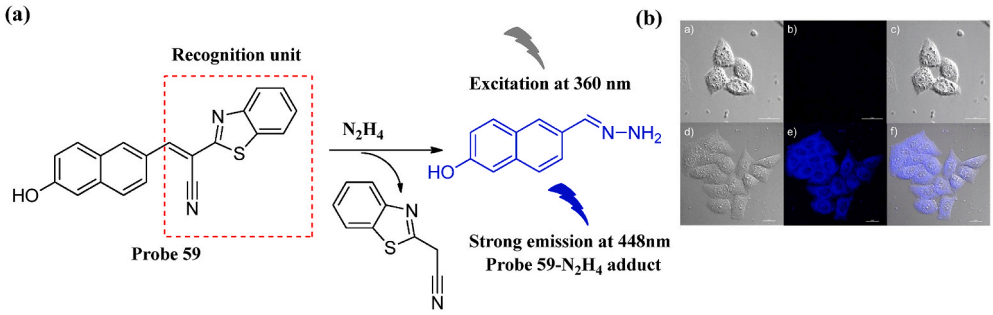

Fig. 68. (a) Suggested sensing mechanism of probe **67** for N_2H_4; (b) Bright-field and fluorescence images of HeLa cells stained with probe **67** in absence and in presence of N_2H_4. Reprinted (adapted) from open access from Fig. 8 in Ref. [104].

presence of DECP, which can be attributed to the transformation of oxime group into the corresponding nitrile during with LOD of 1.3 nM. [Fig. 66]. Confocal microscopic images of probe **65**-composited nanofibers before and after exposure to DECP, exhibited strong yellow fluorescence from the produced cyano-based end-product whereas, the non-exposed nanofibers do not show any such emission [102].

Benzoyl peroxide (BPO) is a popularly known oxidizing agent and effective radical initiator for polymerization and cyclization reactions and thus finds wider applications in several pharmaceutical and food industries. Overconsumption of benzoyl peroxide through food may lead to allergies, and the free radicals obtained from their decomposition products have extremely hazardous effects in humans. Thus, their detection in nature is essential, for which Ma et al. synthesized a novel ratiometric fluorescent probe 66 with an aryl boronate moiety as the recognition unit for BPO. The free probe emits weak blue fluorescence at 460 nm and, upon adding BPO, a strong yellow-greenish fluorescence emission at 546 nm is observed due to cleavage of the arylboronate unit by oxidation and 1,6-elimination processes [Fig. 67]. The probe exhibits a LOD of 0.26 μM. Cellular imaging techniques have confirmed the successful application of the probe to the imaging of BPO in live A549 cells [103].

Hydrazine (N_2H_4) is widely used as a catalyst and reducing agent in pharmaceutical and agricultural industries. Thus, it acts as industrial pollutants to humans and animals, causing lung, liver, and kidney cancers. Wang et al. designed a new "turn-on" two-photon fluorescent probe 67 for hydrazine detection. The free probe did not show any significant fluorescence at an excitation wavelength of 360 nm, but in the presence of N_2H_4 resulted strong fluorescent emission (16 folds) at 448 nm [Fig. 68(a)]. The sensing mechanism can be attributed to the cleavage of the 2-benzothiazoleacetonitrile moiety upon exposure to N_2H_4. The probe was also efficiently applied in the bioimaging of N_2H_4 in tissues

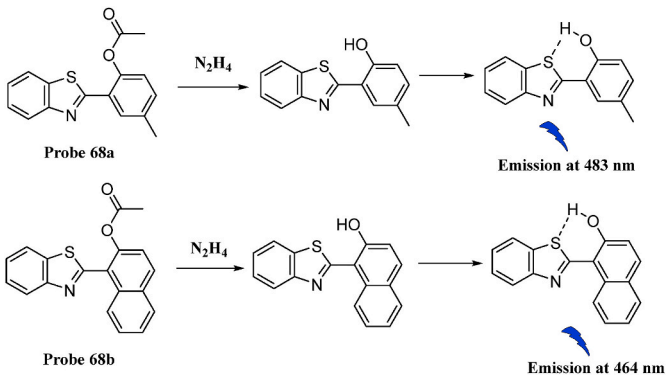

Fig. 69. Detection of N_2H_4 in presence of probes **68a** and **68b**.

and living HeLa cells [Fig. 68(b)] [104].

Liu et al. synthesized two phenolic ester derivatives of benzothiazoles as fluorescent chemosensors **68a** and **68b** for the selective detection of hydrazine. The free probe solutions remain colorless with a very weak fluorescence emission at 370 nm but with the incorporation of N_2H_4, the probes exhibited a bathochromic shift in the absorption peaks of probes **68a** and **68b** at 345 nm and 445 nm, respectively. The corresponding chromogenic change from colorless to yellow was also observed. Probes **68a** and **68b** in presence of N_2H_4 exhibited new emission peaks at 483 nm and 464 nm [Fig. 69]. The fluorescence intensities of probes **68a** and **68b** increased by 20 folds and 17 folds respectively, with increasing concentrations of hydrazine up to 20 equiv. of the probe concentration. The detection limits of the two probes were calculated as 0.37 μM and 0.49 μM, respectively. The probes exhibited

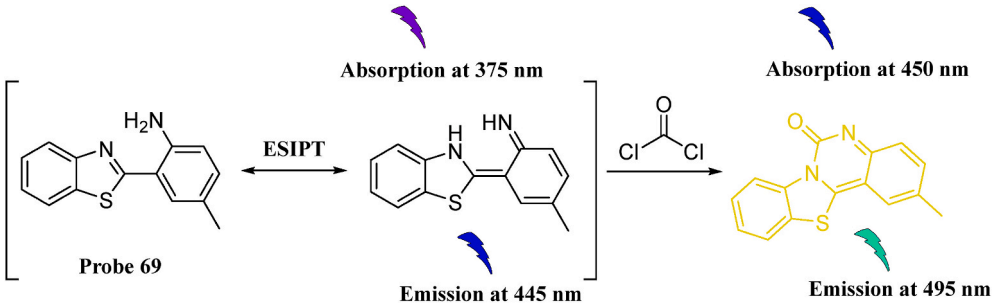

Fig. 70. Chromogenic and fluorometric response of probe **69** in presence of phosgene.

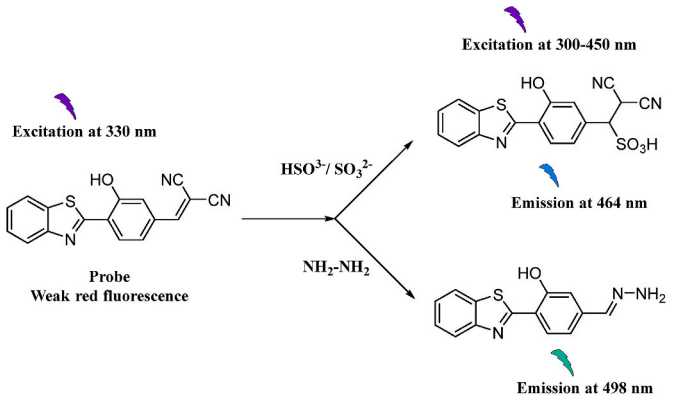

Fig. 71. Fluorescence response of probe **70** in presence of $NaHSO_3$ and NH_2NH_2.

excellent sensitivity and selectivity towards hydrazine and lesser cytotoxicity that facilitates its prospects for use in *vitro* and *in vivo* cell imaging studies. It has been successfully applied to bioimaging of hydrazine in HeLa cells [105].

Chen et al. developed an ESIPT-based colorimetric and ratiometric fluorescence probe **69** for the detection of highly toxic phosgene gas ($COCl_2$) which is accountable for several respiratory tract complications, such as, asphyxia, pulmonary emphysema and edema. The free probe solution in chloroform remained colorless (λ_{max} = 375 nm) and exhibited blue fluorescence emission at 445 nm. Upon addition of triphosgene, the absorption maximum red shifted towards 450 nm with an associated color change to yellow with a concurrent red-shift of the fluorescence emission maximum from 445 nm to 495 nm thereby emitting green fluorescence (Fig. 70). A good linear correlation exists between the emission intensity at 495 and 445 nm and triphosgene concentration upto 3.0 μM of $COCl_2$. Probe 69 exhibited high sensitivity with a detection limit as low as 0.14 ppm and excellent selectivity towards phosgene as compared to other relevant analytes including triphosgene [106].

As mentioned earlier, hydrazine accounts for irreversible cellular or tissue level damages due to its faster penetrability and absorption from mouth and skin. Similarly, sulfur dioxide derivatives (sulfite and bisulfite) cause several of diseases at abnormal levels inside the body. Thus, it is important to develop reliable and instantaneous analytical tools for the detection of sulfur dioxide derivatives and hydrazine. For the simultaneous detection of the differential amounts of two analytes, Zhou et al. designed and synthesized an HBT-based fluorescent probe **70**. The free probe showed very weak red fluorescence due to quenching of the ICT process when excited at 330 nm. Upon addition of $NaHSO_3$ and hydrazine, the maximal absorption wavelength ranged between 300 and 450 nm and a significant enhancement in the fluorescence emission intensity (40-fold and 10-fold) was observed at around 464 nm and 498 nm, respectively, with increasing concentrations of $NaHSO_3$ and hydrazine [Fig. 71]. The detection limits of probe for $NaHSO_3$ and hydrazine were calculated as 6.3×10^{-7} M and 1.7×10^{-5} M, respectively [107].

3. Conclusion

This review covers the recent advances and novel developments made in the field of benzothiazole-based fluorescent probes in the past five years and is mainly classified as detectors of various biomolecules, ions and reactive or catalytic species involved in the mediation of several fatal and gruesome diseases, mainly focusing on different types of cancer, Alzheimer's disease, genetic disorders, and senescence associated with oxidative stress. The benzothiazole probes are mainly composed of two distinct parts: the benzothiazole fluorophore and a detection unit. Upon interaction with a particular analyte, the detection unit undergoes cleavage from benzothiazole fluorophore and leading to the sudden occurrence of or gradual change in the fluorescent signals. These probes interact with various analytes by oxidation, hydrolysis, complexation, nucleophilic addition reactions, etc., to change their photophysical properties. The benzothiazole probes showed advantages of a wide linear range, high quantum yields and low detection limit. These can selectively and quantitatively detect desired analytes in real water samples and also in living biological systems. However, the compulsory requirement of organic solvents for dissolution of probes and detection of analytes limits their scopes in cell imaging due to the severe damaging consequences of organic solvents in living organisms. Thus, future generation probes are required to be completely biocompatible. The benzothiazole scaffold has been widely known to possess pharmacological properties, and several benzothiazole-based drugs are commercially available in the market. Whereas the acute toxicity of many of these probes to be used for *in vivo* applications has been studied on a cellular level. Hence, further studies on toxicity screening should be explored. The fluorescence emission of the benzothiazole scaffold can be improved to achieve red and NIR by enhancing conjugation and push−pull character. Besides that, there is ample room for improvement in enhancing the fluorescence response of the probes by combining them with suitable PET, AIE and/or FRET scaffolds and further the reach of the probes to various challenging analytes. Through this review, we have already established the importance of benzothiazole fluorescent probes for the development of bioimaging and biosensing required for environmental protection and maintenance of healthy life. The prospects involve studies on the development of benzothiazole fluorescent probes with good aqueous solubility and lesser toxicity and further exploration and extension of its applicability. With the advent of new synthetic methodologies, several novel benzothiazole-type sensors will soon become available and may lead to new sensing mechanisms or analyte selectivities that are currently inaccessible.

Declaration of competing interest

The authors declare that they have no known competing financial interests or personal relationships that could have appeared to influence

the work reported in this paper.

Acknowledgement

The authors thank the Department of Biotechnology (DBT), India. Grant Number: 102/IFD/SAN/3016/2019–20.

References

[1] Suss O, Motiei L, Margulies D. Broad applications of thiazole orange in fluorescent sensing of biomolecules and ions. Molecules 2021;26:2828–52.
[2] Lavis LD, Raines RT. Bright ideas for chemical biology. ACS Chem Biol 2008;3:142–55.
[3] Sinkeldam RW, Greco NJ, Tor Y. Fluorescent analogs of biomolecular building blocks: design, properties, and applications. Chem Rev 2010;110:2579–619.
[4] Kobayashi H, Ogawa M, Alford R, Choyke PL, Urano Y. New strategies for fluorescent probe design in medical diagnostic imaging. Chem Rev 2010;110:2620–40.
[5] Zhu J, Gao Q, Tong Q, Wu G. Fluorescent probes based on benzothiazole-spiropyran derivatives for pH monitoring *in vitro* and *in vivo*. Spectrochim Acta Mol Biomol Spectrosc 2020;225:117506–13.
[6] Sun M, Du L, Yu H, Zhang K, Liu Y, Wang S. An intramolecular charge transfer process based fluorescent probe for monitoring subtle pH fluctuation in living cells. Talanta 2017;162:180–6.
[7] Rout B, Motiei L, Margulies D. Combinatorial fluorescent molecular sensors: the road to differential sensing at the molecular level. Synlett 2014;25:1050–4.
[8] de Silva AP, Gunaratne HQN, Gunnlaugsson T, Huxley AJM, McCoy CP, Rademacher JT, Rice TE. Signaling recognition events with fluorescent sensors and switches. Chem Rev 1997;97:1515–66.
[9] Gjorgjieva M, Tomašič T, Kikelj D, Lucija PM. Benzothiazole-based compounds in antibacterial drug discovery. Curr Med Chem 2018;25:1–19.
[10] Pathak N, Rathi E, Kumar N, Kini SG, Rao CM. A review on anticancer potentials of benzothiazole derivatives. Mini Rev Med Chem 2020;20:12–23.
[11] Kamal A, Syed MAH, Mohammed SM. Therapeutic potential of benzothiazoles: a patent review (2010 - 2014). Expert Opin Ther Pat 2015;25:335–49.
[12] Keri RS, Patil MR, Patil SA, Budagupi S. A comprehensive review in current developments of benzothiazole-based molecules in medicinal chemistry. Eur J Med Chem 2015;89:207–51.
[13] Taha M, Ismail NH, Imran S, Wadood A, Rahim F, Khan KM, Riaz M. Hybrid benzothiazole analogs as antiurease agent: synthesis and molecular docking studies. Bioorg Chem 2016;66:80–7.
[14] Cheng J, Liu D, Li W, Bao L, Han K. Comprehensive studies on excited-state proton transfer of a series of 2-(2′-hydroxyphenyl)benzothiazole derivatives: synthesis, optical properties, and theoretical calculations. J Phys Chem C 2015;119:4242–51.
[15] Yan F, Sun J, Zang Y, Sun Z, Zhang H, Wang X. Benzothiazole applications as fluorescent probes for analyte detection. J Iran Chem Soc 2020;17:3179–203.
[16] Sedgwick AC, Wu L, Han H-H, Bull SD, He X-P, James TD, Sessler JL, Tang BZ, Tian H, Yoon J. Excited-state intramolecular proton-transfer (ESIPT) based fluorescence sensors and imaging agents. Chem Soc Rev 2018;47:8842–70.
[17] Li K, Feng Q, Niu G, Zhang W, Li Y, Kang M, Xu K, He J, Hou H, Tang BZ. Benzothiazole-based aiegen with tunable excited-state intramolecular proton transfer and restricted intramolecular rotation processes for highly sensitive physiological pH sensing. ACS Sens 2018;3:920–8.
[18] Ma Q, Li X, Feng S, Liang B, Zhou T, Xu M, Ma Z. A novel acidic pH fluorescent probe based on a benzothiazole derivative. Spectrochim Acta-Part A Mol Biomol Spectrosc 2017;177:6–13.
[19] Capello M, Lee M, Wang H, Babel I, Katz MH, Fleming JB, Maitra A, Wang H, Tian W, Taguchi A, Hanash SM. Carboxylesterase 2 as a determinant of response to irinotecan and neoadjuvant FOLFIRINOX therapy in pancreatic ductal adenocarcinoma. J Natl Cancer Inst (Bethesda) 2015;107:132.
[20] Uchida K, Otake K, Tanaka K, Hashimoto K, Saigusa S, Matsushita K, Koike Y, Inoue M, Ueeda M, Okugawa Y, Inoue Y, Mohri Y, Kusunoki M. Clinical implications of CES2 RNA expression in neuroblastoma. J Pediatr Surg 2013;48:502–9.
[21] Ohtsuka K, Inoue S, Kameyama M, Kanetoshi A, Fujimoto T, Takaoka K, Araya Y, Shida A. Intracellular conversion of irinotecan to its active form, sn-38, by native carboxylesterase in human non-small cell lung cancer. Lung Cancer 2003;41:187–98.
[22] Shaojun C, Li H, Haixin H, Guisheng L. Expression of topoisomerase 1 and carboxylesterase 2 correlates with irinotecan treatment response in metastatic colorectal cancer. Cancer Biol Ther 2018;19:153–9.
[23] Liu S-Y, Qu R-Y, Li R-R, Yan Y-C, Sun Y, Yang W-C, Yang G-F. An activity-based fluorogenic probe enables cellular and *in vivo* profiling of carboxylesterase isozymes. Anal Chem 2020;92:9205–13.
[24] Mao Y, Ma M, Wei P, Zhang P, Liu L, Guan T, Zhang X, Yi T. A sensitive and rapid "off-on" fluorescent probe for the detection of esterase and its application in evaluating cell status and discrimination of living cells and dead cells. Analyst 2020;145:1408–13.
[25] Girault M, Beneyton T, Pekin D, Buisson L, Bichon S, Charbonnier C, delAmo Y, Baret JC. High-content screening of plankton alkaline phosphatase activity in microfluidics. Anal Chem 2018;90:4174–81.
[26] Daryaei I, Ghaffari MM, Jones KM, Pagel MD. Detection of alkaline phosphatase enzyme activity with a CATALYCEST MRI biosensor. ACS Sens 2016;1:857–61.
[27] Ooi K, Shiraki K, Morishita Y, Nobori T. High-molecular intestinal alkaline phosphatase in chronic liver diseases. J Clin Lab Anal 2007;21:133–9.
[28] Zhang P, Fu C, Zhang Q, Li S, Deng C. Ratiometric fluorescent strategy for localizing alkaline phosphatase activity in mitochondria based on the ESIPT process. Anal Chem 2019;91:12377–83.
[29] Kim T-I, Jin H, Bae J, Kim Y. Excimer emission-based fluorescent probe targeting caspase-3. Anal Chem 2017;89:10565–9.
[30] Maes H, Agostinis P. Autophagy and mitophagy interplay in melanoma progression. Mitochondrion 2014;19:58–68.
[31] Honscheid P, Datta K, Muders MH. Autophagy: detection, regulation and its role in cancer and therapy response. Int J Radiat Biol 2014;90:628–35.
[32] Jiang P, Mizushima N. Autophagy and human diseases. Cell Res 2014;24:69–79.
[33] He X, Li J, An S, Jiang C. pH-sensitive drug-delivery systems for tumor targeting. Ther Deliv 2013;4:1499–510.
[34] Reyjal J, Cormier K, Turcotte S. Autophagy and cell death to target cancer cells: exploiting synthetic lethality as cancer therapies. Adv Exp Med Biol 2014:167–88.
[35] Platt FM. Emptying the stores: lysosomal diseases and therapeutic strategies. Nat Rev Drug Discov 2018;17:133.
[36] Abeywickrama CS, Wijesinghe KJ, Stahelin RV, Pang Y. Lysosome imaging in cancer cells by pyrene-benzothiazolium dyes: an alternative imaging approach for LAMP-1 expression based visualization methods to avoid background interference. Bioorg Chem 2019;91:103144.
[37] Abeywickrama CS, Bertman KA, Mcdonald LJ, Alexander N, Dahal D, Baumann HJ, Salmon CR, Wesdemiotis C, Konopka M, Pang Y. Synthesis of highly selective lysosomal markers by coupling 2-(2′-hydroxyphenyl)benzothiazole (HBT) with benzothiazolium cyanine (Cy): the impact of substituents on selectivity and optical properties. J Mater Chem B 2019;7:7502–14.
[38] Ren M, Wang L, Lv X, Liu J, Chen H, Wang J, Guo W. Development of a benzothiazole-functionalized red-emission pyronin dye and its dihydro derivative for imaging lysosomal viscosity and tracking endogenous peroxynitrite. J Mater Chem B 2019;7:6181–6.
[39] Brown JM, Wilson WR. Exploiting tumour hypoxia in cancer treatment. Nat Rev Cancer 2004;4:437–47.
[40] Brown JM. Exploiting tumour hypoxia and overcoming mutant p53 with tirapazamine. Br J Cancer 1998;77:12–4.
[41] Kizaka-Kondoh S, Inoue M, Harada H, Hiraoka M. Tumor hypoxia: a target for selective cancer therapy. Cancer Sci 2003;94:1021–8.
[42] Yang Q, Wang S, Li D, Yuan J, Xu J, Shao S. A mitochondria-targeting nitroreductase fluorescent probe with large Stokes shift and long-wavelength emission for imaging hypoxic status in tumor cells. Anal Chim Acta 2020;1103:202–11.
[43] Blennow K. Biomarkers in Alzheimer's Disease drug development. Nat Med 2010;16:1218–22.
[44] Li C, Yang L, Han Y, Wang X. A simple approach to quantitative determination of soluble amyloid-β peptides using a ratiometric fluorescence probe. Biosens Bioelectron 2019;142:111518–23.
[45] Gabr MT, Pigge FC. Rhenium complexes of bis(benzothiazole)-based tetraarylethylenes as selective luminescent probes for amyloid fibrils. Chem-A Eur J 2018;24:11729–37.
[46] Mora AK, Murudkar S, Alamelu A, Singh PK, Chattopadhyay S, Nath S. Benzothiazole-based neutral ratiometric fluorescence sensor for amyloid fibrils. Chem Eur J 2016;22:1–9.
[47] Rajasekhar K, Narayanaswamy N, Murugan NA, Kuang G, Agren H, Govindaraju T. A high affinity red fluorescence and colorimetric probe for amyloid β aggregates. Sci Rep 2016;6:23668–77.
[48] Zhong K, He Y, Deng L, Yan X, Li X, Tang Y, Hou S, Tang L. A near-infrared fluorescent probe for H_2S based on tandem reaction to construct iminocoumarin-benzothiazole and its application in food, water, living cells. Anal Chim Acta 2020;1127:49–56.
[49] Chen L, Wu D, Lim CS, Kim D, Nam S-J, Lee W, Kim G, Kim HM, Yoon J. A two-photon fluorescent probe for specific detection of hydrogen sulfide based on a familiar ESIPT fluorophore bearing AIE characteristics. Chem Commun 2017;53:4791–4.
[50] Patlolla PR, Desai N, Gupta S, Datta B. Interaction of a dimeric carbocyanine dye aggregate with bovine serum albumin in non-aggregated and aggregated forms. Spectrochim Acta Part A Mol Biomol Spectrosc 2019;209:256–63.
[51] Wang Y-N, Xu B, Qiu L-H, Sun R, Xu Y-J, Ge J-F. Viscosity sensitive fluorescent dyes with excellent photostability based on hemicyanine dyes for targeting cell membrane. Sensor Actuator B Chem 2021;337:129787–94.
[52] Betteridge DJ. What is oxidative stress? Metabolism 2000;49:3–8.
[53] Long Y, Liu J, Tian D, Dai F, Zhang S, Zhou B. Cooperation of ESIPT and ICT processes in the designed 2-(2′-hydroxyphenyl)benzothiazole derivative: a near-infrared two-photon fluorescent probe with a large Stokes shift for the detection of cysteine and its application in biological environments. Anal Chem 2020;92:14236–43.
[54] Li M, Kang N, Zhang C, Liang W, Zhang G, Jia J, Yao Q, Shuang S, Dong C. A turn-on fluorescence probe for cysteine/homocysteine based on the nucleophilic-induced rearrangement of benzothiazole thioether. Spectrochim Acta Part A Mol Biomol Spectrosc 2019;222:117262–7.
[55] Ma X, Hao Y, Liu J, Wu G, Liu L. A green-emitting fluorescent probe based on a benzothiazole derivative for imaging biothiols in living cells. Molecules 2019;24:411–20.

[56] Yu Y, Xu H, Zhang W, Wang B, Jiang Y. A novel benzothiazole-based fluorescent probe or cysteine detection and its application on test paper and in living cells. Talanta 2018;176:151–5.

[57] Zhou Y, Zhang L, Zhang X, Zhu ZJ. Development of a near-infrared ratiometric fluorescent probe for glutathione using an intramolecular charge transfer signaling mechanism and its bioimaging application in living cells. J Mater Chem B 2019;7:809–14.

[58] Zhao Y, Xue Y, Li H, Zhu R, Ren Y, Shi Q, Wang S, Guo W. An excited state intramolecular proton transfer dye based fluorescence turn-on probe for fast detection of thiols and its applications in bioimaging. Spectrochim Acta-Part A Mol Biomol Spectrosc 2017;175:215–21.

[59] Chen S, Li H, Hou P. A novel cyanobiphenyl benzothiazole-based fluorescent probe for detection of biothiols with a large Stokes shift and its application in cell imaging. Tetrahedron 2017;73:589–93.

[60] He L, He T, Farrar S, Ji L, Liu T, Ma X. Antioxidants maintain cellular redox homeostasis by elimination of reactive oxygen species. Cell Physiol Biochem 2017;44:532–53.

[61] Makau JN, Kitagawa A, Kitamura K, Yamaguchi T, Mizuta S. Design and development of an HBT-based ratiometric fluorescent probe to monitor stress-induced premature senescence. ACS Omega 2020;5:11299–307.

[62] Nguyen KH, Hao Y, Zeng K, Fan S, Li F, Yuan S, Ding X, Xu M, Liu YN. A benzothiazole-based fluorescent probe for hypochlorous acid detection and imaging in living cells. Spectrochim Acta-Part A Mol Biomol Spectrosc 2018;199:189–93.

[63] Shen Y, Zhang X, Zhang Y, Li H, Dai L, Peng X, Peng Z, Xie Y. A fluorescent sensor for fast detection of peroxynitrite by removing of C=N in a benzothiazole derivative. Anal Chim Acta 2018;1014:71–6.

[64] Wang M, Wang D, Qiu S, Xiao J, Cai H, Zou J. Multi-wavelength spectrophotometric determination of hydrogen peroxide in water by oxidative coloration of ABTS via fenton reaction. Environ Sci Pollut Res 2019;26:27063–72.

[65] Li RQ, Mao ZQ, Rong L, Wu N, Lei Q, Zhu JY, Zhuang L, Zhang XZ, Liu ZH. A two-photon fluorescent probe for exogenous and endogenous superoxide anion imaging *in vitro* and *in vivo*. Biosens Bioelectron 2017;87:73–80.

[66] Chang C, Wang F, Qiang J, Zhang Z, Chen Y, Zhang W, Wang Y, Chen X. Benzothiazole-based fluorescent sensor for hypochlorite detection and its application for biological imaging. Sensor Actuator B Chem 2017;243:22–8.

[67] Wang Q, Fang T, Zheng J, Shi L, Shi L, Li T. Proximity-dependent switchable ATP aptasensors utilizing a high-performance FRET reporter. ACS Appl Mater & Amp Interfaces 2020;13:9359–68.

[68] Turaev AV, Tsvetkov VB, Tankevich MV, Smirnov IP, Aralov AV, Pozmogova GE, Varizhuk AM. Benzothiazole-based cyanines as fluorescent "light-up" probes for duplex and quadruplex DNA. Biochimie 2019;162:216–28.

[69] Jin M, Liu X, Zhang X, Wang L, Bing T, Zhang N, Zhang Y, Shangguan D. Thiazole orange-modified carbon dots for ratiometric fluorescence detection of G-Quadruplex and double-stranded DNA. ACS Appl Mater Interfaces 2018;10:25166–73.

[70] Lu YJ, Deng Q, Hou JQ, Hu DP, Wang ZY, Zhang K, Luyt LG, Wong WL, Chow CF. Molecular engineering of thiazole orange dye: change of fluorescent signaling from universal to specific upon binding with nucleic acids in bioassay. ACS Chem Biol 2016;11:1019–29.

[71] Luo X, Xue B, Feng G, Zhang J, Lin B, Zeng P, Li H, Yi H, Zhang XL, Zhu H, Nie Z. Lighting up the native viral RNA genome with a fluorogenic probe for the live-cell visualization of virus infection. J Am Chem Soc 2019;141:5182–91.

[72] Gahtory D, Murtola M, Smulders MMJ, Wennekes T, Zuilhof H, Strömberg R, Albada B. Facile functionalization of peptide nucleic acids (PNAs) for antisense and single nucleotide polymorphism detection. Org Biomol Chem 2017;15:6710–4.

[73] Wang X-L, Sun R, Miao J-T, Sheng X. Hemicyanine dyes linked with quaternary ammonium group: near-infrared probes for the detection of nucleic acid. Sensor Actuator B Chem 2016;236:627–34.

[74] Zhu M-S, Zhang X-Q, Ma W, Sun R, Xu Y-J, Ge J-F. Design and synthesis of a series of off-on near infrared fluorescent probes for nucleic acid in aqueous solution. Bioorg Med Chem Lett 2021;48:128239–42.

[75] Väänänen AJ, Salmenperä P, Hukkanen M, Rauhala P, Kankuri E. Cathepsin B is a differentiation-resistant target for nitroxyl (HNO) in THP-1 monocyte/macrophages. Free Radic Biol Med 2006;41:120–31.

[76] Espey MG, Miranda KM, Thomas DD, Wink DA. Ingress and reactive chemistry of nitroxyl-derived species within human cells. Free Radic Biol Med 2002;33:827–34.

[77] Li H, Yao Q, Xu F, Xu N, Ma X, Fan J, Long S, Du J, Wang J, Peng X. Recognition of exogenous and endogenous nitroxyl in living cells via a two-photon fluorescent probe. Anal Chem 2018;90:4641–8.

[78] Gan LL, Chen LH, Nan FJ. Discovery of a novel calcium-sensitive fluorescent probe for α-ketoglutarate. Acta Pharmacol Sin 2017;38:1683–90.

[79] Burgos-Barragan G, Wit N, Meiser J, Dingler FA, Pietzke M, Mulderrig L, Pontel LB, Rosado IV, Brewer TF, Cordell RL, Monks PS, Chang CJ, Vazquez A, Patel KJ. Mammals divert endogenous genotoxic formaldehyde into one-carbon metabolism. Nature 2017;548:549–54.

[80] Tong Z, Han C, Qiang M, Wang W, Lv J, Zhang S, Luo W, Li H, Luo H, Zhou J, Wu B, Su T, Yang X, Wang X, Liu Y, He R. Age-related formaldehyde interferes with dna methyltransferase function, causing memory loss in Alzheimer's Disease. Neurobiol Aging 2015;36:100–10.

[81] Hao Y, Zhang Y, Zhang A, Sun Q, Zhu J, Qu P, Chen S, Xu M. A benzothiazole-based ratiometric fluorescent probe for detection of formaldehyde and its applications for bioimaging. Spectrochim Acta-Part A Mol Biomol Spectrosc 2020;229:117988–93.

[82] Zhou Y, Yan J, Zhang N, Li D, Xiao S, Zheng K. A ratiometric fluorescent probe for formaldehyde in aqueous solution, serum and air using aza-cope reaction. Sensor Actuator B Chem 2018;258:156–62.

[83] Lu X, Hou M, Xia Q, Yan C, Xu Y, Liu R. Mitochondrial targeted fluorescent probe with AIE characteristics for bioimaging. Mater Sci Eng C 2017;77:129–35.

[84] Wei Y-F, Zhang X-Q, Sun R, Xu Y-J, Ge J-F. Fluorescent probes based 1,8-naphthalimide-nitrogen heterocyclic for monitoring the fluctuation of mitochondrial viscosity. Dyes Pigments 2021;194:109559–66.

[85] Li S, Cao D, Meng X, Hu Z, Li Z, Yuan C, Zhou T, Han X, Ma W. A novel fluorescent chemosensor based on coumarin and quinolinyl-benzothiazole for sequential recognition of Cu^{2+} and PPi and its applicability in live cell imaging. Spectrochim Acta-Part A Mol Biomol Spectrosc 2020;230:118022–30.

[86] Zhao YH, Luo Y, Wang H, Wei H, Guo T, Tan H, Yuan L, Zhang XB. A novel ratiometric and reversible fluorescence probe with a large Stokes shift for Cu^{2+} based on a new clamp-on unit. Anal Chim Acta 2019;1065:134–41.

[87] Tang L, He P, Zhong K, Hou S, Bian Y. A new hydroxynaphthyl benzothiazole derived fluorescent probe for highly selective and sensitive Cu^{2+} detection. Spectrochim Acta-Part A Mol Biomol Spectrosc 2016;169:246–51.

[88] Kumar PS, Lakshmi PR, Elango KP. Rational design and application of a fluorogenic chemodosimeter for selective detection of cyanide in an aqueous solution via excimer formation. Spectrochim Acta-Part A Mol Biomol Spectrosc 2019;221:117172–9.

[89] Wang Y, Wang J, Xian Q. A highly selective fluorescent and chromogenic probe for cn^- detection and its applications in bioimaging. Talanta 2018;190:487–91.

[90] Lu ZN, Wang L, Zhang X, Zhu ZJ. A selective fluorescent chemosensor for Cd^{2+} based on 8-hydroxylquinoline-benzothiazole conjugate and imaging application. Spectrochim Acta-Part A Mol Biomol Spectrosc 2019;213:57–63.

[91] Tian ZN, Wu DQ, Sun XJ, Liu TT, Xing ZY. A benzothiazole-based fluorescent probe for ratiometric detection of Al^{3+} and its application in water samples and cell imaging. Int J Mol Sci 2019;20:5993–6104.

[92] Chen Y, Wei T, Zhang Z, Chen T, Li J, Qiang J, Lv J, Wang F, Chen X. A benzothiazole-based fluorescent probe for ratiometric detection of Al^{3+} in aqueous medium and living cells. Ind Eng Chem Res 2017;56:12267–75.

[93] Erami RS, Ovejero K, Meghdadi S, Filice M, Amirnasr M, Rodríguez-Diéguez A, De La Orden MU, Gomez-Ruiz S. Applications of nanomaterials based on magnetite and mesoporous silica on the selective detection of zinc ion in live cell imaging. Nanomaterials 2018;8:434–59.

[94] Chang C, Wang F, Wei T, Chen X. Benzothiazole-based fluorescent sensor for ratiometric detection of Zn(II) ions and secondary sensing PPi and its applications for biological imaging and PPase catalysis assays. Ind Eng Chem Res 2017;56:8797–805.

[95] Kang BH, Gao ZF, Li N, Shi Y, Li NB, Luo HQ. Thiazole orange as a fluorescent probe: label-free and selective detection of silver ions based on the structural change of i-motif DNA at neutral pH. Talanta 2016;156–157:141–6.

[96] Jiao Y, Zhou L, He H, Yin J, Duan C. A new fluorescent chemosensor for recognition of Hg^{2+} ions based on a coumarin derivative. Talanta 2017;162:403–7.

[97] Zhang D, Liu J, Yin H, Wang H, Li S, Wang M, Li M, Zhou L, Zhang J. A turn on ESIPT probe for rapid and ratiometric fluorogenic detection of Hg^{2+} and its application in live-cell imaging. J Fluoresc 2016;26:1367–72.

[98] Zhou Y, He X, Chen H, Wang Y, Xiao S, Zhang N, Li D, Zheng K. An ESIPT/ICT modulation based ratiometric fluorescent probe for sensitive and selective sensing Hg^{2+}. Sensor Actuator B Chem 2017;247:626–31.

[99] Li J, Chen Y, Chen T, Qiang J, Zhang Z, Wei T, Zhang W, Wang F, Chen X. A benzothiazole-based fluorescent probe for efficient detection and discrimination of Zn^{2+} and Cd^{2+}, using cysteine as an auxiliary reagent. Sensor Actuator B Chem 2018;268:446–55.

[100] Gu B, Huang L, Su W, Duan X, Li H, Yao S. A benzothiazole-based fluorescent probe for distinguishing and bioimaging of Hg^{2+} and Cu^{2+}. Anal Chim Acta 2017;954:97–104.

[101] Kaur I, Kaur P, Singh K. 2-(4-amino-2-hydroxyphenyl)benzothiazole based schiff-base: complexation/decomplexation driven photo physical tuning of fluorescence leading to Cu^{2+} and PO_4^{3-} detection. Sensor Actuator B Chem 2018;257:1083–92.

[102] Chen L, Oh H, Wu D, Kim MH, Yoon J. An ESIPT fluorescent probe and a nanofiber platform for selective and sensitive detection of a nerve gas mimic. Chem Commun 2018;54:2276–9.

[103] Ma X, Wu G, Zhao Y, Yuan Z, Xia N, Yang M, Liu L. A benzothiazole-based ratiometric fluorescent probe for benzoyl peroxide and its applications for living cells imaging. Anal Sci 2019;35:91–7.

[104] Wang JY, Liu ZR, Ren M, Lin W. 2-Benzothiazoleacetonitrile based two-photon fluorescent probe for hydrazine and its bio-imaging and environmental applications. Sci Rep 2017;7:1530–7.

[105] Liu C, Wang F, Xiao T, Chi B, Wu Y, Zhu D, Chen X. The ESIPT fluorescent probes for N_2H_4 based on benzothiazole and their applications for gas sensing and bioimaging. Sensor Actuator B Chem 2018;256:55–62.

[106] Chen L, Wu D, Kim J-M, Yoon J. An ESIPT based fluorescence probe for colorimetric, ratiometric and selective detection of phosgene in solutions and the gas phase. Anal Chem 2017;89:12596–601.

[107] Zhou Y, Zeng F, Liu Y, Li M, Xiao S, Yan J, Zhang N, Zheng K. Reaction-based fluorescent probe for detecting of sulfur dioxide derivatives and hydrazine via distinct emission signals. Tetrahedron Lett 2018;59:3253–7.